NRAP
National Risk Assessment Partnership

A Critical Review of the Impacts of Leaking CO_2 Gas and Brine on Groundwater Quality

5 October 2016

U.S. DEPARTMENT OF ENERGY | NATIONAL ENERGY TECHNOLOGY LABORATORY

Office of Fossil Energy

NRAP-TRS-II-008-2016

Disclaimer

This report was prepared as an account of work sponsored by an agency of the United States Government. Neither the United States Government nor any agency thereof, nor any of their employees, makes any warranty, express or implied, or assumes any legal liability or responsibility for the accuracy, completeness, or usefulness of any information, apparatus, product, or process disclosed, or represents that its use would not infringe privately owned rights. Reference therein to any specific commercial product, process, or service by trade name, trademark, manufacturer, or otherwise does not necessarily constitute or imply its endorsement, recommendation, or favoring by the United States Government or any agency thereof. The views and opinions of authors expressed therein do not necessarily state or reflect those of the United States Government or any agency thereof.

This report (PNNL-24897) has been reviewed by Pacific Northwest National Laboratory and approved for public release.

Cover Illustration: This is a photograph of the column experiment set up. Solutions are pumped upward into the columns (bottom), past the in-line pH and Eh probes (top), and into the fraction collectors (left).

Suggested Citation: Qafoku, N. P.; Bacon, D. H.; Zheng, L.; Lawter, A. R.; Brown, C. F. *A Critical Review of the Impacts of Leaking CO_2 Gas and Brine on Groundwater Quality*; NRAP-TRS-II-008-2016; NRAP Technical Report Series; U.S. Department of Energy, National Energy Technology Laboratory: Morgantown, WV, 2016; p 88.

An electronic version of this report can be found at:
http://www.netl.doe.gov/research/on-site-research/publications/featured-technical-reports

https://edx.netl.doe.gov/nrap

A Critical Review of the Impacts of Leaking CO_2 Gas and Brine on Groundwater Quality

N. P. Qafoku, D. H. Bacon, L. Zheng, A. R. Lawter, C. F. Brown

[1]Pacific Northwest National Laboratory, 902 Battelle Boulevard, Richland, WA 99354

[2]Lawrence Berkeley National Laboratory, 1 Cyclotron Road, Berkeley, CA 94720

NRAP-TRS-II-008-2016

Level II Technical Report Series

5 October 2016

This page intentionally left blank.

Table of Contents

ABSTRACT **1**

1. INTRODUCTION **2**

2. OBJECTIVES **4**

3. GEOCHEMICAL DATA REQUIRED TO ASSESS AND PREDICT AQUIFER RESPONSES TO CO_2 AND BRINE LEAKAGE **5**

3.1 THRESHOLD VALUES AND AVERAGE GROUNDWATER CONCENTRATIONS 5

3.2 SOLID PHASE PROPERTIES: MINERALOGY 11

3.3 OTHER AQUIFERS 15

3.4 RELEVANT PROCESSES AND REACTIONS 21

3.5 DEVELOPMENT OF CONCEPTUAL AND REDUCED-ORDER MODELS 35

4. POTENTIAL RISK FOR GROUNDWATER POLLUTION DUE TO CO_2 GAS AND BRINE INTRUSION **40**

4.1 THE EFFECTS ON TDS AND PH 40

4.2 CHANGES IN MAJOR, MINOR, AND TRACE ELEMENT CONCENTRATION 44

4.3 CHANGES IN ORGANIC CONTAMINANT CONCENTRATIONS 52

5. CONCLUSIVE REMARKS **63**

5.1 CRUCIAL SITE-SPECIFIC DATA 63

5.2 POTENTIAL RISK TO GROUNDWATER 64

5.3 FUTURE EFFORTS 66

6. REFERENCES **67**

This page intentionally left blank.

List of Figures

Figure 1: Comparison of background values of pH for the High Plains Aquifer and shallow, urban unconfined portion of the Edwards Aquifer used in NRAP studies with ranges for various aquifer types in the U.S. Symbols represent median value and error bars the 10th percentile. 9

Figure 2: Comparison of background values of TDS for the High Plains Aquifer and shallow, urban unconfined portion of the Edwards Aquifer used in NRAP studies with ranges for various aquifer types in the U.S. Symbols represent median value and error bars the 90th percentile. 10

Figure 3: Comparison of background values of Arsenic for the High Plains Aquifer and shallow, urban unconfined portion of the Edwards Aquifer used in NRAP studies with ranges for various aquifer types in the U.S. Symbols represent median value and error bars the 90th percentile. 10

Figure 4: Comparison of background values of Barium for the High Plains Aquifer and shallow, urban unconfined portion of the Edwards Aquifer used in NRAP studies with ranges for various aquifer types in the U.S. Symbols represent median value and error bars the 90th percentile. 11

Figure 5: Comparison of background values of Lead for the High Plains Aquifer and shallow, urban unconfined portion of the Edwards Aquifer used in NRAP studies with ranges for various aquifer types in the U.S. Symbols represent median value and error bars the 90th percentile. 11

Figure 6: SEM/EDS for (a) CNG 8, (b) CNG 60, (c) CNG 150, and (d) CAL 121 91. 13

Figure 7: SEM/EDS for Edwards samples: (a) Set A #1, (b) Set A #7, and (c) Set B # 2. 15

Figure 8: Schematic of the CO_2 and brine leakage model parameters and profiles in the generalized model. 37

Figure 9: Simulated and observed breakthrough curves of pH for the column test of sample CNG60. 41

Figure 10: Major ion modeling results compared to column experiment results. 44

Figure 11: Simulated and observed breakthrough curves of Ca for the column test of sample CNG60. 45

Figure 12: Simulated and observed breakthrough curves of As for the column test of sample CNG60. 46

Figure 13: As modeling results compared to column experiment results and aquifer concentrations. 48

Figure 14: Ba modeling results compared to experimental results and aquifer concentrations. 48

Figure 15: Cr modeling results compared to experimental results and aquifer concentrations. 49

List of Figures (cont.)

Figure 16: Cu modeling results compared to experimental results and aquifer concentrations. 49

Figure 17: Pb modeling results compared to experimental results and aquifer concentrations. Aquifer median concentrations are below detection. 50

Figure 18: Sb modeling results compared to experimental results and aquifer concentrations. Aquifer median concentrations are below detection. 50

Figure 19: Se modeling results compared to experimental results and aquifer concentrations 51

Figure 20: Cross section views of the spatial distribution of pH at 50, 200 years: (a) at y=2,600 m, (b) at x = 2,000 m, and (c) at z = -202.5 m. 55

Figure 21: Cross section views of the spatial distribution of total aqueous benzene concentration at 200 years: (a) at y=2,600 m, (b) at x = 2,000 m, and (c) at z = -202.5 m 56

Figure 22: An iso-surface at benzene concentration of 3.84e-10 mol/L (0.03 µg/L, threshold value). 56

Figure 23: Cross section views of the spatial distribution of total aqueous naphthalene concentration at 200 years: (a) at y=2,600 m, (b) at x = 2,000 m, and (c) at z = -202.5 m. 57

Figure 24: An iso-surface at naphthalene concentration of 1.53e-9 mol/L (0.2 µg/L, threshold value). 57

Figure 25: Cross section views of the spatial distribution of total aqueous phenol concentration at 200 years: (a) at y=2,600 m, (b) at x = 2,000 m, and (c) at z = -202.5 m 58

Figure 26: An iso-surface at naphthalene concentration of 3.19e-11 mol/L (0.003 µg/L, threshold value). 58

Figure 27: Cumulative density function of aquifer volume exceeding organic no-impact thresholds during 200 years of well leakage. 61

List of Tables

Table 1: Initial Aquifer Concentrations Used in the Simulations, Estimated Mean Aquifer Values, and No-Impact Thresholds 6
Table 2: Initial Values, Tolerance Limits, and Regulatory Standards for each Variable 7
Table 3: Aquifer Name Abbreviations 9
Table 4: A Summary of Recent Studies Conducted in Different Aquifers 16
Table 5: Surface Protonation and Complexation Reactions on Goethite 23
Table 6: Surface Protonation and Complexation Reactions on HFO 24
Table 7: Surface Protonation and Complexation Reactions of Cations on Illite 25
Table 8: Surface Protonation and Complexation Reactions of Cations on Kaolinite 26
Table 9: Surface Protonation and Complexation Reactions of Cations on Montmorillonite 27
Table 10: Surface Protonation and Complexation Reactions of Anions on Calcite 28
Table 11: Cation Exchange Reactions and Selectivity Coefficients, Using the Gaines-Thomas Convention 28
Table 12: Compilation of Published Kd for Benzene Between Soil and Water 29
Table 13: K_{oc} (L/kg) for Benzene, Phenol, and Naphthalene 30
Table 14: Degradation Rate Constant (1/day) for Benzene, Phenol, and Naphthalene 31
Table 15: Kinetic Mineral Reactions and Neutral Mechanism Rates for the Edwards Aquifer at 25°C 32
Table 16: Equilibrium Constants of the Major Rock-Forming Minerals for the High Plains Aquifer. 32
Table 17: Kinetic Properties for Minerals Considered in the Model 34
Table 18: Proposed Parameter Ranges for Generalized CO_2 and Brine Leakage Models 37
Table 19: Sodium, Trace Metals and Organics Concentrations Considered in the Groundwater Simulations and ROM. 38
Table 20: Parameter Definition and Ranges for Hydrologic Simulations and Emulations 38
Table 21: Input Parameters of the Development of the Scaling Functions 39
Table 22: Mineral Reactions 42
Table 23: Aqueous Complexation Reactions 43
Table 24: Summary of Column Experiment Trace Metal Concentrations at the End of Each Experimental Stage, Relative to Aquifer Maximum Concentrations and MCL Regulatory Limits 47
Table 25: Organics Concentrations in Brine Considered in the Reactive Transport Model 53
Table 26: Distribution Coefficient and Degradation Constant for Organic Compounds 53

List of Tables (cont.)

Table 27: Flow and Chemical Parameters used in Simulations that Model Results 54
Table 28: Input Parameters for Organic Adsorption and Biodegradation 59
Table 29: Organic Concentration Ranges in Brine 59
Table 30: Initial Values, Tolerance Limits, and Regulatory Standards for Each Variable 60

Acronyms, Abbreviations, and Symbols

Term	Description
3-D	Three-dimensional
BR	Basin and Range basin-fill sand and gravel aquifers
BTEX	Benzene, toluene, ethylbenzene, and xylene-volatile aromatic compounds typically found in petroleum
CEC	Cation exchange capacity
CH_4	Methane
CL	Coastal lowlands sand aquifer system
CO_2	Carbon dioxide
DIC	Dissolved inorganic carbon
EDS	Energy dispersive spectrometry
EMSL	Environmental Molecular Sciences Laboratory
EOR	Enhanced oil recovery
EPA	U.S. Environmental Protection Agency
Eu	NRAP Edwards shallow, urban carbonate-rock aquifer
F	Floridan carbonate-rock aquifer system
Gc	Central glacial sand and gravel aquifers
GCS	Geological carbon sequestration
HBSL	USGS Health-Based Screening Levels
HFO	Hydrous ferric oxide
HP	NRAP High Plains sand and gravel aquifer
LBNL	Lawrence Berkley National Laboratory
LLNL	Lawrence Livermore National Laboratory
LT	Lower Tertiary and Upper Cretaceous sandstone aquifers
M	Mississippian sandstone and carbonate-rock aquifers
MCL	Maximum contaminant levels
MSU-ZERT	Montana State University-Zero Emission Research and Technology site
NAWQA	USGS National Water-Quality Assessment
NEx	New England crystalline-rock aquifers
NRAP	National Risk Assessment Partnership
PAH	Poly-aromatic hydrocarbons
PCA	Principal component analysis
PNNL	Pacific Northwest National Laboratory

Acronyms, Abbreviations, Symbols (cont.)

Term	Description
QXRD	Quantitative X-ray diffraction analyses
ROM	Reduced-order model
SACROC	Scurry Area Canyon Reef Operators Committee
SCM	Surface complexation model
SEM	Scanning electron microscope
SGW	Synthetic groundwater
SPb	Snake River Plain basaltic-rock aquifers
TDS	Total dissolved solids
USGS	U.S. Geological Survey

Acknowledgments

This work was completed as part of the National Risk Assessment Partnership (NRAP) project. Support for this project came from the U.S. Department of Energy's (DOE) Office of Fossil Energy's Crosscutting Research program. The authors wish to acknowledge Traci Rodosta (Carbon Storage Technology Manager), Kanwal Majajan (Carbon Storage Division Director), M. Kylee Rice (Project Manager), Mark Ackiewicz (Division of CCS Research - Program Manager), Susan Maley and Steve Seachman (NETL Strategic Center for Coal), and Regis Conrad (DOE Office of Fossil Energy) for programmatic guidance, direction, and support.

The authors also wish to acknowledge Bruce Arey and Mark Bowden who conducted the quantitative X-ray diffraction analyses (QXRD) analyses and scanning electron microscope/ energy dispersive spectrometry (SEM/EDS) inspections performed in the Environmental Molecular Sciences Laboratory (EMSL), a national scientific user facility sponsored by the U.S. DOE's Office of Biological and Environmental Research and located at PNNL. The authors also wish to acknowledge Keith Geiszler, Steven Baum, and Ian Leavy for laboratory analysis and Heather Culley for editorial assistance.

This page intentionally left blank

ABSTRACT

This report is a summary of modeling efforts, in combination with laboratory batch and column experiments and a review of current literature, undertaken to determine the effect of carbon dioxide (CO_2) and brine leakage from deep storage reservoirs on the quality of overlying groundwater aquifers. For two aquifer types (i.e., carbonate and unconsolidated sand and gravel aquifers), "no-impact" thresholds were determined to evaluate the results of the laboratory and modeling.

Modeling and laboratory results emphasized the importance of site-specific data and analysis for determining potential impacts of CO_2 and brine intrusion into overlying groundwater aquifers. "No-impact" thresholds were variable between the two studied sites, and were mostly more conservative than the U.S. Environmental Protection Agency (EPA) maximum contaminant levels (MCLs). The aquifer calcite and clay content, as well as the storage reservoir salinity and organic and trace metals contents are all crucial site-specific data that must be collected for successful evaluation by the developed models. Using these inputs, the site-specific reduced-order models (ROMS) were able to predict aquifer response and the degree of impact due to leaking CO_2. Results have indicated that the risk to aquifers is site-specific, and directly proportional to the mass of CO_2 or brine leaked.

Several questions remain unanswered, in particular, related to aquifer recovery time, partitioning of organic matter between phases, and the limitations of existing ROMs to infinite buffering capacity, requiring further investigation to enhance understanding of the impact of leaking CO_2 and brine on groundwater aquifers.

1. INTRODUCTION

Geological carbon sequestration (GCS) is a global carbon emission reduction strategy involving the capture of carbon dioxide (CO_2) emitted from fossil fuel burning power plants, as well as the subsequent injection of the captured CO_2 gas into deep saline aquifers or depleted oil and gas reservoirs. A critical question that arises from the proposed GCS is the potential impacts of CO_2 injection on the quality of drinking-water systems overlying CO_2 sequestration storage sites.

Although storage reservoirs are evaluated and selected based on their ability to safely and securely store emplaced fluids, leakage of CO_2 from storage reservoirs is a primary risk factor and potential barrier to the widespread acceptance of geologic CO_2 sequestration (Harvey et al., 2013; Jun et al., 2013; DOE, 2007). Therefore, a systematic understanding of how CO_2 leakage would affect the geochemistry of potable aquifers, and subsequently control or affect elemental and contaminant release via sequential and/or simultaneous abiotic and biotic processes and reactions is vital.

Two possible scenarios for CO_2 leakage have been identified: a sudden, fast, and short-lived release of CO_2, as seen in the case of a well failure during injection or a sudden blowout (Holloway et al., 2007; Jordan and Benson, 2009; Skinner, 2003), or a slower, more gradual leak, occurring along undetected faults, fractures, or well linings (Annunziatellis et al., 2008; Bachu, 2008; Celia and Nordbotten, 2009; Damen et al., 2005; Lewicki et al., 2007; Nordbotten et al., 2005; Scherer et al., 2011); however, well related leaks appear to be declining thanks to improved construction and operation (Newmark et al., 2010).

Upon entering an aquifer, a portion of the CO_2 gas will dissolve into the groundwater, which will cause a subsequent decrease in aqueous pH (Trautz et al., 2013) due to the formation and disassociation of carbonic acid (Harvey et al., 2013). The reduced pH can then cause an increase in the mobilization of major (Ca, Mg, K, Na, etc.) and minor (Fe, Al, Ba, etc.) elements as well as potential contaminants via desorption and/or dissolution reactions. Changes in other water quality parameters, such as alkalinity, salinity, and total dissolved solids (TDS), may also occur.

Properties of the aquifer and the network of processes and reactions may also impact a system's behavior and response, and may also have an impact on potential risks associated with CO_2 sequestration. Brine can be brought upward into an overlying groundwater aquifer with increased pressure due to CO_2 injection (Oldenburg and Rinaldi, 2011). Salinity of the brine, as well as presence of contaminants, such as and Cd, can vary and can increase negative effects of CO_2 leakage.

Over the last decade, a number of studies have been undertaken to assess the impacts of potential CO_2 leakage from deep storage reservoirs on the quality of overlying freshwater aquifers. These studies include natural analogs (Caritat et al., 2013; Lewicki et al., 2007; Keating et al., 2010), field in-situ CO_2 injection (Kharaka et al., 2010b; Nisi et al., 2013; Peter et al., 2012; Smyth et al., 2009; Trautz et al., 2013), and experimental column and batch studies (Humez et al., 2013; Little and Jackson, 2010; Lu et al., 2010; Montes-Hernandez et al., 2013; Wang et al., 2016; Wei et al., 2011). However, the results of the studies are contradictory as some indicate CO_2 leaks pose a serious risk (Cahill et al., 2013; Kharaka et al., 2010b; Little and Jackson, 2010; Lu et al., 2010; Wang and Jaffe, 2004; Wei et al., 2011; Zheng et al., 2009; Vong et al., 2011), some indicate low levels of risk (Frye et al., 2012; Kirsch et al., 2014; Mickler et al., 2013; Keating et al., 2010), and others have found some possible benefits (such as the removal of As, U, V, and Cr) related to CO_2 leakage into groundwater (Lu et al., 2010; Smyth et al., 2009). Clearly, the

scientific community has not yet reached an agreement on the important issue of deciding whether the impacts from the leakage of CO_2 into groundwater are negative, insignificant, or positive.

This report summarizes data and findings that are already published in the literature over the last several years. In addition, a summary of the results collected over the last four years from batch and column experiments conducted at the Pacific Northwest National Laboratory (PNNL) and the associated modeling efforts conducted at PNNL and Lawrence Berkley National Laboratory (LBNL) will be presented and discussed.

The experiments were conducted with materials from two representative aquifer types that commonly overlie potential CO_2 sequestration reservoirs: the Edwards Aquifer in Texas, representative of unconfined limestone aquifers, and the High Plains Aquifer in Kansas, representative of typical unconsolidated sand and gravel aquifers. Column experiments in which CO_2 charged synthetic groundwater flows through a column packed with material from the aquifers were conducted to simulate the impact of a gradual leak of CO_2 on a shallow aquifer. Batch experiments were conducted to simulate sudden, short-lived CO_2 release. A reactive transport model was then developed using solid phase characterization data of the aquifer materials to interpret the observed concentration changes in the effluent water, attempting to shed light on the chemical reactions, water-rock interaction mechanisms, and key parameters that control the concentration changes of some constituents.

Although the effects of water-rock interactions may be site-specific, the results from the experimental and modeling efforts will help in developing a systematic understanding of how CO_2 leakage is likely to influence pertinent geochemical processes (e.g., dissolution/precipitation, sorption/desorption). A three-dimensional (3-D) multiphase flow and reactive transport simulation of CO_2 leakage from an abandoned wellbore into a generalized model of the shallow, unconfined portion of the Edwards Aquifer was also developed to determine potential impacts on groundwater quality.

In addition to the work that focused on aquifer composition, further experiments have been conducted to observe the effects of gaseous impurities and inorganic contaminants on aquifer response. Specifically, methane (CH_4), present with CO_2, was used to represent possible impurities in the gas stream. Additionally, As and Cd spikes were added to the synthetic groundwater used in batch and column experiments based on the maximum As and Cd levels predicted to reach the aquifer from the brine source term within the reservoir, according to modeling simulations by Bacon (2013). Supplementary experiments were performed to investigate the effect of autotrophic methanogenesis, stimulated by CO_2, on the mobility of metals. Collectively, these tests were conducted to study the effect of gas, trace metal, and biological variations likely to be found in GCS sites.

2. OBJECTIVES

The objectives of this report are to:

- Identify the set of geochemical data required to assess and predict aquifer responses to CO_2 and brine leakage
- Present and discuss potential risks for groundwater degradation due to CO_2 gas and brine exposure

Specifically, this report will discuss the following issues:

- Aquifer responses:
    - Changes in aqueous phase (groundwater) chemical composition
    - Changes in solid phase chemistry and mineralogy
    - Changes in the extent and rate of reactions and processes and possible establishment of a new network of reactions and processes affecting or controlling overall mobility of major, minor, and trace elements
    - Development of conceptual and reduced-order models (ROMs) to describe and predict aquifer responses
- The degree of impact:
    - Significant or insignificant changes in pH and major, minor, and trace element release that depend on the following controlling variables:
        - Leaking plume characteristics
            - Gas composition (pure CO_2, CO_2 -CH_4 -H_2S mixtures)
            - Brine concentration and composition (trace metals)
        - Aquifer properties:
            - Initial aqueous phase conditions
            - Mineralogy: minerals controlling sediments' response (e.g., calcite, Si bearing minerals, etc.)
- Overview of relevant hydrogeological and geochemical processes related to the impact of CO_2 gas and brine on groundwater quality
- The fate of the elements released from sediments or transported with brine:
    - Precipitation/incorporation into minerals (calcite and other minerals)
    - Adsorption
    - Electron transfer reactions
    - The role of natural attenuation
- Whether or not the release of metals following exposure to CO_2 harmful
    - Risk assessment.

3. GEOCHEMICAL DATA REQUIRED TO ASSESS AND PREDICT AQUIFER RESPONSES TO CO_2 AND BRINE LEAKAGE

3.1 THRESHOLD VALUES AND AVERAGE GROUNDWATER CONCENTRATIONS

In order to determine whether CO_2 and brine leakage has an impact on groundwater quality, a protocol was established for determining statistically significant changes in groundwater concentrations of regulated contaminants (Last et al., 2013). The effort examined selected portions of two aquifer systems: the urban shallow-unconfined aquifer system of the Edwards-Trinity Aquifer System (being used to develop the ROM for carbon-rock aquifers), and a portion of the High Plains Aquifer (an unconsolidated and semi-consolidated sand and gravel aquifer being used to develop the ROM for unconsolidated aquifers).

No-impact threshold values were determined for cadmium, lead, arsenic, pH, TDS, and select organic compounds that could be used to identify potential areas of contamination predicted by numerical models of carbon sequestration storage reservoirs. No-impact threshold values were later determined for chromium specifically to support the ROM being developed by Lawrence Livermore National Laboratory (LLNL) for the High Plains Aquifer. These threshold values are based on an interwell approach for determining background groundwater concentrations as recommended in the U.S. Environmental Protection Agency's (EPA, 2009) document titled, "Unified Guidance for Statistical Analysis of Groundwater Monitoring Data at RCRA Facilities".

The resulting no-impact threshold values can be used to inform a "no change" scenario with respect to groundwater impacts, rather than use a maximum concentration limit or secondary drinking-water standard that in some cases could be significantly higher than existing concentrations in the aquifer. These no-impact threshold values are intended for use in helping to predict areas of potential impact. They are not intended for use as alternate regulatory limits.

Development of "generic" no-impact threshold values that could be used for a number of locations appears unlikely. Instead, the threshold values must be based on site-specific groundwater quality data. However, the scarcity of existing data, proximity of the data to the target model domain, potential spatial heterogeneity, and temporal trends make the development of statistically robust data sets and the use of valid statistical assumptions challenging. In some cases, the calculated no-impact threshold values may exceed regulatory standards. Other approaches, such as the hybrid intrawell-interwell approach also examined in the study by Last et al. (2013), may provide alternate mechanisms for calculating no-impact threshold limits. Examples are presented in the following sections to demonstrate the development and use of threshold values in two representative aquifers.

3.1.1 High Plains Aquifer

The hydrology ROMs and chemical scaling functions generated in the third-generation ROM are specific to thresholds that represent no net degradation to the groundwater quality. The impact thresholds defined for pH, TDS, trace metals, and select organics in Table 1 represent concentrations above (or below for pH) the background water chemistry that could be used to assess impact from brine and/or CO_2 leakage into the aquifer. Each threshold was calculated as the 95%-confidence, 95%-coverage tolerance from data collected in a 2010 U.S. Geological

Survey (USGS) groundwater survey of 30 wells within the High Plains Aquifer from an area outside of the lithology model site.

This dataset was chosen because spatial and temporal data were not available from wells located within the model domain. This study considered benzene, naphthalene, and phenol as representative of benzene, toluene, ethylbenzene, and xylene-volatile aromatic compounds typically found in petroleum (BTEX), poly-aromatic hydrocarbons (PAH), and phenol organic compounds that could be present in the leaking brine (Zheng et al., 2010). Table 1 also includes regulatory standards referring to concentrations that exceed primary or secondary maximum contaminant levels designated by the U.S. EPA (2009). Primary drinking-water standards are for trace metals, such as, Ba, Cd, Cr, Cu, Pb, and BTEX organics among others, and are legally enforced for the protection of public health by limiting the levels of contaminants in drinking water. Secondary drinking-water standards are for elements such as Fe, Mn, and Zn. Usually, they are non-enforceable guidelines regulating contaminants that may cause cosmetic or aesthetic effects in drinking water. Currently PAHs and phenols are unregulated.

Table 1: Initial Aquifer Concentrations Used in the Simulations, Estimated Mean Aquifer Values, and No-Impact Thresholds

Parameter	Initial Value Used in Third-Generation Simulations	Mean of Selected and Adjusted 2010 Data[b]	"No-Impact" Threshold[c]	U.S. EPA Regulatory Standard
pH	7.6[a]	7.5[c]	7.0	6.5
TDS	570 mg/L[a,d]	440 mg/L[d]	1,300 mg/L[d,e]	500 mg/L[e]
Arsenic	1.50 µg/L	1.50 µg/L	9.30 µg/L	10.00 µg/L
Barium	43.00 µg/L[b]	43.00 µg/L[b]	140.00 µg/L	2,000 µg/L
Cadmium	0.06 µg/L	0.06 µg/L	0.25 µg/L	5 µg/L
Chromium	1.00 µg/L	1.00 µg/L	3.90 µg/L	100 µg/L
Iron	5.40 µg/L[b]	5.40 µg/L[b]	43.00 µg/L[b]	300 µg/L
Lead	0.09 µg/L	0.09 µg/L	0.63 µg/L	15 µg/L
Manganese	0.35 µg/L[d]	0.35 µg/L[d]	7.00 µg/L[d]	50 µg/L
Benzene	0	<0.03 µg/L[d]	0.03 µg/L[g]	5 µg/L
Naphthalene	0	<0.20 µg/L[d]	0.20 µg/L[g]	700 µg/L
Phenol	0	<0.003 µg/L[f]	0.003 µg/L[g]	10,000 µg/L[h]

(a) Based on Carroll et al. (2009)
(b) Geometric mean except for pH
(c) 95%-confidence, 95%-coverage tolerance limit based on log values except for pH
(d) Rounded to two significant digits
(e) Threshold value exceeds regulatory standard; using the regulatory standard may result in widespread false positives under field conditions
(f) As 4-Chloro-2-methylphenol
(g) Detection limit for the 2010 U.S. Geologic Survey National Water-Quality Assessment Program (NAWQA) sample data
(h) Recommended Water Quality Criteria for Human Health, consumption of Water + Organism (74 FR 27535); http://water.epa.gov/scitech/swguidance/standards/criteria/current/index.cfm#hhtable.

3.1.2 Edwards Aquifer

As part of the USGS National Water-Quality Assessment (NAWQA) Program, the USGS collected and analyzed groundwater samples from 1996 to 2006 from the San Antonio segment of the Edwards Aquifer of central Texas, a productive karst aquifer developed in Cretaceous-age carbonate rocks (Musgrove et al., 2010). The National Water-Quality Assessment Program studies provide an extensive dataset of groundwater geochemistry and water quality, consisting of 249 groundwater samples collected from 136 sites (wells and springs), including: 1) wells completed in the shallow, unconfined, and urbanized part of the aquifer in the vicinity of San Antonio (shallow/urban unconfined category); 2) wells completed in the unconfined (outcrop area) part of the regional aquifer (unconfined category); and 3) wells completed in springs discharging from the confined part of the regional aquifer (confined category).

Ninety water samples from the shallow, unconfined portion of the Edwards Aquifer in Texas (Musgrove et al., 2010) were used to examine methodologies for establishing baseline data sets and statistical protocols for determining statistically significant changes between background concentrations and predicted concentrations that would be used to represent a contamination plume in the modeling presented in this report (Last et al., 2013). No-impact threshold values were determined for As, Ba, Cd, Pb, benzene, naphthalene, phenol, pH, and TDS that could be used to identify potential areas of contamination predicted by numerical models of carbon sequestration storage reservoirs (Table 2). Initial values of these concentrations were also determined using selected statistical methods. For comparison, the EPA maximum contaminant levels (MCLs) are also shown in Table 2.

Table 2: Initial Values, Tolerance Limits, and Regulatory Standards for each Variable

Analyte	Initial Value	"No-Impact" Threshold	Maximum Contaminant Level	Units
Arsenic	0.31	0.55	10	µg/L
Barium	38	54	2000	µg/L
Cadmium	0	0.04	5	µg/L
Lead	0.064	0.15	15	µg/L
Benzene	0	0.016	5	µg/L
Naphthalene	0	0.4	0.20	µg/L
Phenol	0	0.005	10000	µg/L
pH	6.9	6.6	6.5	$-\log[H^+]$
TDS	330	420	500	mg/L

3.1.3 Other Aquifers

As part of the NAWQA Program, water samples were collected during 1991–2004 from domestic wells (private wells used for household drinking water) across the United States (U.S.) for analysis of drinking-water contaminants, where contaminants are considered, as defined by the Safe Drinking Water Act, to be all substances in water. The concentrations of major ions, trace elements, nutrients, radon, and organic compounds (pesticides and volatile organic compounds) were measured in as many as 2,167 wells. The wells were located within major hydrogeologic settings of 30 regionally extensive aquifers used for water supply in the U.S. One sample was collected from each well prior to any in-home treatment. Concentrations were compared to water quality benchmarks for human health, either EPA MCLs for public water supplies or USGS Health-Based Screening Levels (HBSLs).

Measurements of pH, TDS, and selected trace metals and organic compounds for eight aquifers were compared to the High Plains and Edwards Aquifers considered in the National Risk Assessment Partnership (NRAP) studies. To simplify comparison, abbreviations for the aquifer names are listed in Table 3. Median and 90th percentile values (10th percentile for pH) reported in DeSimone (2009) are compared to the initial and no-impact threshold values for the NRAP study aquifers.

All of the aquifers have median pH values ranging from 6.8 to 8.1 (Figure 1). Only two aquifers have 10th percentile values that are less than the regulatory limit of 6.5: the Coastal Lowlands sand aquifer (5.1) and New England crystalline-rock aquifer (5.9).

All of the aquifers have median TDS values less than the regulatory limit of 500 mg/L, with the exception of the Lower Tertiary and Upper Cretaceous sandstone aquifers (Figure 2). However, many have 90th percentile values above the regulatory limit, with some above 1,000 mg/L (HP, BR, LT).

All of the aquifers have median As concentrations less than the regulatory limit of 10 µg/L (Figure 3), but many have 90th percentile values above the regulatory limit (BR, GC, M, SPb, and NEx). All of the aquifers have median and 90th percentile Ba concentrations below the regulatory limit of 2,000 µg/L (Figure 4). Most aquifers have undetectable levels of Cd, and so the 90th percentile values are set to the detection limit. All of the aquifers have very low median concentrations of Pb (Figure 5) and most have 90th percentile concentrations of less than 1, well below the regulatory limit of 15 µg/L.

Only summary data for benzene, naphthalene, and phenol were provided in DeSimone (2009). Benzene was detected (> 0.2 µg/L) in 2 out of 1,948 samples. Naphthalene was detected (> 0.2 µg/L) in 2 out of 1,928 samples. Phenol was not detected (> 0.2 µg/L) in any of the 919 samples analyzed. This indicates that these organic compounds are not normally present in drinking-water aquifers, except due to contamination.

Table 3: Aquifer Name Abbreviations

Abbreviation	Description
HP	NRAP High Plains sand and gravel aquifer
Eu	NRAP Edwards shallow, urban carbonate-rock aquifer
BR	Basin and Range basin-fill sand and gravel aquifers
Gc	Central glacial sand and gravel aquifers
CL	Coastal lowlands sand aquifer system
LT	Lower Tertiary and Upper Cretaceous sandstone aquifers
M	Mississippian sandstone and carbonate-rock aquifers
F	Floridan carbonate-rock aquifer system
SPb	Snake River Plain basaltic-rock aquifers
NEx	New England crystalline-rock aquifers

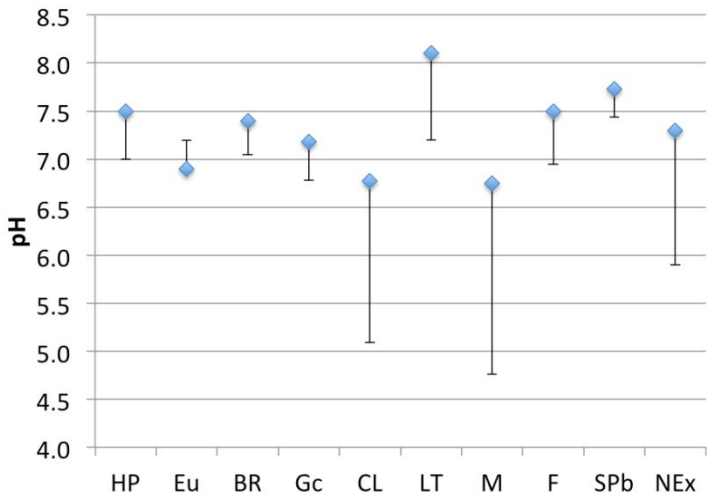

Figure 1: Comparison of background values of pH for the High Plains Aquifer and shallow, urban unconfined portion of the Edwards Aquifer used in NRAP studies with ranges for various aquifer types in the U.S. Symbols represent median value and error bars the 10th percentile.

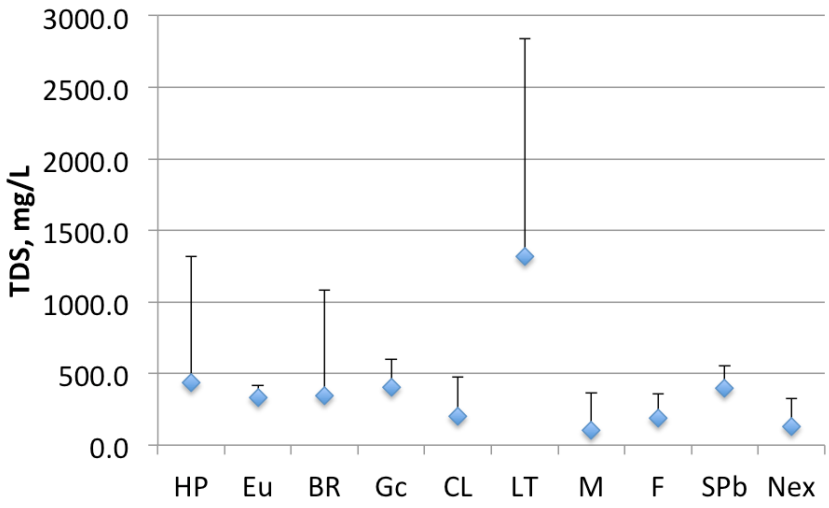

Figure 2: Comparison of background values of TDS for the High Plains Aquifer and shallow, urban unconfined portion of the Edwards Aquifer used in NRAP studies with ranges for various aquifer types in the U.S. Symbols represent median value and error bars the 90th percentile.

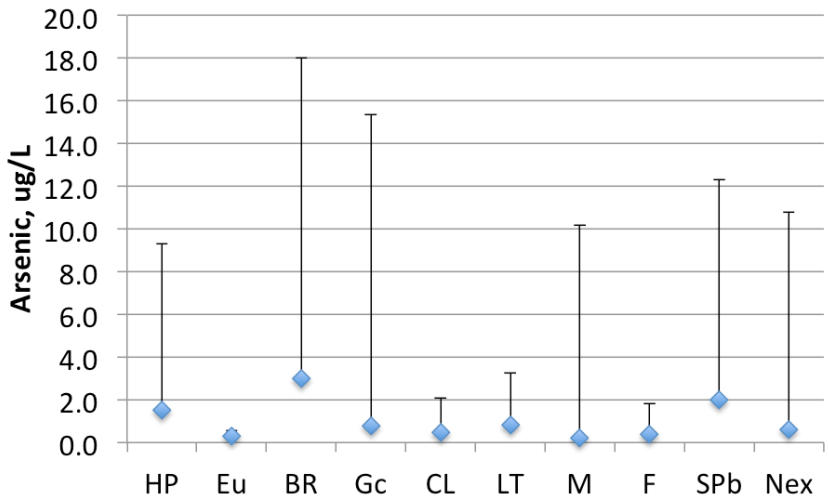

Figure 3: Comparison of background values of Arsenic for the High Plains Aquifer and shallow, urban unconfined portion of the Edwards Aquifer used in NRAP studies with ranges for various aquifer types in the U.S. Symbols represent median value and error bars the 90th percentile.

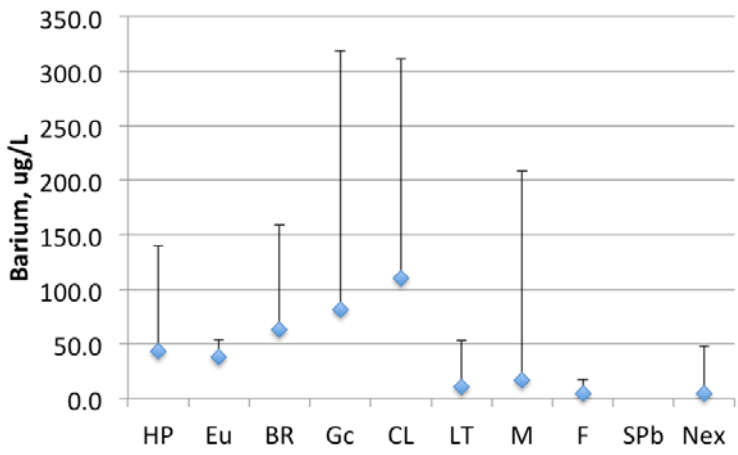

Figure 4: Comparison of background values of Barium for the High Plains Aquifer and shallow, urban unconfined portion of the Edwards Aquifer used in NRAP studies with ranges for various aquifer types in the U.S. Symbols represent median value and error bars the 90th percentile.

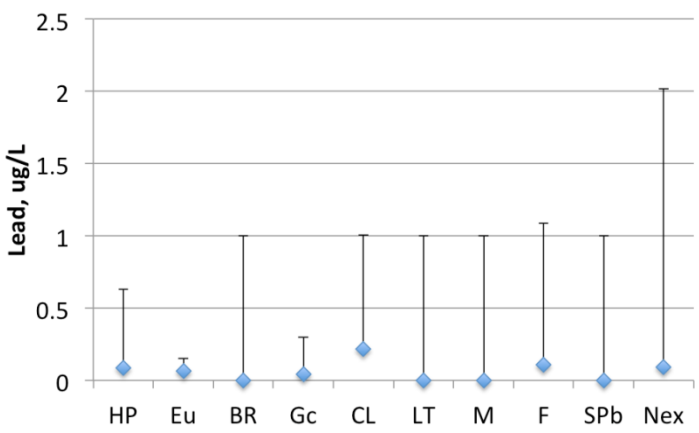

Figure 5: Comparison of background values of Lead for the High Plains Aquifer and shallow, urban unconfined portion of the Edwards Aquifer used in NRAP studies with ranges for various aquifer types in the U.S. Symbols represent median value and error bars the 90th percentile.

3.2 SOLID PHASE PROPERTIES: MINERALOGY

Mineralogical properties of the aquifer are important determinants of the way the aquifer will respond to the exposure of leaking CO_2 (and other gases) and brine from the deep subsurface reservoirs. The mineralogy of two representative aquifers was studied and a summary of the results is presented below.

3.2.1 High Plains Aquifer

The mineralogy of the High Plains Aquifer was determined in a set of samples obtained from the Kansas Geological Survey. These sediment samples were used in a series of batch and column experiments (Qafoku et al., 2013). The sediments originated from three different wells (named CNG [latitude 37.0635, longitude -101.7193], CAL 121 [latitude 37.7736, longitude 100.8187], and CAL 122 [latitude 37.7368, longitude 100.7588]), all located in the central High Plains Aquifer area in Kansas. Four of the samples came from well CNG (CNG 8, CNG 60, CNG 110, and CNG 150), two samples came from well CAL 121 (CAL 121 150 and CAL 121 91), and two samples came from well CAL 122 (CAL 122 4 and CAL 122 29).

Sediment samples from Kansas were received as loose, sandy materials. Texture determination found the samples of the CAL well were classified as “sand” while the samples from the CNG well were classified as a “sandy loam” (CNG-8) and “loamy sand” (CNG 60 and CNG 110).

Quantitative X-ray diffraction analyses (QXRD) showed that calcite contents of the sediments varied from zero to ~4% (Qafoku et al., 2013). QXRD results also showed that the sediments contained appreciable amounts of feldspars, montmorillonite, quartz, and mica. QXRD analysis of the silt and clay fractions separated from these sediments confirm the presence of small amounts of carbonate minerals (calcite and/or dolomite) in all samples except one (Shao et al., 2015). This is important because small-sized calcite particles undergo fast dissolution after sediment exposure to CO_2 gas, buffering the pH of the aqueous phase.

In addition to the QXRD analyses, a series of scanning electron microscope (SEM) inspections and energy dispersive spectrometry (EDS) measurements were performed to characterize the morphology of the mineral particles and determine their chemical composition (Figure 6). EDS results showed a low amount of Ca and high concentration of Si for CNG 60. The SEM images showed the samples had rough surfaces (i.e., a high reactive surface area and potentially high adsorption and dissolution rates). EDS results, in agreement with previous QXRD data, suggested the presence of feldspars and/or micas in the High Plains Aquifer CNG sediments. Additional SEM/EDS related analyses and figures are presented in Shao et al. (2015), Lawter et al. (2015), and Lawter et al. (2016).

Microwave digestion analyses were conducted to determine the elemental composition of the aquifer sediments. In addition, 8M nitric acid extractions were conducted to determine the identity of different inorganic elements and potential contaminants that may be released from the sediments during CO_2 injection. The results indicate that the solid phase of the sediments contains varied amounts of trace metals that are of environmental concern, such as, Ba, Cd, Cr, and Pb, which are regulated with primary MCLs; and Fe, Mn, and Zn, which are regulated with secondary MCLs. Potentially, appreciable amounts of several contaminants (e.g., As) could be released from the sediments when contacted with CO_2 saturated groundwater (Shao et al., 2015; Qafoku et al., 2013).

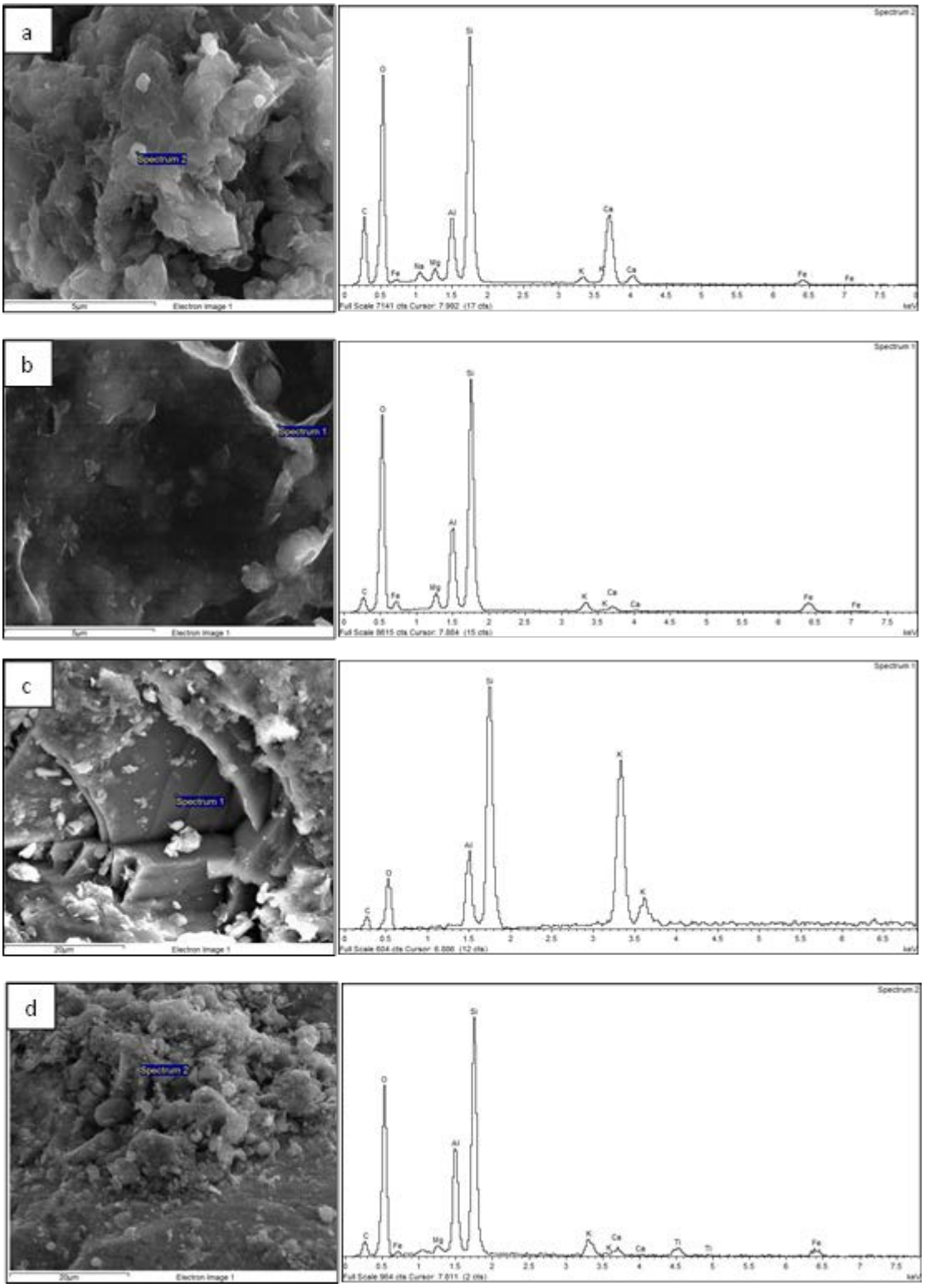

Figure 6: SEM/EDS for (a) CNG 8, (b) CNG 60, (c) CNG 150, and (d) CAL 121 91.

3.2.2 Edwards Aquifer

Two sets (of seven samples each) from the unconfined section of the Edwards Aquifer were used in a series of batch and column experiments; they are referred to as Set A (weathered rock) and Set B (unweathered rock). The samples were received as mostly large rocks, but were ground to <2 mm before use in experiments and characterization. XRD analyses conducted on the Edwards Aquifer showed samples from Set B were exclusively dominated by calcite, while samples from Set A (weathered rock) were dominated by calcite, but also contained quartz and montmorillonite.

SEM micrographs and EDS chemical analysis measurements were used to describe the morphology of calcite, the predominant mineral in these samples, and to locate other minerals determined by XRD. For example, calcite and quartz were both present in the relatively weathered rocks (Set A). The rough surfaces of calcite explain the fast rate of dissolution observed in batch experiments in response to CO_2 gas exposure.

Phyllosilicates were also located in weathered samples (in one location, a 2:1 concentration ratio for Al and Si was found, which is a typical ratio for 2:1 phyllosilicates and montmorillonite). SEM and EDS results for Sample 2 from Set B (which is a representative of the unweathered rock samples) found only calcite (Figure 7). Additional information and figures related to the SEM/EDS analyses are presented in recent papers published by the NRAP group at PNNL and LBNL (Wang et al., 2016; Bacon et al., 2016).

As with the High Plains sediments, 8 M nitric acid extractions were conducted on the Edwards Aquifer sediments. The main objective for conducting the 8 M acid extractions was to understand the types of potential contaminants present in the sediments, which may (or may not) be mobilized when these solid materials are exposed to a CO_2 gas stream or CO_2 saturated synthetic groundwater (SGW). Results of these extractions show the materials contained potentially releasable contaminants, including As, Cd, Cr, Pb, and Zn (Qafoku et al., 2013).

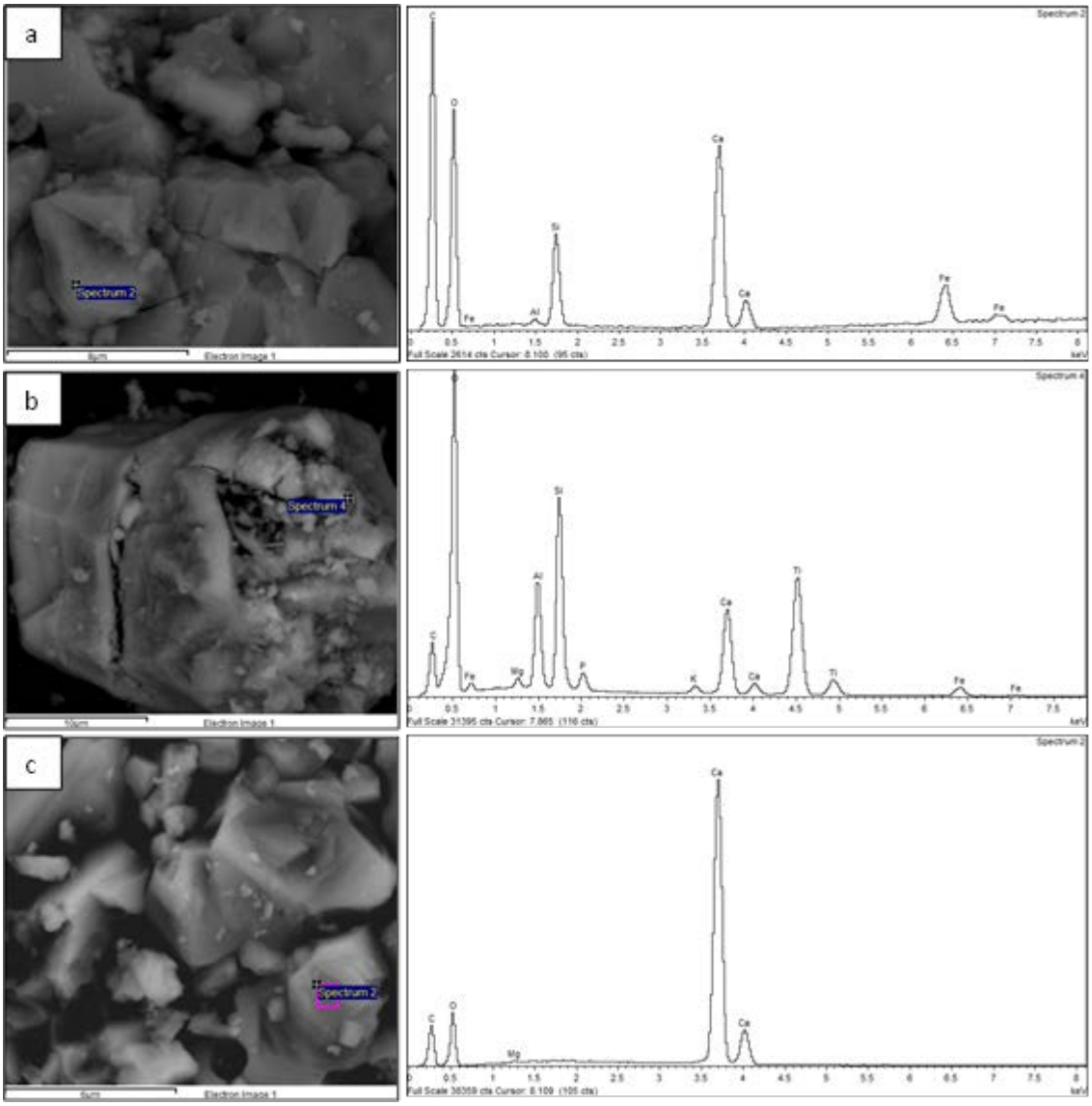

Figure 7: SEM/EDS for Edwards samples: (a) Set A #1, (b) Set A #7, and (c) Set B # 2.

3.3 OTHER AQUIFERS

Several other sites have been studied, such as the Montana State University-Zero Emission Research and Technology site (MSU-ZERT, Bozeman, MT), a natural analog site in Chimayo, NM, and Scurry Area Canyon Reef Operators Committee (SACROC) oil field in Scurry County, TX. The sites studied most extensively are all sandstone or unconsolidated sand and gravel aquifers; carbonate aquifers have received much less attention, although the abundance of carbonate aquifers and specific concerns related to these sites make carbonate sites important.

The importance of mineralogy (and especially calcite content) in the sediment is clearly stated in recent studies (Frye et al., 2012; Wunsch et al., 2014; Wunsch et al., 2013; Cahill and Jakobsen, 2013; Little and Jackson, 2010; Lu et al., 2010; Keating et al., 2010). On one side, calcite may buffer the pH of the aquifer, decreasing the extent of mineral dissolution and release of

contaminants. For example, in a column study conducted with artificial lake and river sediments (created by mixing purchased calcite, quartz sand, and illite minerals), Frye et al. (2012) observed that the mineralogical properties of aquifer materials significantly influenced the response of groundwater quality to the intrusion of CO_2. They found that calcite content as low as 10% can mitigate the effect of pH reduction and may result in zero Cd desorption from Cd laden illite (Frye et al., 2012). Studies also show that carbonates buffer the system to avoid further decreases in pH (Cahill et al., 2013; Little and Jackson, 2010). In an analog study conducted in New Mexico, Keating et al. (2010) reported that despite relatively high levels of dissolved CO_2, trace element mobility was not significant due to the high buffering capacity of the groundwater aquifer they studied.

On the other side, Kirsch et al. (2014) found that the contaminants released in their laboratory experiment were directly correlated with calcite dissolution, leading them to conclude that calcite dissolution is the source of the contaminants. A batch experiment conducted by Lu et al. (2010) also suggests aquifers containing carbonate rocks are of particular concern due to the presence of Ba, Mn, and Sr in carbonates, in addition to increased alkalinity which followed carbonate dissolution. A summary of additional sites that have been subject to recent investigations is presented in Table 4.

Table 4: A Summary of Recent Studies Conducted in Different Aquifers

Project Site	Paper	Details/Results
ZERT- Food grade CO_2 injected 1–2 m below the water table for 30 days at MSU-ZERT in Bozeman, MT	(Viswanathan et al., 2012)	PCA (principal component analysis) of the 80 water samples mentioned below; used to simulate the processes responsible for increased dissolved constituents using a multicomponent reaction path model
	(Apps et al., 2011)	Water samples taken before, during and after injection; geochemical model used to simulate processes likely to be responsible for dissolved constituents
	(Kharaka et al., 2010b)	Field study: collected 80 water samples from the site before/during/after injection. Rapid and systematic changes in pH, alk, Ec; major increases in Ca, Mg, Fe and Mn, CO_2 caused increase of BTEX, metals, lower pH, and other solutes; significantly below MCLs
High Plains:		
Ogallala aquifer, TX (Southern High Plains)	(Little and Jackson, 2010)	Lab experiments; compared results with materials from aquifers in MD/VA and IL; Al, Mn, Fe, Zn, Cd, Se, Ba, Tl, and U approached or exceeded MCLs
Central High Plains	(Lawter et al., 2015)	Batch and column (lab) studies using HP sediments and SGW
	(Zheng et al., 2016)	Modeling done to determine likely processes controlling geochemical changes observed in Lawter et al. (2015)

Table 4: A Summary of Recent Studies Conducted in Different Aquifers (cont.)

Project Site	Paper	Details/Results
	(Shao et al., 2015)	Laboratory column and batch studies using As/Cd spiked SGW
	(Lawter et al., 2016)	Laboratory batch and column studies using 1% CH_4 and As/Cd spiked SGW
	(Carroll et al., 2014)	Model simulated CO_2 leakage to predict plume size, potential impacts, detection, time scale, and "no-impact" thresholds
Chimayo, NM- natural analog site (field study)	(Keating et al., 2013)	A 3-D reactive transport model which captures the essential geochemical reactions that control CO_2/aquifer interactions at the site and which may determine trace metal concentrations
	(Keating et al., 2013)	Compared to Springerville, AZ where CO_2 leaks through brine but salinity is not increased; in Chimayo, salinity is significantly increased. Used multiphase transport simulations to show which conditions favor increased salinity
	(Keating et al., 2010)	Found high levels of CO_2 did not have a major effect on pH or trace metal mobility, but the addition of brakish waters did have a major effect on the aquifer
Springerville, AZ	(Keating et al., 2014)	Site also studied in some Chimayo, NM papers, this paper found dissolved CO_2 upward movement was much greater than buoyant free gas movement
SACROC- 35 year CO_2 enhanced oil recovery site sitting under Dockum aquifer in TX (sandstone and conglomerate)	(Romanak et al., 2012)	Geochemical characterization of Dockum aquifer followed by hypothetical leakage model
	(Smyth et al., 2009)	Also studied Cranfield, MS EOR site. Laboratory batch experiments were conducted, then field studies to see if any CO_2 might have been leaking (no degradation of water sources was identified)
Edwards	(Carroll et al., 2014)	Model simulated CO_2 leakage to predict plume size, potential impacts, detection, time scale, and "no-impact" thresholds
	(Bacon et al., 2016)	Modeling of the results from the batch and column studies presented in the paper by Wang et al. (2016)
	(Wang et al., 2016)	Edwards Aquifer batch and column studies conducted (lab)

Table 4: A Summary of Recent Studies Conducted in Different Aquifers (cont.)

Project Site	Paper	Details/Results
	(Qafoku et al., 2013)	PNNL report covering Edwards and High Plains batch and column studies conducted during or before 2013
Frio Formation, TX		
Saline sandstone aquifer	(Kharaka et al., 2006a; Kharaka et al., 2006b)	Study of changes to the reservoir brine after CO_2 injection in a saline storage reservoir. Rapid changes in pH and carbonate dissolution suggest conditions that may create pathways upward into overlying aquifers
	(Kharaka et al., 2009)	Monitoring was done to observe migration of injected CO_2 from the lower Frio formation into a section 15 m above the injection section 6 months after injection. However, 15 months after injection found no additional CO_2 in the upper Frio formation and no CO_2 leakage was detectable in the overlying groundwater
Plant Daniel, MS (EPRI site): Field-scale test site at Plant Daniel Power plant	(Trautz et al., 2013)	Groundwater sampling after injection of CO_2 showed a decrease in pH (~3 units) but pulse-like behavior for alkalinity and conductivity. No inorganics regulated by the EPA exceeded MCLs during testing. A reactive transport model was then tested using the obtained data, with good agreement for pH, Ca, Mg, K, and Sr, and lesser agreement for Mn, Ba, Cr, and Fe
	(Varadharajan et al., 2013)	Sediment characterization of the Plant Daniel site combined with laboratory studies to determine to compare results with field studies and determine the cause of elemental changes
Cranfield, MS	(Hovorka et al., 2011)	Summary of completed, continuing, and future studies conducted at the Cranfield site
	(Yang et al., 2013)	A push-pull test was conducted to determine the effect of CO_2 on the aquifer. XRD and SEM characterization of the site are also included
	(Nicot et al., 2013)	Well logs were used to assess the risk related to CO_2 leakage from wells within the Cranfield EOR site. The risk assessment concluded that no more than two, but likely none, of the wells were likely to leak CO_2

3.3.1 Carbonate Aquifers

Few studies have been conducted with carbonate aquifers, although some studies have included sediments with varying amounts of carbonate materials. The results from three such studies (two focused on aquifers and one on sediments with variable carbonate content) are summarized below.

Wunsch et al. (2013, 2014) use laboratory experiments to study metal release from limestones and dolomites, respectively. These carbonate aquifer materials were placed in batch reactors with a 1:5 solid to solution ratio, with pCO_2 ranging from 0.01 to 1 bar. Results of the limestone experiments showed an increase in Ca following an increase in pCO_2, then stabilizing with time. Ba, Sr, Co, and As followed the Ca trend, as did Mg in one of the limestone samples. Pb, Tl, Si, and U were also released from one or both limestone samples, but did not follow the same trend as Ca, and sulfates continually increased for the duration of the experiment. The pH initially decreased during the first 1–2 days of each stage of the experiment, then increased for the remainder, ranging from an initial pH of approximately 9.5 to less than 6.5. The same pH trend was seen in the dolomite batch study, with pH reaching a low of <5.6. In the dolomite experiments, both Ca and Mg concentrations began to increase immediately. Concentrations of As, Ba, Co, Cs, Ge, Mn, Mo, Ni, Rb, Sb, Sr, Tl, and Zn were also elevated in at least one of the dolomite leachate samples. The two studies concluded that carbonates were the source of several contaminants found in the aqueous samples. After opening the reactors at the conclusion of the experiment, however, many of these contaminants were removed from the solution with the return to atmospheric conditions. These studies show the potential for contaminant release from carbonate aquifers, despite the potential for high buffering capacities in these aquifers, as well as the importance of site-specific studies (Wunsch et al., 2013; 2014).

Caritat et al. (2013) studied two limestone aquifers at a sequestration demonstration site in Victoria, Australia at the Otway project site. Groundwater composition was monitored before, during, and after the injection of CO_2, but no significant changes related to CO_2 leakage were detected during the 3 years of monitoring. To aid in the detection of a leak, and to distinguish the injected CO_2 from natural CO_2, tracers were added twice during injection. These tracers were not detected in the atmospheric, soil, or aquifer samples collected from the site (Underschultz et al., 2011).

Cahill et al. (2013) used eight different sediments in a laboratory batch experiment to determine contaminant release from sediments with carbonate content varying from 0 to 100%. The silicate dominated sediments were found to be more prone to acidification, but less likely to release elevated amounts of contaminants due to a low amount of easily dissolved minerals. Carbonate dominated samples (TIC > 2%) were found to release greater concentrations of elements, although the carbonate systems were able to buffer against greater pH decreases. Results from the Cahill et al. (2013) study show the distinctive potential issues with several different aquifer types, demonstrating the importance of evaluating each possible aquifer type.

3.3.2 Sandstone and Unconsolidated Sand and Gravel Aquifers

Sandstone aquifers have received more attention than carbonate aquifers; a summary of the findings in recent studies is presented below.

SACROC is an oil field near Cranfield, MS, where CO_2 has been used for enhanced oil recovery (EOR) for over 35 years. Geochemical characterization has been conducted on the Dockum

aquifer, a minor sandstone and conglomerate aquifer overlying the SACROC injection area. The characterization was followed by a hypothetical leakage model to show expected reactions in the aquifer due to CO_2 leakage (Romanak et al., 2012).

The hypothetical leakage model showed dedolomitization as the dominant process in this system; calcite dissolution cannot be assumed. Romanak et al. (2012) conclude that current parameters used in leakage detection are site-specific, but the use of dissolved inorganic carbon (DIC) as a parameter may reduce the need for site-specific parameters, as they found the DIC response to be similar across many modeled environments. Laboratory batch studies indicated several constituents would increase and pH would decrease if CO_2 were to leak into the overlying Dockum aquifer. However, a field study of several wells located inside and outside the SACROC oil field shows no degradation of groundwater resources due to CO_2 injection. While some elemental concentrations exceeded EPA MCLs, this occurred more outside the SACROC area than inside the oil field (Smyth et al., 2009).

At the MSU-ZERT site in Bozeman, MT, food grade CO_2 was injected below the water table for 30 days. The water table is located beneath the topsoil, in a sandy gravel deposit (Zheng et al., 2012). Water samples were collected before, during, and after injection. Analysis of the samples showed that although pH, alkalinity, and several constituents changed within the groundwater during injection, none of the changes exceeded EPA MCL's (Kharaka et al., 2010). Modeling was done to determine the processes responsible for the increased dissolved constituents (Apps et al., 2011; Zheng et al., 2012).

Chimayo, NM is the location of a natural analog site where shallow wells release CO_2 into a drinking-water aquifer. Field studies coupled with modeling have been used to study the impact of CO_2 gas on the aquifer, as well as the transport of brine with CO_2 along fault zones (Keating et al., 2013a; Keating et al., 2013b; Keating et al., 2010). The Chimayo, NM site was compared with a site in Springerville, AZ, another natural analog site where brine is present but, in this case, the salinity of the affected aquifer was not significantly increased. Reactive transport models were used to determine what conditions favor the transport of brine with CO_2, and found the width of the leakage pathway to be a major factor (i.e., narrow pathways increase co-transport) (Keating et al., 2013b).

3.3.3 Comparison of Different Aquifers

Many of the previous studies have focused on sandstone or unconsolidated sand and gravel aquifers with variable carbonate content (Spangler et al., 2010; Varadharajan et al., 2013; Dafflon et al., 2013; Cahill and Jakobsen, 2013; Kirsch et al., 2014; Carroll et al., 2009; Kharaka et al., 2010; Yang et al., 2014; Keating et al., 2010; Zheng et al., 2012). A study by Cahill et al. (2013) considered samples with >2% total inorganic carbon to be "carbonate dominated," and concluded that these samples released greater amounts of trace elements but decreased pH less than silicate dominated samples. Using Cd laden illite, Frye et al. (2012) determined carbonate content as low as 10% mitigated the effect of CO_2 injection; no Cd was desorbed.

Fewer studies have been conducted with carbonate aquifer materials in relation to CO_2 sequestration, and given their prevalence as sources of potable water overlying potential sequestration reservoirs within the continental U.S., there is a need to better understand their response to potential CO_2 gas intrusions. Nisi et al. (2013) established geochemical and isotopic data for spring and surface waters located at a CO_2 injection site that included some limestone

units. However, the manuscript was written prior to CO_2 injection and does not provide insight to consequences of CO_2 leakage interactions with carbonate materials. The demonstration site studied by Caritat et al. (2013) did involve research post-injection, but no leakage into the overlying limestone aquifer was detected. In two laboratory batch experiments, both limestone and dolomite aquifer materials were tested for metal release by Wunsch et al. (2014) and Wunsch et al. (2013), respectively, with conclusions that calcite is the primary source for several released contaminants; regulatory limits were exceeded for As, Mn, and Ni in one or both studies.

Other studies focused on the effect of carbonate materials in smaller amounts (i.e., carbonate minerals are present but the aquifer is not dominated by carbonates). These studies give insight to the effect of carbonates on aquifer response to CO_2 exposure. One such study, Montes-Hernandez et al. (2013), used synthetic goethite and calcite in batch experiments. The results showed the presence of these two minerals prevented remobilization of Cu(II), Cd(II), Se(IV), and As(V), and increased adsorption of Se(IV) and As(V), although As(III) was partially remobilized with the presence of CO_2.

Cahill et al. (2013) used batch experiments to study differences in water chemistry changes for chalk, calcareous sand, and siliceous sand, concluding that carbonate materials had the greatest change in chemistry but the least change in pH. According to this study, the greater change in pH in the siliceous sand represented a greater risk for mobilization of toxic elements, although less toxic elements released from carbonates could also present a risk to water quality. Wang and Jaffe (2004) used numerical simulations and geochemical transport modeling to predict the solubilization of trace metals, with a focus on Pb in galena-quartz and galena-calcite systems, concluding the higher alkalinity and pH of the calcite system significantly reduced the detrimental effects of the presence of CO_2.

Other studies on trace element release in carbonate aquifers, although not studied in the context of CO_2 sequestration risk evaluation, have been conducted with an emphasis on As mobility. While the calcite content can buffer the change in pH, As can be incorporated into the crystal lattice of carbonates such as limestone and calcite (Di Benedetto et al., 2006; Costagliola et al., 2013; Yokoyama et al., 2012), causing As to be released as the carbonate minerals dissolve (Lazareva et al., 2014; Arthur et al., 2002).

3.4 RELEVANT PROCESSES AND REACTIONS

The way groundwater in shallow aquifers responds to the leakage of CO_2 and brine is controlled by coupled transport (advection and diffusion) and chemical reactions. This section lists possible reactions that could affect the fate of the pH, TDS, trace metals, and organic compounds in the aquifer, keeping in mind that it is likely that only a subset of these reactions will be important for a particular aquifer.

While the increase in concentration of dissolved constituents raises concerns, a lot of effort has been invested in understanding the controlling chemical processes and source minerals via model interpretation of laboratory experiments (e.g., Viswanathan et al., 2012) and field tests (Zheng et al., 2012), hopefully facilitating the development of numerical models with better predictability.

The chemical processes potentially responsible for the mobilization of trace elements include the dissolution of carbonates (Kharaka et al., 2006; McGrath et al., 2007; Birkholzer et al., 2008), sulfides (Wang and Jaffe, 2004; Apps et al., 2010; Zheng et al., 2009), and iron oxyhydroxide

minerals (Kharaka et al., 2006; Kharaka et al., 2009), as well as surface reactions such as adsorption/desorption and ion exchange (Kharaka et al., 2006; Apps et al., 2010; Zheng et al., 2009; Kharaka et al., 2009).

The release of alkali and alkaline earth metals, including Na, K, Ca, Mg, Sr, and Ba, which are most commonly observed both in laboratory and field experiments, is thought to be controlled by the dissolution of calcite and Ca-driven cation exchange reactions (Zheng et al., 2012). The reaction path and kinetic model study conducted by Wilkin and Digiulio (2010) further indicates that the geochemical response of an aquifer to CO_2 leakage is closely related to the aquifer mineralogy. It is thus expected that differences in geology (the type of aquifer), mineralogy (the type of minerals), and groundwater chemistry (the ion composition and pH) at any particular site could all lead to different responses to CO_2 leakage. For this reason, as noted by Apps et al. (2010), field tests integrated with modeling studies are necessary to further assess hydrogeochemical processes potentially affecting groundwater quality upon a CO_2 release. In general, there are three type of reactions, as discussed in the following sections.

3.4.1 Surface Reactions

3.4.1.1 Surface Reactions for Trace Metals

In a typical aquifer sediment, Fe oxides and hydroxides [such as, goethite, hydrous ferric oxide (HFO)] and clay minerals (such as illite, kaolinite, montmorillonite) are important adsorbents. Other minerals could also have some adsorption capacity, but become less relevant when Fe oxides and hydroxides and clay minerals are present in the sediment (which is the case in almost all soils and sediments).

Zheng et al. (2012) summarized the adsorption/desorption reactions H+ (surface protonation), Cd, Cu, Pb, As, Ca, Fe, Ba, Cr, Sb, and aqueous carbonate on goethite, HFO, illite, kaolinite, and montmorillonite. There are two popular methods to model adsorption/desorption reactions: a linear sorption isotherm via a distribution coefficient (Kd) or as a surface complexation model (SCM). SCM is currently used in NRAP to model adsorption/desorption reactions. The surface complexation reactions for the trace metals that are included in the third-generation ROM, namely As, Pb, Cd, and Ba, are listed in Tables 5–10. Note that surface protonation reactions are also included in these tables. These reactions play an important role in buffering pH when pH buffering by calcite dissolution is minimal. Table 10 lists the adsorption/desorption reactions for arsenate and arsenite on calcite, which is an important process that controls the fate of As in carbonate aquifers.

Table 5: Surface Protonation and Complexation Reactions on Goethite

Reactions	Log k_{int}	Site Density (mol/m^2)	Surface Area (m^2/g)	Amount of Solid (g/kg water)	Type of SCM Model	Reference
$goe^1_OH_2^+ = goe^1_OH + H^+$	-7.38	3.9-8	80	10	DLM	(Swedlund et al., 2009)
$goe^1_O^- + H^+ = goe^1_OH$	10.74	3.9-8	80	10	DLM	
$goe^2_OH_2^+ = goe^2_OH + H^+$	-7.38	3.8e-6	80	10	DLM	(Swedlund et al., 2009)
$goe^2_O^- + H^+ = goe^2_OH$	10.74	3.8e-6	80	10	DLM	
$goe^1_OCd^+ + H^+ = goe^1_OH + Cd^{+2}$	-1.29	3.9-8	80	2	DLM	(Swedlund et al., 2009)
$goe^2_OCd^+ + H^+ = goe^2_OH + Cd^{+2}$	1.83	3.8e-6	80	2	DLM	
$goe^1_OPb^+ + H^+ = goe^1_OH + Pb^{+2}$	-4.78	3.9-8	80	10	DLM	(Swedlund et al., 2009)
$goe^2_OPb^+ + H^+ = goe^2_OH + Pb^{+2}$	-1.52	3.8e-6	80	10	DLM	
$goe^2_H_2AsO_3 + H_2O = goe^2_OH + H_3AsO_3$	-5.19[a]	3.32e-6	54	0.5	DLM	(Dixit and Hering, 2003)
$goe^2_HAsO_3^- + H_2O + H^+ = goe^2_OH + H_3AsO_3$	2.34[a]	3.32e-6	54	0.5	DLM	
$goe^2_H_2AsO_4 + H_2O = goe^2_OH + AsO_4^{+3} + 3H^+$	-31.0	3.32e-6	54	0.5	DLM	(Dixit and Hering, 2003)
$goe^2_HAsO_4^- + H_2O = goe^2_OH + AsO_4^{+3} + 2H^+$	-26.81	3.32e-6	54	0.5	DLM	
$goe^2_AsO_4^{-2} + H_2O = goe^2_OH + AsO_4^{+3} + H^+$	-20.2	3.32e-6	54	0.5	DLM	

Table 6: Surface Protonation and Complexation Reactions on HFO

Reactions	Log k_{int}	Site Density (mol/m^2)	Surface Area (m^2/g)	Amount of Solid (g/kg water)	Type of SCM Model	Reference
$HFO^1_OH_2^+ = HFO^1_OH + H^+$	-7.29	8.5e-8	600	0.1	DLM	(Dzombak and Morel, 1990)
$HFO^1_O^- + H^+ = HFO^1_OH$	8.93	8.5e-8	600	0.1	DLM	
$HFO^2_OH_2^+ = HFO^2_OH + H^+$	-7.29	3.4e-6	600	0.1	DLM	(Dzombak and Morel, 1990)
$HFO^2_O^- + H^+ = HFO^2_OH$	8.93	3.4e-6	600	0.1	DLM	
$HFO^1_OCd^+ + H^+ = HFO^1_OH + Cd^{+2}$	-0.47	8.5e-8	600	0.1	DLM	(Dzombak and Morel, 1990)
$HFO^2_OCd+H^+ = HFO_OH + Cd^{+2}$	2.9	3.4e-6	600	0.1	DLM	
$HFO^1_OPb^+ + H^+ = HFO^1_OH + Pb^{+2}$	-4.65	8.5e-8	600	0.1	DLM	(Dzombak and Morel, 1990)
$HFO^2_OPb+H^+ = HFO_OH + Pb^{+2}$	-0.3	3.4e-6	600	0.1	DLM	
$HFO^1_OBa^+ + H^+ = HFO^1_OH + Ba^{+2}$	-5.46	8.5e-8	600	0.1	DLM	(Dzombak and Morel, 1990)
$HFO^2_OBa^+ + H^+ = HFO_OH + Ba^{+2}$	7.20	3.4e-6	600	0.1	DLM	
$HFO^1_H_2AsO_3 + H_2O = HFO^1_OH + AsO_3^{-3} + 3H^+$	-38.76	3.32e-6	54	0.5	DLM	(Dixit and Hering, 2003)
$HFO^1_HAsO_3^- + H_2O + H^+ = HFO^1_OH + AsO_3^{-3} + 2H^+$	-31.87	3.32e-6	54	0.5	DLM	
$HFO^1_H_2AsO_4 + H_2O = HFO^1_OH + AsO_4^{+3} + 3H^+$	-29.88	3.32e-6	54	0.5	DLM	(Dixit and Hering, 2003)
$HFO^1_HAsO_4^- + H_2O = HFO^1_OH + AsO_4^{+3} + 2H^+$	-24.43	3.32e-6	54	0.5	DLM	
$HFO^1_AsO_4^{-2} + H_2O = HFO^1_OH + AsO_4^{+3} + H^+$	-18.10	3.32e-6	54	0.5	DLM	

Table 7: Surface Protonation and Complexation Reactions of Cations on Illite

Reactions	Log k_{int}	Site Density (mol/m^2)	Surface Area (m^2/g)	Amount of Solid (g/kg water)	Type of SCM Model with Capacitance	Reference
ill_OH_2^+ = ill_OH + H^+	-8.02	2.27e-6	66.8	0.03	CCM, κ =2.0 F/m^2	(Gu and Evans, 2007)
ill_O^- + H^+ = ill_OH	8.93	2.27e-6	66.8	0.03	CCM, κ =2.0 F/m^2	
ill_Na + H^+ = ill_H + Na	1.58	1.3e-6	66.8	0.03	CCM, κ =2.0 F/m^2	
ill_OCd^+ + H^+ = ill_OH + Cd^{+2}	3.62	2.27e-6	66.8	0.03	CCM, κ =2.0 F/m^2	(Gu and Evans, 2007)
(ill_)$_2$Cd + 2H^+ = 2ill_H + Cd^{+2}	-0.63	1.3e-6	66.8	0.03	CCM, κ =2.0 F/m^2	
ill_CdOH + 2H^+ = ill_H + Cd^{+2} + H_2O	6.49	1.3e-6	66.8	0.03	CCM, κ =2.0 F/m^2	
ill_OPb^+ + H^+ = ill_OH + Pb^{+2}	0.70	2.27e-6	66.8	0.03	CCM, κ =2.0 F/m^2	(Gu and Evans, 2007)
(ill_)$_2$Pb + 2H^+ = 2ill_H + Pb^{+2}	-1.37	1.3e-6	66.8	0.03	CCM, κ =2.0 F/m^2	
ill_PbOH + 2H^+ = ill_H + Pb^{+2} + H_2O	3.65	1.3e-6	66.8	0.03	CCM, κ =2.0 F/m^2	
ill _H_2AsO_3 + H_2O = ill_OH + H_3AsO_3	-2.12	3.83e-6	22.6	40	CCM, κ =1.06 F/m^2	(Goldberg, 2002)
ill _$HAsO_3^-$ + H_2O + H^+ = ill_OH + H_3AsO_3	5.66	3.83e-6	22.6	40	CCM, κ =1.06 F/m^2	
ill_AsO_4^{-2} + H_2O + 2H^+ = ill_OH + H_3AsO_4	5.21	3.83e-6	22.6	40	CCM, κ =1.06 F/m^2	(Goldberg, 2002)

Table 8: Surface Protonation and Complexation Reactions of Cations on Kaolinite

Reactions	Log k_{int}	Site Density (mol/m^2)	Surface Area (m^2/g)	Amount of Solid (g/kg water)	Type of SCM Model	Reference
$kao_OH_2^+ = kao_OH + H^+$	-4.63	2.24e-6	22.42	7.8	CCM, κ =1.2 F/m^2	(Gu and Evans, 2008)
$kao_O^- + H^+ = kao_OH$	7.54	2.24e-6	22.42	7.8	CCM, κ =1.2 F/m^2	
$Kao_Na^+ + H^+ = Kao_H + Na^+$	2.02	3.57e-7	22.42	7.8	CCM, κ =1.2 F/m^2	
$Kao_OCd^+ + H^+ = Kao_OH + Cd^{+2}$	3.23	2.24e-6	22.42	7.8	CCM, κ =1.2 F/m^2	(Gu and Evans, 2008)
$(Kao_)_2Cd + 2H^+ = 2Kao_H + Cd^{+2}$	-1.22	3.57e-7	22.42	7.8	CCM, κ =1.2 F/m^2	
$Kao_OPb^+ + H^+ = Kao_OH + Pb^{+2}$	0.64	2.24e-6	22.42	7.8	CCM, κ =1.2 F/m^2	(Gu and Evans, 2008)
$(Kao_)_2Pb + 2H^+ = 2Kao_H + Pb^{+2}$	-2.36	3.57e-7	22.42	7.8	CCM, κ =1.2 F/m^2	
$kao_HAsO_3^- + H_2O + H^+ = kao_OH + H_3AsO_3$	5.43	3.83e-6	21.6	40	CCM, κ =1.06 F/m^2	(Goldberg, 2002)
$kao_AsO_4^{-2} + H_2O + 2H^+ = kao_OH + H_3AsO_4$	4.69	3.83e-6	21.6	40	CCM, κ =1.06 F/m^2	(Goldberg, 2002)

Table 9: Surface Protonation and Complexation Reactions of Cations on Montmorillonite

Reactions	Log k_{int}	Site Density (mol/m^2)	Surface Area (m^2/g)	Amount of Solid (g/kg water)	Type of SCM Model and Capacitance	Reference
$mon_OH_2^+ = mon_OH + H^+$	-6.04	4.41e-6	46	1.5	CCM, κ =3.2 F/m^2	(Gu et al., 2010)
$mon_O^- + H^+ = mon_OH$	6.63	4.41e-6	46	1.5	CCM, κ =3.2 F/m^2	
$mon_Na^+ + H^+ = mon_H + Na^+$	-0.18	1.53e-5	46	1.5	CCM, κ =3.2 F/m^2	
$mon_OCd^+ + H^+ = mon_OH + Cd^{+2}$	2.93	4.41e-6	46	1.5	CCM, κ =3.2 F/m^2	(Gu et al., 2010)
$(mon_)_2Cd + 2H^+ = 2mon_H + Cd^{+2}$	-2.37	1.53e-5	46	1.5	CCM, κ =3.2 F/m^2	
$mon_OPb^+ + H^+ = mon_OH + Pb^{+2}$	-0.49	4.41e-6	46	1.5	CCM, κ =3.2 F/m^2	(Gu et al., 2010; Goldberg, 2002)
$(mon_)_2Pb + 2H^+ = 2mon_H + Pb^{+2}$	-2.56	1.53e-5	46	1.5	CCM, κ =3.2 F/m^2	
$mon_H_2AsO_3 + H_2O = mon_OH + H_3AsO_3$	-1.19	3.83e-6	68.9	40	CCM, κ =1.06 F/m^2	(Goldberg, 2002)
$mon_HAsO_3^- + H_2O + H^+ = mon_OH + H_3AsO_3$	3.92	3.83e-6	68.9	40	CCM, κ =1.06 F/m^2	(Goldberg, 2002)
$mon_HAsO_4^- + H_2O + H^+ = mon_OH + H_3AsO_4$	4.52	3.83e-6	68.9	40	CCM, κ =1.06 F/m^2	(Goldberg, 2002)

Table 10: Surface Protonation and Complexation Reactions of Anions on Calcite

Reactions	Log k_{int}	Site Density (mol/m²)	Surface Area (m²/g)	Amount of Solid (g/kg water)	Type of SCM Model	Reference
$cal_CO_3H^0 = cal_CO_3^- + H^+$	-5.1	8.22e-6	0.22	200	DLM	(Sø et al., 2008)
$cal_CO_3H^0 + Ca^{2+} = cal_CO_3Ca^+ + H^+$	-1.7	8.22e-6	0.22	200	DLM	
$cal_CaCO_3^- + H_2O = cal_CaOH^{2+} + CO_3^{2-}$	-5.25	7.99e-6	0.22	200	DLM	
$cal_CaCO_3^- + HCO_3^- = cal_CaHCO_3^0 + CO_3^{2-}$	-3.929	7.99e-6	0.22	200	DLM	
$cal\ CaCO_3^- + H_2AsO_4^- = cal_CaHAs\ O_4^- + H^+ + CO_3^{2-}$	-8.97	7.99e-6	0.22	200	DLM	
$cal\ CaCO_3^- + CaHAsO_4^0 = cal_CaAsO4Ca0 + H^+ + CO_3^{2-}$	-9.81	7.99e-6	0.22	200	DLM	
$cal_sCaCO_3^- + H_2O = cal_sCaOH_2^+ + CO_3^{2-}$	-5.25	2.3e-7	0.22	200	DLM	
$cal_sCaCO_3^- + HCO_3^- = cal_sCaHCO_3^0 + CO_3^{2-}$	-3.929	2.3e-7	0.22	200	DLM	
$cal_sCaCO_3^- + H_2AsO_4^- = cal_sCaHAsO_4^- + H^+ + CO_3^{2-}$	-7.98	2.3e-7	0.22	200	DLM	
$cal_sCaCO_3^- + CaHAsO_4^0 = cal_sCaAsO_4Ca^0 + H^+ + CO_3^{2-}$	-7.22	2.3e-7	0.22	200	DLM	

Several experimental and modeling studies (Zheng et al., 2012; Trautz et al., 2013; Zheng et al., 2016) revealed that cation exchange reactions control the fate of the alkali and alkaline earth metals. Among them, Ba is of particular importance because it is more of an environmental concern. The cation exchange reactions that are typically involved when CO_2 leaks into a shallow aquifer are listed in Table 11.

Table 11: Cation Exchange Reactions and Selectivity Coefficients, Using the Gaines-Thomas Convention (Appelo and Postma, 1994)

Cation Exchange Reaction	$K_{Na/M}$
$Na^+ + X\text{-}H = X\text{-}Na + H^+$	1
$Na^+ + X\text{-}K = X\text{-}Na + K^+$	0.2
$Na^+ + 0.5X\text{-}Ca = X\text{-}Na + 0.5Ca^{+2}$	0.4
$Na^+ + 0.5X\text{-}Mg = X\text{-}Na + 0.5Mg^{+2}$	0.6
$Na^+ + 0.5X\text{-}Ba = X\text{-}Na + 0.5Ba^{+2}$	0.2
$Na^+ + 0.5X\text{-}Sr = X\text{-}Na + 0.5Sr^{+2}$	0.15
$Na^+ + X\text{-}Li = X\text{-}Li + Li^+$	0.08

3.4.1.2 Surface Reactions for Organic Compounds

Because linear adsorption isotherms are widely used to model the transport of organic compounds in aquifers, the NRAP groundwater model uses the same approach and the key parameter is the distribution coefficient, Kd. The distribution coefficient between soil and water is defined as:

$$K_d = \frac{m_i^S / m^S}{m_i^{H_2O} / m^{H_2O}} \tag{1}$$

where m_i^S and m_i^{H2O} is the mass of organic species *i* in the sediments and water respectively, and m^S and m^{H_2O} is the mass of sediments and water, respectively. Note that K_d in Equation 1 is dimensionless. Alternatively, K_d can also take units of mL/g or L/kg if expressed as a ratio of concentrations (i.e., mg/kg_{soil} divided by mg/L_{water}). Table 2 lists some published K_d values for benzene, which are highly variable. Also shown in Table 12 is the weight fraction of organic carbon in sediments, f_{oc}, calculated based on a K_{oc} of 79 ($logK_{oc}$=1.9); the definition of f_{oc} and K_{oc} will be discussed later.

Table 12: Compilation of Published Kd for Benzene Between Soil and Water

Reference	K_d (mL/g)	f_{oc}	Comments
(Larsen et al., 1992)	0.05-0.65	0.00063-0.0082	Measured for aquifer samples which are located at various locations in Denmark and have a great variety
(Donahue et al., 1999)	0.1-1.0	0.0013-0.013	Measured for Regina clay in Canada
(Jean et al., 2002)	0.16-0.5	0.0021-0.0063	Measured in a laboratory experiment for artificial medium-size sand
(Hawthorne and Miller, 2003)	28-59	0.35-0.75	Measured for manufactured gas plant soils (contaminated by organic compounds)

The large range of measured K_d values is primarily due to the dependence of K_d on the organic matter content of soils, which is quite variable. In other words, K_d is sediment specific, and the same K_d value is not necessarily applicable to a range of different soil types. Although the value of K_d depends on the properties of sediments, the hydrophobic partitioning theory as reviewed by Karickhoff et al. (1979) implies that the partitioning of a specific compound between water and organic carbon, as expressed by K_{oc}, is largely independent of the organic content of the solid material. K_d can be calculated from K_{oc} by the equation:

$$K_d = f_{oc} \times K_{oc} \tag{2}$$

where $f_{oc} = m_{oc}^{s} / m^{s}$ is the mass fraction of organic carbon in sediments, defined as the mass of organic carbon in sediments, m_{oc}^{s}, divided by the mass of sediments. K_{oc} may be thought of as the ratio of the amount of chemical adsorbed per unit weight of organic carbon in the soil to the concentration of the chemical in solution at equilibrium:

$$K_{oc} = \frac{m_i^S / m_{oc}^S}{m_i^{H_2O} / m^{H_2O}} \tag{3}$$

K_{oc} is usually related to K_{ow} by:

$$\log K_{oc} = a \log K_{ow} + b \tag{4}$$

where K_{ow} is the octanol/water partition coefficient. Karickhoff et al. (1979) reported the following equation from least squares fitting for $logK_{oc}$ versus $logK_{ow}$.

$$\log K_{oc} = 1.0 \cdot \log K_{ow} - 0.21 \tag{5}$$

Mackay et al. (1992) reported that the *log* K_{oc} ranges from 1.09 to 2.53 with a median around 1.8–2.0.

Table 13: K_{oc} (L/kg) for Benzene, Phenol, and Naphthalene

Organic Compound	Max	Min	Geometric Mean
Benzene	100	31	62
Phenol	No data available	No data available	28.8[a]
Naphthalene	1950	830	1191

(a) calculated rather than measured

Oxidation of the organics was calculated with the first-order degradation kinetics:

$$\frac{dC}{dt} = -KC \tag{6}$$

where C is the concentration of the organic compound and K is the first-order rate constant which was treated as a variable parameter.

The K_{oc} for benzene, phenol, and naphthalene is included in Table 13 and the degradation rate constants for these same organic compounds are included in Table 14.

Table 14: Degradation Rate Constant (1/day) for Benzene, Phenol, and Naphthalene (Saleem, 1999)

Organic Compound	Max	Min	Median
Benzene	0.071	0	0
Phenol	0.2	0	0.032
Naphthalene	0.03	0	0

3.4.2 Dissolution/Precipitation

The dissolution/precipitation of minerals in aquifer sediments is critical for how aquifers respond to incoming CO_2 and brine. First, the dissolution of minerals, typically carbonate minerals such as calcite, is the major pH buffering process.

Second, the dissolution of minerals could lead to the release of trace metals directly or indirectly. For example, the dissolution of some sulfide minerals (e.g., galena or asenopyrite) could be responsible for the increase of lead and arsenic concentration (Zheng et al., 2009; Apps et al., 2010; Wang and Jaffe, 2004) and the dissolution of calcite could lead to the release of some impurities in calcite, such as Sr and Ba (Lu et al., 2010). The dissolution of calcite could also cause indirect release of Cs and Ba by triggering Ca-driven cation exchange reactions (Zheng et al., 2012). It is noteworthy that not only the fast reacting minerals such as calcite play a significant role, but also the slow reacting minerals in certain circumstances. For instance, a field test in Mississippi (Trautz et al., 2013) showed that the dissolution of plagioclase (which reacts much slower than calcite) started to release calcium and subsequently trigger the increase in concentrations of Sr and Ba after the injection of CO_2-saturated water stopped, which illustrated that when the groundwater flow rate is fairly low, slow reacting minerals could also have significant impacts on the release of trace metals.

Third, dissolution/precipitation of minerals can alter the pore structure of sediments and, subsequently, the flow pathways. However, such an effect is more important for the mineral trapping of CO_2 in the storage formation than for the impact of the CO_2 and brine leakage on groundwater. Although in the last decade studies have shown fast reacting minerals, such as carbonate and sulfide minerals, and a few slow reacting minerals, such as plagioclase, play a major role in controlling the response of aquifers to the leakage of CO_2 and brine, these reactions are chains of complex reaction networks. It is therefore necessary to take into account all of the minerals' phases when developing a reactive transport model, despite the fact that most of the time a subset of these minerals is selected due to pragmatic reasons, such as computation time. This report focused on the mineral phases that are related to two aquifers, the Edwards and High Plains Aquifers, because it is not possible to have an exhaustive list of minerals. Table 15 shows the minerals for the Edwards Aquifer and their kinetic reaction rates.

Table 15: Kinetic Mineral Reactions and Neutral Mechanism Rates (Palandri and Kharaka, 2004) for the Edwards Aquifer at 25°C

Kinetic Reaction	Equilibrium Coefficient at 25°C, log	Forward Rate at 25°C, mol/m^2/s	Activation Energy, kJ/mol
Calcite + H^+ = HCO_3^- + Ca^{+2}	1.847	1.5e-6	23.5
Dolomite + $2H^+$ = $2HCO_3^-$ + Ca^{+2} + Mg^{+2}	3.533	2.9e-8	52.2
Strontianite = CO_3^- + Sr^{+2}	-9.271	Same as calcite	Same as calcite

Table 16: Equilibrium Constants of the Major Rock-Forming Minerals for the High Plains Aquifer. Chemical reactions for the minerals in the first column are written as the chemical species in the first row with stoichiometric coefficients listed under each species.

Minerals	logK (25°C)
Calcite + H^+ = Ca^{+2} + HCO_3^-	1.853
Illite + 6.3 H_2O = H^+ + 0.25Mg^{+2} + 0.85K^+ +3.4 H_4SiO_4(aq)+ 2.35AlO_2^-	-43.490
Kaolinite +3H2O = 2H+ +2H_4SiO_4(aq)+ 2AlO_2^-	-39.262
Smectite + 7.32 H_2O = 0.68H^+ + 0.17Ca^{+2} + 0.335Mg^{+2} + 3.99 H_4SiO_4(aq)+ 1.68AlO_2^-	-32.834
goethite + $3H^+$ = $2H_2O$ + Fe^{+3}	0.363
Albite + $6H_2O$ = Na^+ + $3H_4SiO_4$(aq)+ AlO_2^-	-20.126
Quartz +$2H_2O$ = H_4SiO_4(aq)	-3.740
K-Feldspar + $6H_2O$ = K^+ + $3H_4SiO_4$(aq)+ AlO_2^-	-22.394
Dolomite + $2H^+$ = Ca^{+2} + Mg^{+2} + HCO_3^-	3.545
Magnesite + H^+ = Mg^{+2} + HCO_3^-	1.420
Dawsonite = H^+ + Na^+ + HCO_3^- + 2.35AlO_2^-	-18.535
Muscovite + $6H_2O$ =$2H^+$ + K^+ + $3H_4SiO_4$(aq)+ 3AlO_2^-	-57.264
Ferrihydrite + $3H^+$ = $3H_2O$ + Fe^{+3}	3.404
Gibbsite = H_2O + H^+ + AlO_2^-	-15.129

Table 16 lists all the major rock-forming minerals for the High Plains Aquifer. Kinetic rate parameters for most rock-forming minerals for the High Plains Aquifer were taken from Palandri and Kharaka (2004), which are based mainly on experimental studies conducted under far-from-equilibrium conditions. The overall rate equation is tied to mineral equilibria through Q/K with a pH dependent rate consisting of acid, neutral, and base mechanisms as indicated below:

$$r = \pm k\, A \left[1 - \left(\frac{Q}{K}\right)^{\theta}\right]^{\eta} \tag{7}$$

and

$$k = k_{25}^{nu} \exp\left[\frac{-E_a^{nu}}{R}\left(\frac{1}{T} - \frac{1}{298.15}\right)\right] + k_{25}^{H} \exp\left[\frac{-E_a^{H}}{R}\left(\frac{1}{T} - \frac{1}{298.15}\right)\right] a_H^{n_H} + k_{25}^{OH} \exp\left[\frac{-E_a^{OH}}{R}\left(\frac{1}{T} - \frac{1}{298.15}\right)\right] a_{OH}^{n_{OH}} \tag{8}$$

where
- r = the kinetic rate
- k = the rate constant
- A = the specific reactive surface area
- K = the equilibrium constant for the mineral–water reaction
- Q = the reaction quotient
- nu = neutral mechanism
- H = acid mechanism
- OH = base mechanisms
- E_a = activation energy that accounts for the dependence of the rate on temperature
- T = absolute temperature
- a_H = hydrogen ion activity
- a_{OH} = hydroxyl ion activity
- n = an empirical constant

The parameters θ and η are assumed equal to unity. The mineral reactive surface areas were taken from Xu et al. (2006), based on the work of Sonnenthal et al. (2005). A thorough review and discussion of the kinetic rates for arsenian pyrite, pyrite, and galena was given in Zheng et al. (2009). The kinetic properties for the minerals in the High Plains Aquifer are given in Table 17.

Table 17: Kinetic Properties for Minerals Considered in the Model (see text for data sources). "Primary" minerals are initially present in the aquifer. "Secondary" minerals are formed by precipitation.

		Parameters for Kinetic Rate Law							
		Neutral Mechanism		Acid Mechanism			Base Mechanism		
Mineral	A (cm^2/g)	k_{25} $mol/m^2/s$	E_a KJ /mol	k_{25}	E_a	$n(H^+)$	k_{25}	E_a	$n(OH^-)$
Primary:									
Calcite	3.05	1.6×10^{-6}	62.76						
Illite	151.60	1.66×10^{-13}	35.00	1.05×10^{-11}	23.60	0.34	3.02×10^{-17}	58.9	-0.40
Kaolinite	151.60	6.91×10^{-14}	22.20	4.89×10^{-12}	65.90	0.78	8.91×10^{-18}	17.9	-0.47
Smectite	151.60	1.66×10^{-13}	35.00	1.05×10^{-11}	23.60	0.34	3.02×10^{-17}	58.9	-0.4
Goethite	12.90	2.51×10^{-15}	66.20	4.07×10^{-10}	66.20	1.00			
Albite	9.80	3.89×10^{-13}	38.00	8.71×10^{-11}	51.70	0.50	6.31×10^{-12}	94.1	-0.82
Quartz	9.80	3.98×10^{-14}	87.7						
K-feldspar	9.80	3.89×10^{-13}	38.00	8.71×10^{-11}	51.70	0.50	6.31×10^{-12}	94.1	-0.82
Secondary:									
Dolomite	12.90	2.95×10^{-8}	62.76	2.34×10^{-7}	43.54	1.00			
Magnesite	9.80	4.57×10^{-10}	23.50	4.17×10^{-7}	14.40	1.00			
Dawsonite	9.80	3.89×10^{-13}	38.00	8.71×10^{-11}	51.70	0.50	6.31×10^{-12}	94.1	-0.82
Muscovite	9.80	3.89×10^{-13}	38.00	8.71×10^{-11}	51.70	0.50	6.31×10^{-12}	94.1	-0.82
Gibbsite	9.80	3.89×10^{-13}	38.00	8.71×10^{-11}	51.70	0.50	6.31×10^{-12}	94.1	-0.82
Pyrite	12.90	2.52×10^{-12}	62.76						

3.4.3 Redox Reactions

Redox potential is very important in determining the fate of redox-sensitive trace metals and organic compounds when groundwater in a shallow aquifer is affected by the leakage of CO_2. For example, it is known that As(III) has much higher mobility and is of more environmental concern than As(V). Also, the biodegradation rate for an organic compound is much higher in oxidizing than reducing conditions. When CO_2 or CO_2-saturated brine leaks into the aquifer, it primarily causes a decrease of pH. Meanwhile, Eh will change as well due to the interrelation of pH and Eh. It is therefore critical to determine the background redox condition in the aquifer and the change of redox condition after the intrusion of CO_2.

For confined aquifers, because of the fairly low redox potential, a sufficient increase in redox potential to cause a shift of speciation of redox-sensitive species, such as, is unlikely. For unconfined aquifers, changes in redox potential are more likely and could shift the speciation and key parameters of potential contaminants (e.g., degradation rate for organic compounds). However, in either case, redox reactions have to be included in the reactive transport models and redox potentials have to be evaluated. The most prevalent redox reactions are those involving the following pairs of redox couples: Fe(II)/Fe(III), HS-/SO4-2, and As(III)/As(V).

3.5 DEVELOPMENT OF CONCEPTUAL AND REDUCED-ORDER MODELS

The development of a ROM requires multiple runs of the reactive transport models that simulate the leakage of CO_2 and brine into a shallow aquifer. The core of the reactive transport model is the geochemical conceptual model. The following work is helpful, and sometimes necessary, to build a defensible conceptual model.

First, it is necessary to gather detailed water and mineral composition data. This basic information, with the help of geochemical equilibrium calculations, can reveal which mineral phase controls the major and trace elements and which reactions are important for pH and Eh. It is also necessary to measure the cation exchange capacity (CEC) and sorption capacity of the aquifer sediments.

Second, batch experiments that typically involve the release of CO_2 into a pre-equilibrated water-sediment environment are very useful in two ways. First, the batch experiment is a great screening tool to determine which elements could be released. Such experiments have features, including the well mixing of sediment with water, that lead to a very aggressive release of trace elements (Zheng et al., 2015), and they therefore provide the upper bound of the type of elements and their concentrations that could be caused by the introduction of CO_2 into an aquifer. In other words, if a given element is not released by the batch experiment, it is unlikely to show up in the aquifer in a large scale CO_2 leakage scenario, although one should pay attention to the heterogeneity issue and make sure to do a series of batch experiments with sediments from different locations of the aquifer. Secondly, the batch experiment, integrated with geochemical modeling, is very useful for determining the chemical reactions that control the release of trace elements. Because of the aggressiveness of the batch experiment, some reactions that are relevant for the batch experiment may become less important, or even irrelevant, for the real condition.

Third, it is desirable to have a column test to evaluate transport processes, such as the column test with High Plains Aquifer sediments (Lawter et al., 2016). Such tests give us more realistic estimates of the type of elements and their concentrations that could result from the introduction

of CO_2 into aquifer, and provide an insight of the interaction of chemicals with transport processes. A reactive transport model for the column test (Zheng et al., 2016) can further narrow down the key reactions and parameters and lay a strong foundation for a reactive transport model at appropriate field scales.

After the establishment of the conceptual model, simulations can be conducted for the time steps and spatial resolution needed. A sensitivity analysis, which can be performed by manually tuning some key parameters, is useful to double-check the model setup.

The development of the third-generation hydrology ROM (Carroll et al., 2014) is an example of the procedure to develop a ROM. First, the parameter ranges are needed for the development of the aquifer model, hydrologic flow, leakage flux, brine concentrations, and geochemical parameters. Second, these parameters are sampled to design a number of simulations. For example, for the third-generation hydrology ROM (Carroll et al., 2014), 1,000 simulations were designed. Third, model results are processed to calculate the entities used to build the ROM. Then the ROM is derived. Depending on the nature of the ROM (e.g., polynomial-based ROMs, lookup tables, etc.), the derivation method is different. The ROM should be able to emulate the outcome of the numerical model, but with less complexity, more thorough sampling of the parameter space, and significantly faster simulation times to generate risk-based profiles that can be used in decision making processes.

Development of the groundwater ROMs required the following data:

- Threshold values
- Initial groundwater concentrations
- Rock mineralogy
- Thermodynamic data (log K's) for rock mineral and aqueous complexes
- Surface complexation reactions for trace metals
- Koc and biodegradation rates for organics

Parameters needed to drive the second-generation and third-generation ROMs can be grouped in three categories: parameters that are related to the source term, parameters to define the hydrological properties of the aquifer, and parameters used to define the chemical properties of the aquifer. In the third-generation ROM (Carroll et al., 2014), the leakage models and variable parameters are illustrated in Figure 8. Variability in the CO_2 leakage profile was generated using four parameters:

1. q_{CO2} – the peak flux
2. T_{1C} – the time needed to reach peak flux
3. dT_{2C} – the duration of the peak flux
4. dT_{3C} – the duration of the transition to zero flux after injection has stopped

Brine leakage profiles are different from that of CO_2. Brine leakage was characterized with a maximum and constant flux during injection, which falls off to a final flux after injection stops. Uncertainty in the brine leakage profile was generated using four parameters:

1. q_{BRN} – the initial and maximum flux

2. λq_{BRN} – the final flux
3. T_{1B} – the injection time
4. dT_{2B} – the duration of the transition between the maximum and final flux

An additional parameter, TM, was included to represent wellbore mitigation time. The ranges of these parameters are given in Table 18 (Carroll et al., 2014). Another set of the parameters that are related to the source term are the concentrations of major ions (i.e., Na and Cl), trace metals, and organic compounds, which are listed in Table 19. Note that in Table 19, chloride concentration is assumed to be the same as sodium concentration and there is no barium in the leaking brine.

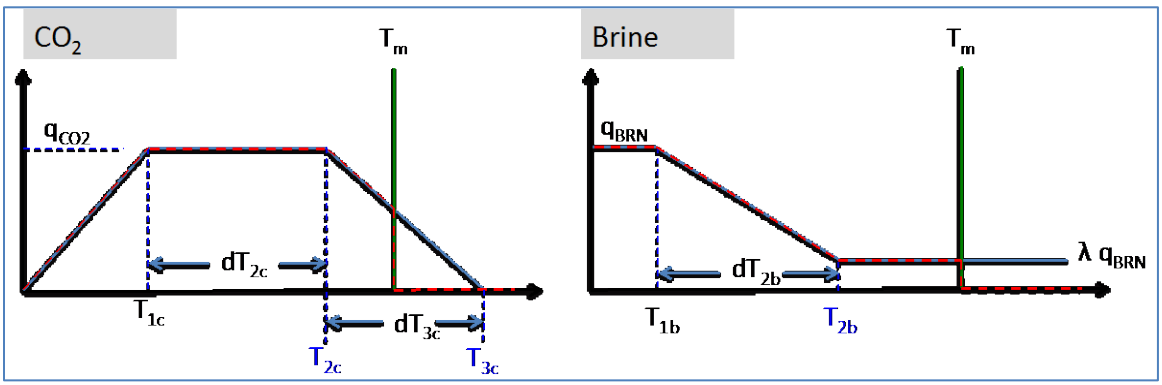

Figure 8: Schematic of the CO_2 and brine leakage model parameters and profiles in the generalized model.

Table 18: Proposed Parameter Ranges for Generalized CO_2 and Brine Leakage Models

Parameter	Min	Max	Notes
q_{CO2}	-3.000	-0.301	Log_{10} (0.001 – 0.5) kg s^{-1}
q_{BRN}	-2.301	-1.125	Log_{10} (0.005 – 0.075) kg s^{-1}
λ	0.200	0.300	Ratio for brine leakage tail
T_{1c}	5.000	50.000	yr
dT_{2c}	0	100.000	yr
dT_{3c}	5.000	50.000	yr
T_{1b}	1.000	50.000	yr
dT_{2b}	1.000	10.000	yr
T_m	50.000	200.000	Mitigation time, yr

Table 19: Sodium, Trace Metals and Organics Concentrations Considered in the Groundwater Simulations and ROM. Trace metals are based on experiments (Karamalidis et al., 2013) and organic concentrations are based on Zheng et al. (2010).

Trace Metal	Minimum	Maximum	Unit
Sodium Molality	-3	1	Log_{10}[mol kg^{-1}]
Barium			Log_{10}[mol kg^{-1}]
Cadmium	-8.87	-6.43	Log_{10}[mol kg^{-1}]
Chromium	-6.42	-4.02	Log_{10}[mol kg^{-1}]
Iron	-6.07	-2.79	Log_{10}[mol kg^{-1}]
Lead	-8.12	-4.74	Log_{10}[mol kg^{-1}]
Manganese	-5.13	-2.10	Log_{10}[mol kg^{-1}]
Benzene	-10	-3.2	Log_{10}[mol kg^{-1}]
Naphthalene	-10	-3.7	Log_{10}[mol kg^{-1}]
Phenol	-10	-4.1	Log_{10}[mol kg^{-1}]

Five parameters are needed to define the hydrological conditions in the aquifers, which are listed in Table 20. Table 21 lists the parameters related to the chemical properties of the aquifer.

Table 20: Parameter Definition and Ranges for Hydrologic Simulations and Emulations

	Parameter	Minimum	Maximum	Unit
1	Sand volume fraction	0.35	0.65	-
2	Correlation length in X-direction	200	2500	[m]
3	Correlation length in Z-direction	0.5	25	[m]
4	Permeability in sand	-14	-10	$Log_{10}[m^2]$
5	Permeability in clay	-18	-15	$Log_{10}[m^2]$

Table 21: Input Parameters of the Development of the Scaling Functions

Parameter	Range
Calcite volume fraction	0.0 to 0.2
Goethite volume fraction	0.0 to 0.2
Illite volume fraction	0.0 to 0.3
Kaolinite volume fraction	0.0 to 0.2
Montmorillonite volume fraction	0.0 to 0.5
Cation exchange capacity (CEC meq/100)	0.1 to 40.0
Benzene concentration in the leaking brine (mol/L)	-10.0 to -3.2[a]
Phenol concentration in the leaking brine (mol/L)	-10.0 to -3.7[a]
Naphtalene concentration in the leaking brine (mol/L)	-10.0 to -4.1[a]
Benzene distribution coefficient (L/kg)	-4.5 to 0.69[a]
Phenol distribution coefficient (L/kg)	-6.0 to 0.15[a]
Naphtalene distribution coefficient (L/kg)	-3.1 to 1.98[a]
Benzene degradation constant (1/s)	0 to -6.1[a]
Phenol degradation constant (1/s)	0 to -5.63[a]
Naphtalene degradation constant (1/s)	0 to -6.45[a]
Time (years)	0 to 200

(a) indicates log10 values

4. POTENTIAL RISK FOR GROUNDWATER POLLUTION DUE TO CO_2 GAS AND BRINE INTRUSION

This section of the report establishes the overall potential risk for groundwater pollution of CO_2/brine leakage based on literature review and data from modeling, laboratory, and field experiments conducted at PNNL and LBNL.

4.1 THE EFFECTS ON TDS AND PH

4.1.1 High Plains Aquifer

4.1.1.1 Experimental Results

Results from a series of batch and column experiments revealed important differences in pH and TDS that will be discussed in detail in the following section on modeling. Briefly, some of the sediment samples have detectable amounts of calcite, while some other samples had no XRD detectable calcite. In these latter samples, the pH remained lower than the pH measured in experiments conducted with calcite-containing sediments, mainly due to reduced buffering capacity of sediments that had no calcite. The pH for the calcite-containing sediments decreased to no less than ~6, while the pH for calcite-free sediments decreased to ~5. Aqueous samples from the calcite-free sediment showed a greater release of elements, including several regulated by the EPA, such as, Cr, and Pb.

Contaminants, such as and Cd present in saline brines, could travel upward with leaking CO_2 into the overlying aquifer. Batch and column experiments were conducted with As and Cd spikes (114 µg/L and 40 µg/L, respectively) to determine the fate of these contaminants if this were to happen. These solutions had no significant effect on pH.

Methane can also be transported upward with a CO_2 plume, so experiments were conducted with a 1% CH_4 and 99% CO_2 gas mix. These experiments revealed that the effect on pH was not significant.

4.1.1.2 Modeling

In this section the discussion is focused on input and fitted modeling parameters, sensitive and non-sensitive parameters, the impact of site-specific data on modeling, and whether the changes are short- or long-term.

The assessment of the risk of CO_2 and brine leakage on groundwater overlying a CO_2 sequestration site relies heavily on numerical models. Correct geochemical conceptual models and reliable key parameters are critical for the predictability of a numerical model. In light of modeling the impact of CO_2 and brine leakage on groundwater, conceptual models look at the chemical reactions that control the release of trace metals and the fate of organic compounds. Therefore, the most important parameters are those needed to describe these reactions. Model interpretation of the laboratory and field experiments is an effective way to develop the right conceptual model and calibrate key parameters.

A series of batch and column tests were conducted for the sediments from the High Plains Aquifer (Lawter et al., 2016). In the column experiments, CO_2 saturated synthetic groundwater (which mimics the water composition of the High Plains Aquifer) was injected through a column packed with material from the High Plains Aquifer to simulate the impact of a gradual leak of CO_2 on a shallow aquifer. A reactive transport model was developed to interpret the observed

concentration changes in the column effluent water (Zheng et al., 2016), attempting to shed light on the chemical reactions and key parameters that control the concentration changes of some constituents.

The geochemical conceptual model used in the reactive transport model for the column test was consistent with those revealed by modeling two field tests (Zheng et al., 2012; Trautz et al., 2013): the MSU-ZERT field test in Montana (Kharaka et al., 2010), and a field test conducted in Plant Daniel, Mississippi (Trautz et al., 2013). Note that both of these tests were conducted on a sandstone aquifer, for which the composition of key minerals in the aquifer sediments were similar to that of the High Plains Aquifer. Due to similarities between the two aquifer systems, it is not a surprise that the geochemical conceptual model developed for the field test in Mississippi is applicable to the model for the column test with High Plains Aquifer materials (Lawter et al., 2016). In these models, dissolution of calcite is the primary pH buffering process, with the dissolution of magnesite and surface protonation playing a secondary role. Figure 9 shows the comparison of the model results with experimental data.

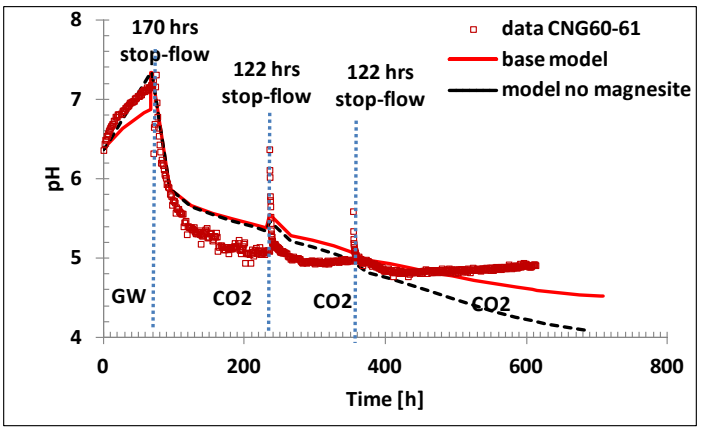

Figure 9: Simulated and observed breakthrough curves of pH for the column test of sample CNG60.

4.1.2 Edwards Aquifer

4.1.2.1 Experimental Results

Materials from the Edwards Aquifer in Texas were used to represent a potential unconfined carbonate aquifer overlying a CO_2 sequestration site. As with the High Plains Aquifer sediments, both column and batch experiments were conducted using samples from the Edwards Aquifer. Unlike the unconsolidated sand and gravel aquifer sediments, the unweathered or slightly weathered rocks of the Edward aquifer were ground by mortar and pestle and used in these experiments in the form of powder. Column studies were conducted with a steady CO_2 flow rate of 0.5 mL/min into the SGW, which was pumped through the columns at 0.03 mL/min. Because of the high calcite content and buffering capacity of these sediments, the effect on pH was similar in all tested materials. The pH of all experiments did not decrease below pH ~ 6 due to the high carbonate content and buffering capacity of these materials. Data from these experiments are presented in a previously published report (Qafoku et al., 2013) and will be also discussed in the following section on modeling.

4.1.2.2 Modeling

Results from mineralogical analyses show that the limestone consists almost entirely of calcite (Wang et al., 2016). Previous publications indicate that the predominant mineral in this limestone is calcite with a small amount of dolomite (Maclay and Small, 1994); and a minor amount of the mineral strontianite was included in solid solution with calcite (Tesoriero and Pankow, 1996) (Table 22).

Table 22: Mineral Reactions

Kinetic Reaction	Equilibrium Coefficient at 25°C, log	Forward Rate at 25°C, mol/m²/s	Activation Energy, kJ/mol
Calcite + H^+ = HCO_3^- + Ca^{+2}	1.847	1.5e-6	23.5
Dolomite + $2H^+$ = $2HCO_3^-$ + Ca^{+2} + Mg^{+2}	3.533	2.9e-8	52.2
Strontianite = CO_3^- + Sr^{+2}	-9.271	Same as calcite	Same as calcite

Modeling of the batch experiments was conducted using PHREEQC (Parkhurst and Appelo, 1999) and the thermo.com.V8.R6 database (Wolery and Jarek, 2003). Modeling of the column experiments was conducted using the multiphase flow and reactive transport solver STOMP-CO2-R (White et al., 2012) with ECKEChem (White and McGrail, 2005). The STOMP simulations used a smaller subset of equilibrium aqueous complexation reactions extracted from PHREEQC simulations of the batch experiments and groundwater samples (Musgrove et al., 2010) taken from the unconfined/urban portion of the Edwards Aquifer (Table 23).

Table 23: Aqueous Complexation Reactions

Equilibrium Reaction	Equilibrium Coefficient at 25°C, log
$HCO_3^- + H^+ = CO_2 + H_2O$	6.3447
$HCO_3^- + Ca^{+2} = CaHCO_3^+$	1.0467
$HPO_4^{-2} + Ca^{+2} = CaHPO_4$	2.7400
$HPO_4^{-2} + Ca^{+2} = CaPO_4^- + H^+$	-5.8618
$SO_4^{-2} + Ca^{+2} = CaSO_4$	2.1111
$Cl^- + Cd^{+2} = CdCl^+$	2.7059
$HCO_3^- + Cd^{+2} = CdHCO_3^+$	1.5000
$HPO_4^{-2} + H^+ = H_2PO_4^-$	7.2054
$Mg^{+2} + HCO_3^- = MgHCO3+$	1.0357
$Mg^{+2} + HPO_4^{-2} = MgHPO_4$	2.9100
$SO_4^{-2} + Mg^{+2} = MgSO_4$	2.4117
$H_2O = OH^- + H^+$	-13.9951
$Na^+ + HCO_3^- = NaHCO_3$	0.1541
$Pb^{+2} + HCO_3^- = PbCO_3 + H^+$	-3.7488
$Pb^{+2} + H_2O = PbOH^+ + H^+$	-7.6951
$Sr^{+2} + SO_4^{-2} = SrSO_4$	2.3000
$2H_2O + Cr^{+3} = Cr(OH)_2^+ + 2H^+$	-9.7000
$3H_2O + Cr^{+3} = Cr(OH)_3 + 3H^+$	-18.0000
$H_2O + Cr^{+2} = CrOH^{+2} + H^+$	-4.0000
$HCO_3^- + Cu^{+2} = CuCO_3 + H^+$	-3.3735
$H_2O + Cu^{+2} = CuOH^+ + H^+$	-7.2875
$SeO_3^{-2} + H^+ = HSeO_3^-$	7.2861

The column experiments utilizing unweathered rock samples were modeled by including calcite and dolomite, and adjusting the amount of strontium in solid solution with calcite. For the first sample, the concentration of dissolved CO_2 in the inlet water was adjusted to match the observed pH (Figure 10), which decreases to a value of around 6.5. TDS was calculated based on major ion concentrations (Figure 10), and increased from a value of 161 mg/L at the beginning of the experiment to a value of 353 mg/L at the end of the column experiment. The reported median value of TDS in the urban, unconfined portion of the Edwards Aquifer is 329 mg/L (M

Musgrove et al. 2010). The experimentally observed TDS is lower than the reported 75th percentile value of 360 mg/L.

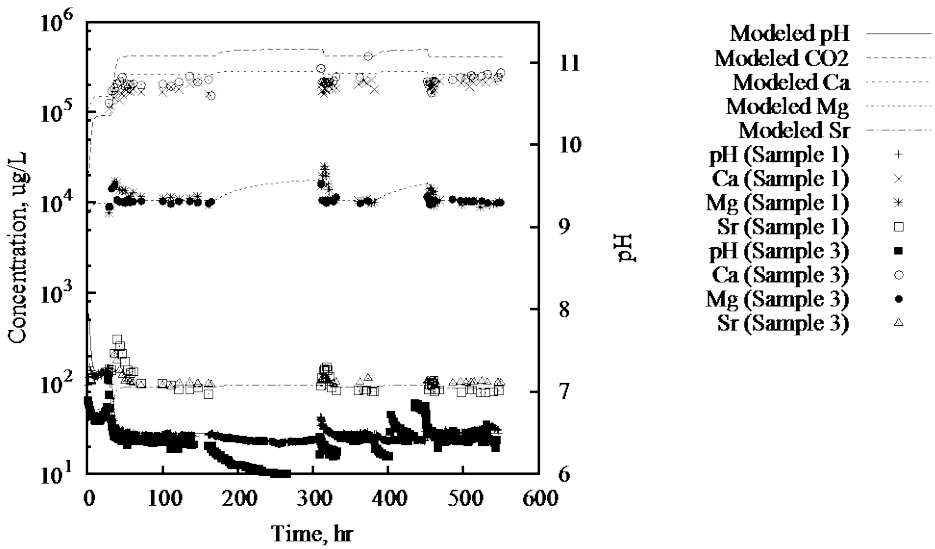

Figure 10: Major ion modeling results compared to column experiment results.

4.2 CHANGES IN MAJOR, MINOR, AND TRACE ELEMENT CONCENTRATION

4.2.1 <u>High Plains Aquifer</u>

4.2.1.1 Experimental Results

The release of major, minor, and trace elements from sediments exposed to CO_2 gas streams was studied in a series of batch and column experiments. The data will be presented in the modeling section that follows.

As mentioned previously, contaminants, such as and Cd, could travel upward with the leaking CO_2 into the overlying aquifer. Batch and column experiments were conducted with an As and Cd spike (114 µg/L and 40 µg/L, respectively) to determine contaminant fate if this were to happen. Results showed the sandstone aquifer sediments had a large adsorption capacity for these contaminants, with a 90–95 % reduction of Cd and a 60–70% reduction of As within 4 hours in the gas injected reactors and a greater reduction in the blank (no gas) reactors. Cd concentrations fell below detection limits and As fell below 73%.

Methane can also be transported upward with a CO_2 plume, so experiments were conducted with a 1% CH_4 and 99% CO_2 gas mix. Calcite-free sediments and sediments containing calcite were used in batch and column experiments. Results show little effect of CH_4 on contaminant release and again confirmed the large adsorption capacity for As and Cd in these sediments.

4.2.1.2 Modeling

The effluent water from the column test (Lawter et al., 2016) has high concentrations of major elements (e.g., Si, Ca, Mg, Na, K), minor elements (e.g., Al, Fe, Mn), and trace elements (e.g., Sb, Sr, Ba, Cr, Se, As, Pb, Cs, Cu, and Zn). Reactive transport models were developed to interpret the concentration change of the alkali and alkaline earth metals, As and Pb. In these models, calcite dissolution and Ca-driven cation exchange are responsible for the release of alkali and alkaline earth metals, including Ca, Mg, Na, K, Sr, Cs, and Ba; adsorption/desorption are the reactions that control the release of As and Pb. Because Pb, As, and Ba are included in the third-generation ROM, the reactive transport models for the column are very helpful to define the key reactions that control Pb, As, and Ba. Note that Cd is considered in the third-generation ROM, but the Cd was not detected in the column test; the reactive transport model for the column test thus cannot help to define the reactions for Cd. The details of these reactions are listed in Zheng et al. (2016).

Model interpretation of the column test also helped us to constrain key parameters. The parameters that were calibrated based on experimental data were calcite volume fraction, CEC, and the volume fraction of adsorbent (goethite). A limited amount of calcite that would be depleted after the intrusion of CO_2 was key to reproducing the pulse-like breakthrough curve of the concentration of alkali and alkaline earth metals in the effluent of the column test. A volume fraction of 0.045% and a specific surface area of 60 cm^2/g were used for calcite, which led to a decent fit of the measured breakthrough curve of pH and Ca (Figure 9 and Figure 11). Calcite was not observed by XRD because the volume fraction was well below the detection limit of 1%, but a Ca bearing coating was detected in CNG 60 by SEM/EDS analysis. It is also noteworthy that a volume fraction of calcite below the XRD detection limit was also used in the model for the field test described in Trautz et al. (2013), where the presence of calcite in the sediments was later confirmed by micro-X ray spectroscopy. When deriving the third-generation ROM, a range of 0─20% was used for calcite volume fraction, which covers the value calibrated based on the column test data.

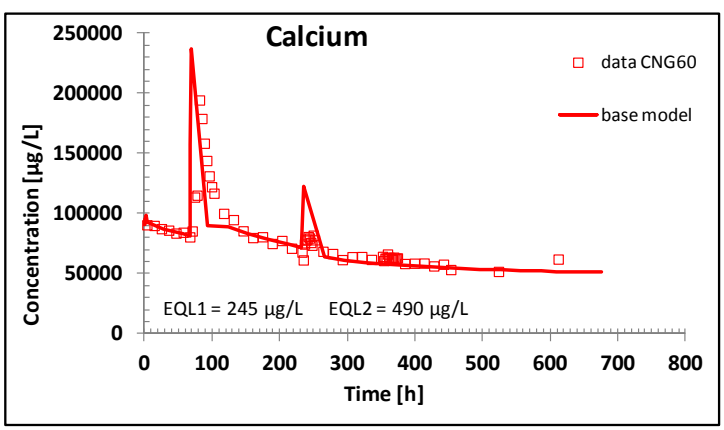

Figure 11: Simulated and observed breakthrough curves of Ca for the column test of sample CNG60.

The key parameter relevant to Ba is the cation exchange capacity of the sediment; the calibrated CEC is 1.55 meq/100 g, which falls in the range of CECs that were used in the third-generation ROM. Another parameter is related to the adsorption/desorption reactions that control the release of As and Pb. In the reactive transport model that was used to derive the third-generation ROM, the adsorption capacity depends on the product of the amount of adsorbent and the surface area of the adsorbent. Therefore, the amount of adsorbent is considered as an input parameter in the ROM, while the surface area of adsorbent is fixed. Using a surface area of 40 m^2/g, the calibrated amount of adsorbent (volume fraction of the goethite in this case) is 0.019 based on the column test data, which leads to a decent fit of measured data (Figure 12).

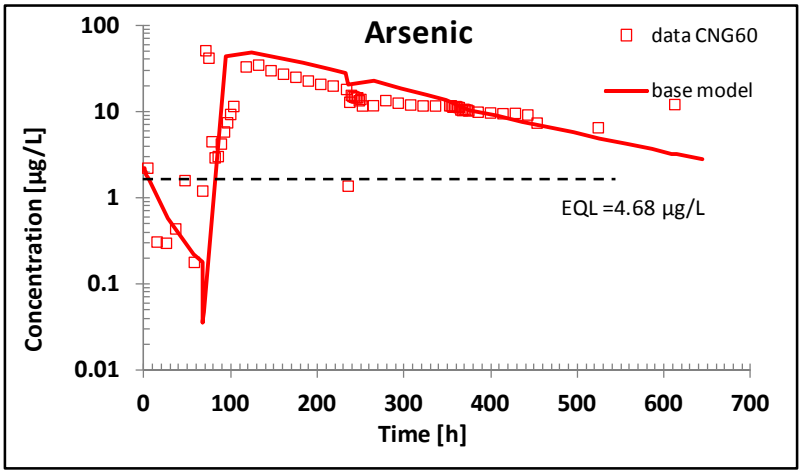

Figure 12: Simulated and observed breakthrough curves of As for the column test of sample CNG60.

In summary, laboratory experiments integrated with reactive transport model simulations are very useful to find out the key chemical reactions and parameters that control the response of an aquifer to the leakage of CO_2. Regarding the third-generation ROM that is based on the conditions of the High Plains Aquifer, the reactive transport models for the column tests confirm the reactions taken into account in the ROM and parameter ranges for reactions related to Pb, As, and Ba. Because Cd and organic compounds were not detected or measured in the column test, reactions and parameters for these constituents cannot be evaluated via a reactive transport model for the column tests.

4.2.2 Edwards Aquifer

4.2.2.1 Experimental Results

The outcomes of the column experiments relative to the aquifer maximum concentrations and MCLs are summarized in Table 24. Concentrations are generally higher during the stop-flow periods. At the end of the first stop-flow period, all of the trace metals except for Cr exceed the maximum aquifer-observed values, and As, Pb, Sb, and Se exceed the MCL limits. However, concentrations of the trace metals generally decrease during the flow periods, and at the end of the second stop-flow period, Ba and Cr exceed the observed aquifer maximums and only As, Pb, and Sb exceed the MCL. By the last flow period, only Sb and Se exceed the aquifer maximum threshold and no trace metals exceed their respective MCLs.

Table 24: Summary of Column Experiment Trace Metal Concentrations at the End of Each Experimental Stage, Relative to Aquifer Maximum Concentrations and MCL Regulatory Limits (grey background indicates aquifer maximum exceeded, black background indicates MCL exceeded)

Experiment Stage	As	Ba	Cr	Cu	Pb	Sb	Se
Flow 1	1.00	19.5	0.590	1.52	1.32	0.690	3.01
Stop-Flow 1	44.7	203	2.03	58.2	817	17.8	150
Flow 2	0.460	10.8	0.580	1.80	0.180	0.170	1.07
Stop-Flow 2	10.1	88.2	18.1	10.9	45.0	8.64	34.5
Flow 3	0.750	5.66	0.460	0.660	0.150	0.210	2.56
Threshold	**As**	**Ba**	**Cr**	**Cu**	**Pb**	**Sb**	**Se**
Aquifer Max, µg/L	1.11	69.9	5.57	57.3	0.15	0.06	1.40
MCL, µg/L	10	2,000	100	1,300	15	6	50

4.2.2.2 Modeling

Figures 13–19 show the model predictions for trace metal concentrations compared to column experimental results for Samples 1 and 3, and are compared to aquifer median and maximum concentrations, as well as the EPA MCL values. The release of the trace metals with time is very different in shape than that of the major ions. Whereas the major ions increase to a stable value with time and show small spikes during the stop-flow events, the trace metal concentrations generally decrease with time and show relatively large spikes during the stop-flow events. Arsenic concentrations during the flow periods are relatively stable, decreasing slightly between the first and second flow periods and increasing again during the third flow period, spiking above the MCL during the first stop-flow period, and reaching the MCL at the start of the second stop-flow period (Figure 13). Barium concentrations spike above the aquifer maximum during the stop-flow periods, but fall below the aquifer median during the flow periods (Figure 14). Chromium concentrations spike above the aquifer maximum during the stop-flow periods, but fall below the aquifer median during the flow periods (Figure 15). Copper concentrations remain between the aquifer median and maximum for the duration of the experiment (Figure 16). Lead concentrations spike above the MCL threshold initially and during both stop-flow events, finally falling beneath the aquifer maximum near the end of the experiment (Figure 17). Antimony concentrations spike above the MCL thresholds during the two stop-flow events, and remain above the aquifer maximum for the duration of the experiment (Figure 18). Selenium concentrations spike above the MCL threshold during the two stop-flow events and average close to the aquifer maximum for the duration of the experiment (Figure 19).

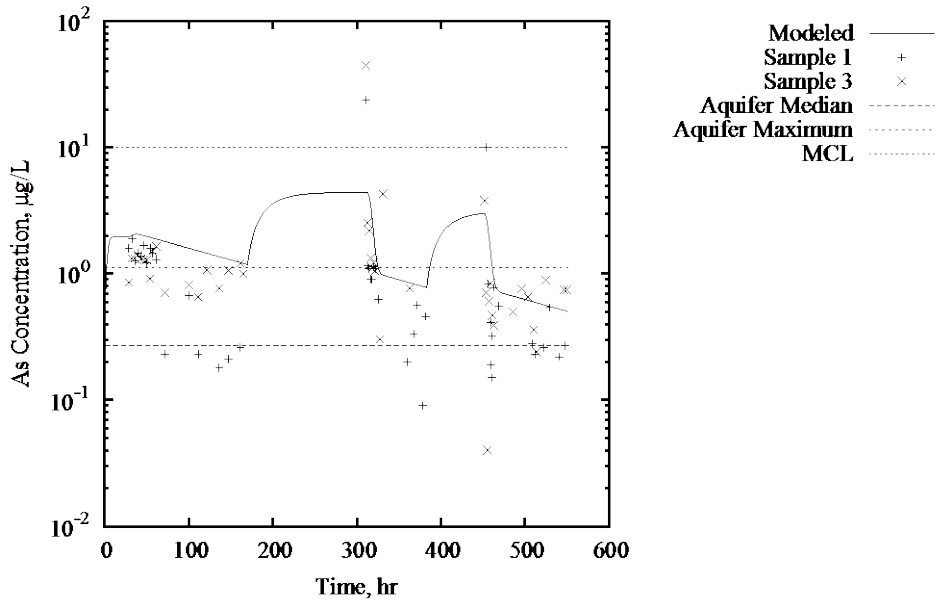

Figure 13: As modeling results compared to column experiment results and aquifer concentrations.

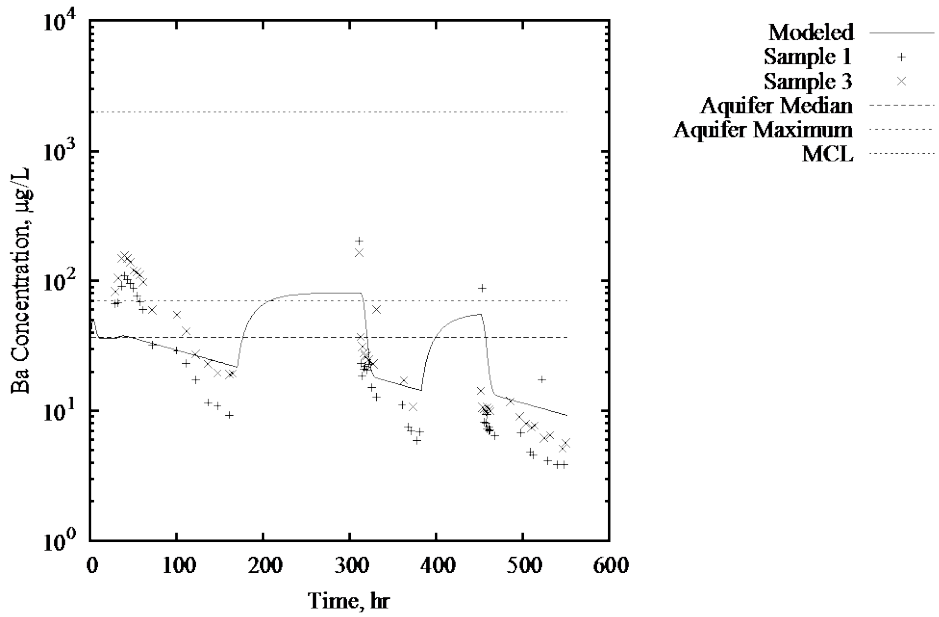

Figure 14: Ba modeling results compared to experimental results and aquifer concentrations.

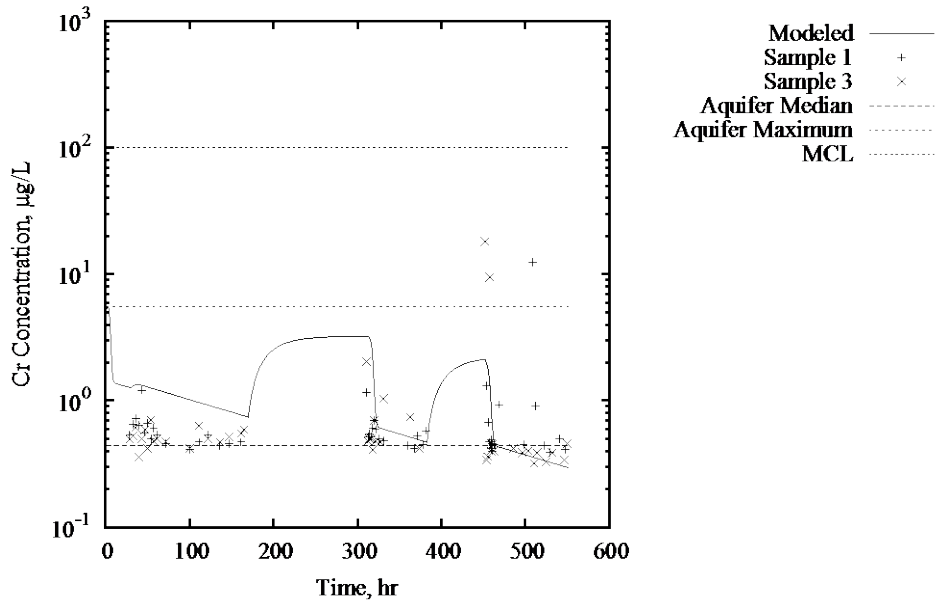

Figure 15: Cr modeling results compared to experimental results and aquifer concentrations.

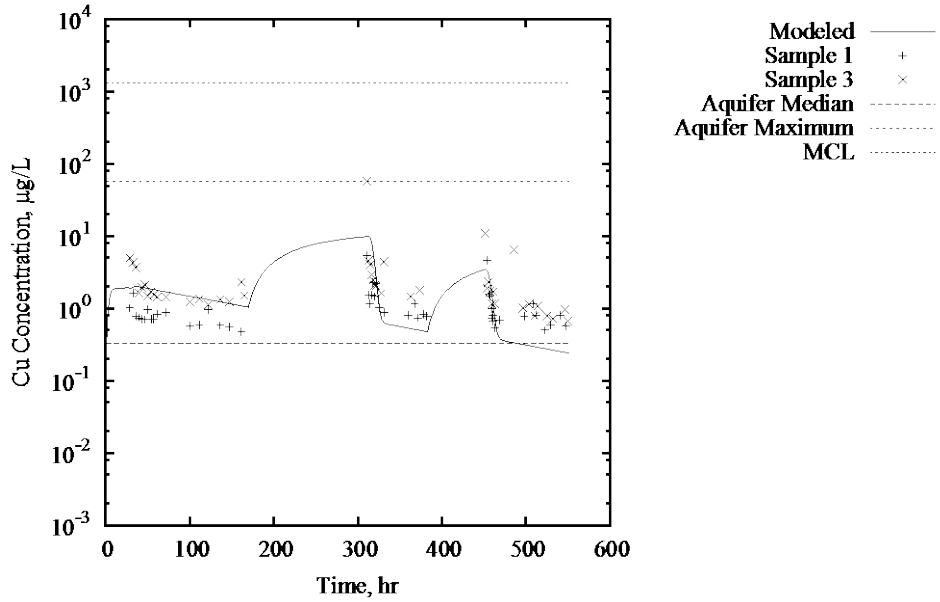

Figure 16: Cu modeling results compared to experimental results and aquifer concentrations.

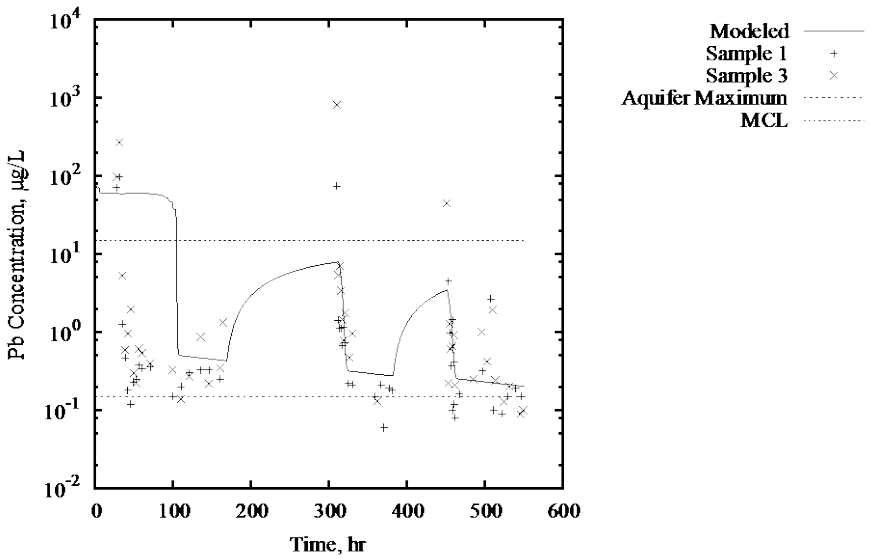

Figure 17: Pb modeling results compared to experimental results and aquifer concentrations. Aquifer median concentrations are below detection.

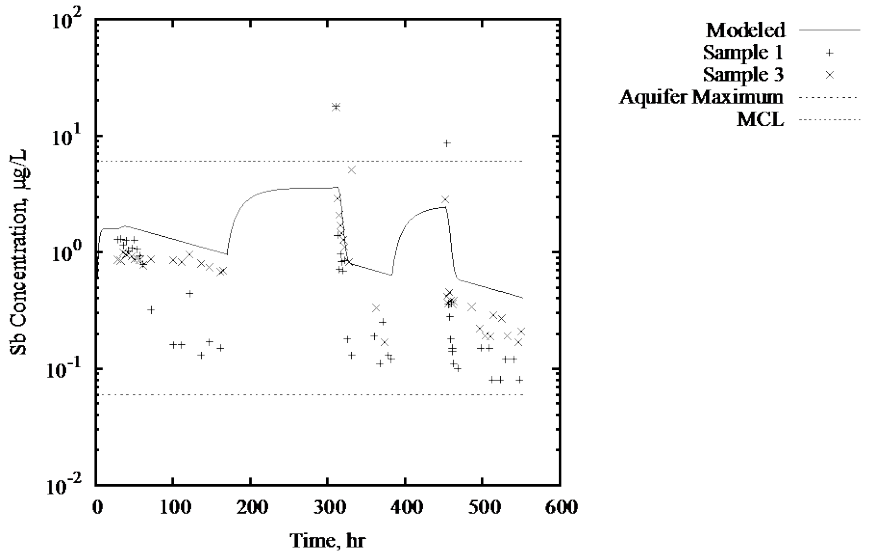

Figure 18: Sb modeling results compared to experimental results and aquifer concentrations. Aquifer median concentrations are below detection.

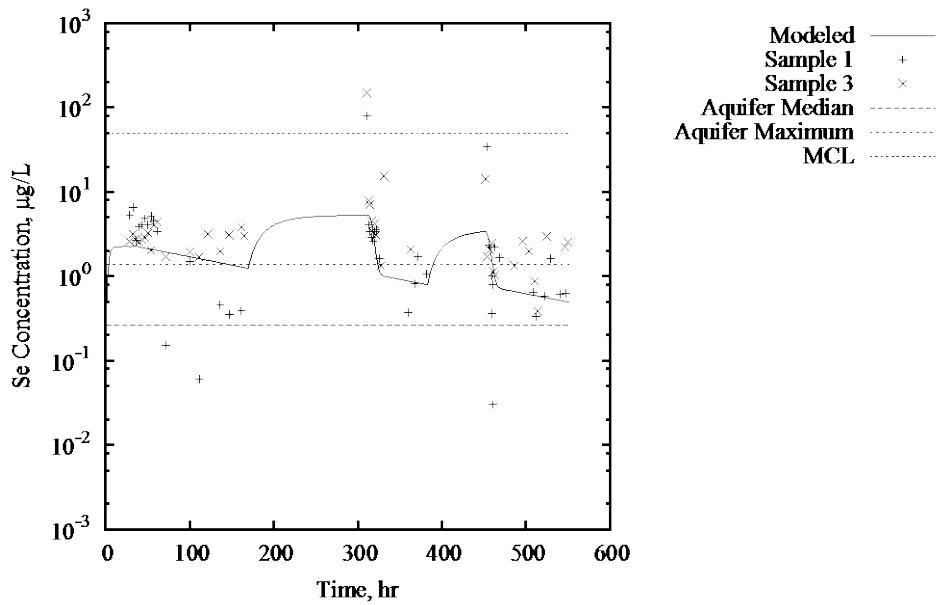

Figure 19: Se modeling results compared to experimental results and aquifer concentrations

4.2.3 Other Aquifers

Despite detectable contaminant concentrations in their batch study, Kirsch et al. (2014) concluded that the low level of released contaminants during experiments also indicates a low risk for impacting groundwater quality. Mickler et al. (2013) conducted laboratory batch experiments as well as a single-well push-pull field test and found that several of the elements initially mobilized after introduction of CO_2 (Mo, V, Zn, Se, and Cd) were removed from solution by the end of the experiment. Mickler et al. (2013) observed several other elements increase in concentration, but only Mn exceeded EPA MCLs.

In addition to experimental work, numerical modeling has been used to conduct a generic evaluation of the potential groundwater quality changes as a result of the hypothetical leakage of CO_2 (Apps et al., 2010; Carroll et al., 2009; Wang and Jaffe, 2004; Wilkin and Digiulio, 2010; Zheng et al., 2009; Vong et al., 2011; Altevogt and Jaffe, 2005; Jacquemet et al., 2011), and also to understand the chemical processes that control the CO_2-induced release of metals via model interpretation of laboratory experiments (Kirsch et al., 2014; Viswanathan et al., 2012; Wunsch et al., 2014) and field tests (Trautz et al., 2013; Zheng et al., 2012). In general, these models predicted the release of trace metals such as Pb and As (Wang and Jaffe, 2004; Apps et al., 2010; Zheng et al., 2009), which is largely consistent with the observations from laboratory experiments (Smyth et al., 2009; Lu et al., 2010; Little and Jackson, 2010; Humez et al., 2013; Wunsch et al., 2014; Viswanathan et al., 2012; Varadharajan et al., 2013; Kirsch et al., 2014), although the type of metal being released and the severity of release vary among these experiments.

However, release of trace metals, especially those of environmental relevance such as As, Pb, Ba, and Cd, have not been observed in field tests (Peter et al., 2012; Yang et al., 2013; Trautz et al., 2013; Spangler et al., 2010; Cahill and Jakobsen, 2013; Kharaka et al., 2010). The difference between the observation of laboratory and field tests in terms of the release of trace metals is

likely because the laboratory experiments are more aggressive in leaching out trace metals due to the use of DI water, manipulation of the particle size of material tested, oxidation, high water/solid ratios, and longer reaction time. However, release of alkali and alkaline earth metals, including Na, K, Ca, Mg, Sr, and Ba, were commonly observed in both the laboratory and field experiments, although the degree of release is different in the laboratory versus the field tests. The rise in concentrations of dissolved constituents observed during field tests is typically much less pronounced than in laboratory experiments—field tests show increases of about an order of magnitude or less compared to pre-CO_2 levels (20% to 700% in the studies cited above), while orders-of-magnitude increases have been observed in laboratory tests.

Despite potential trace metal release, most current research results show releases below the EPA MCL requirements for drinking water, resulting in a small potential risk for groundwater aquifers due to CO_2 leakage when considering current water quality regulations. However, if studies used a "no-impact" threshold, as discussed in Section 3.1, the risk might be larger. In addition, studies thus far have focused on aquifer variability; very few have been published on variables in the injected or upward migrating gas stream or aquifer brine composition. A variety of compositions may be present in the gas stream due to the presence of trace contaminants remaining after the CO_2 capture process. Methane, for example, can be present as an impurity in the injection gas (Blanco et al., 2012; Mohd Amin et al., 2014). Methane can also be present as a native gas within the reservoir (Taggart, 2010; Oldenburg and Doughty, 2011; Hosseini et al., 2012), or could be produced through methanogenesis either in the reservoir or after CO_2 enters the aquifer (Leu et al., 2011). Inclusion of methane prior to injection can lead to several challenges, including increased pressure needed for transport and reduced CO_2 capacity during transport and storage due to the buoyancy of methane (Blanco et al., 2012; Hosseini et al., 2012). Despite problematic properties of methane, presence of this gas has also been shown to be beneficial. Modeling by Mohd Amin et al. (2014) showed reduced transportation of acidic CO_2 saturated brine, resulting in reduced dissolution of the storage reservoir caprock. Taggart (2010) created a model showing CO_2 driving out dissolved methane from reservoir brine, creating a leading CH_4 plume that could be useful for monitoring leakage. Taggart (2010) also suggests the methane could be recovered for energy production.

4.3 CHANGES IN ORGANIC CONTAMINANT CONCENTRATIONS

4.3.1 High Plains Aquifer

In the experiments conducted with the High Plains Aquifer sediments (Lawter et al., 2016), no measurements were conducted to determine the organic compounds in the aqueous phase of the batch experiments or in the column effluents, although the organic matter concentration in these sediments seems to be low based on visual observations. However, when CO_2 and brine move up from the storage reservoir, they can carry organic compounds, especially if the CO_2 is stored in a depleted oil reservoir. Therefore, in the third-generation ROM for High Plains Aquifers, organic compounds were included in reactive transport models, and subsequently in the derived ROM.

When organic compounds were included in the reactive transport models, it was necessary to determine which compounds to include and what their prospective concentrations in the leaking CO_2 and brine were. Although the organic compounds present in deep saline aquifers were seldom reported, their compositions in waters produced from oil fields have been extensively studied (RøeUtvik, 1999; Witter and Jones, 1999). The most common dissolved hydrocarbons

are benzene, toluene, ethylbenzene, xylenes BTEX, PAHs, and phenols. To simplify the model, benzene is used to represent BTEX, naphthalene to represent PAHs, and phenol to represent phenols. The respective maximum concentrations in the brine were taken from Zheng et al. (2010) (Table 25), which were largely based on the concentration of these compounds in the production water (Kharaka and Hanor, 2007). The minimum concentrations were arbitrary.

Table 25: Organics Concentrations in Brine Considered in the Reactive Transport Model (Zheng et al., 2010)

Organic Compounds	Minimum	Maximum	Unit
Benzene	-10	-3.2	Log_{10}[mol kg^{-1}]
Naphthalene	-10	-3.7	Log_{10}[mol kg^{-1}]
Phenol	-10	-4.1	Log_{10}[mol kg^{-1}]

Oxidation of the organics was calculated with first-order degradation kinetics:

$$\frac{dC}{dt} = -KC \tag{9}$$

where C is the concentration of the organic compound and K is the first-order rate constant, which was treated as a variable parameter.

Linear adsorption isotherms are used to model the adsorption of organic compounds; the key parameter is the distribution coefficient, Kd. The range for the distribution coefficient and degradation constant are listed in Table 26.

Table 26: Distribution Coefficient and Degradation Constant for Organic Compounds

Parameter	Range
Benzene distribution coefficient (L/kg)	-4.5* to 0.69[a]
Phenol distribution coefficient (L/kg)	-6.0* to 0.15[a]
Naphtalene distribution coefficient (L/kg)	-3.1* to 1.98[a]
Benzene degradation constant (1/s)	0 to -6.1[a]
Phenol degradation constant (1/s)	0 to -5.63[a]
Naphtalene degradation constant (1/s)	0 to -6.45[a]

(a) indicates log10 values

Around 500 simulations have been conducted to account for the uncertainties of both flow and chemical parameters. The following graphs show results from one of the simulations to illustrate the spatial distribution of organic compounds after 200 years of leakage. For details of other

conditions of the model, refer to Carroll et al. (2014). The key parameters used in this particular simulation are listed in Table 27.

Table 27: Flow and Chemical Parameters used in Simulations that Model Results

Parameter	Value
Benzene concentration in the leaking brine (mol/L)	2.51E-7
phenol concentration in the leaking brine (mol/L)	1.41E-7
Naphthalene concentration in the leaking brine (mol/L)	8.9E-8
Benzene distribution coefficient (L/kg)	1.24E-2
phenol distribution coefficient (L/kg)	1.18E-3
Naphthalene distribution coefficient (L/kg)	2.75E-1
Benzene degradation constant (1/s)	0
phenol degradation constant (1/s)	3.7E-7
Naphthalene degradation constant (1/s)	0

Figure 20 shows the plume of pH, which can be used to approximate the movement of CO_2. In comparison, the plumes for organic compounds are very small. Figures 21 and 22 show the spatial distribution of benzene. Despite the continuous leakage of brine that contained a high concentration of benzene, the plume was fairly small and always surrounded the leakage point. The plume for naphthalene (Figures 23 and 24) was smaller than that of benzene because of stronger adsorption of naphthalene by aquifer sediments as manifested by the higher distribution coefficient for naphthalene. Phenol (Figures 25 and 26) had the smallest plume in comparison with that of benzene and naphthalene because phenol undergoes both adsorption and biodegradation.

In summary, the model results suggest that in comparison to the plume of pH or dissolved CO_2, the plumes for organic compounds were very small, and if the leakage stops, the plumes could quickly disappear due to adsorption and biodegradation.

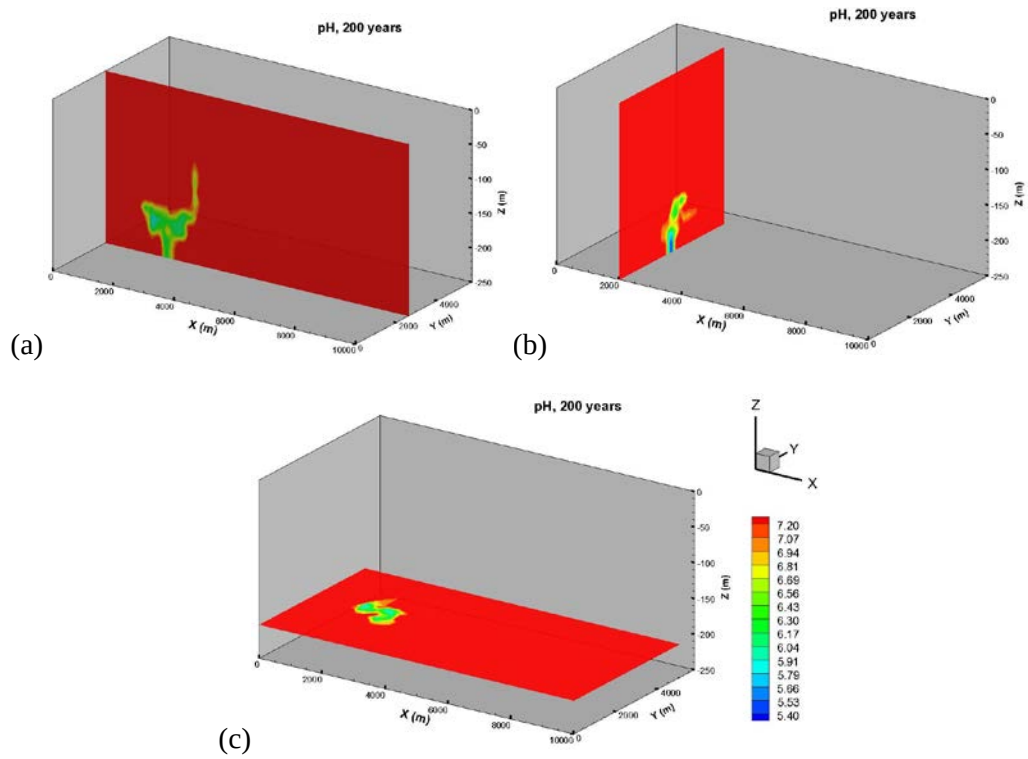

Figure 20: Cross section views of the spatial distribution of pH at 50, 200 years: (a) at y=2,600 m, (b) at x = 2,000 m, and (c) at z = -202.5 m.

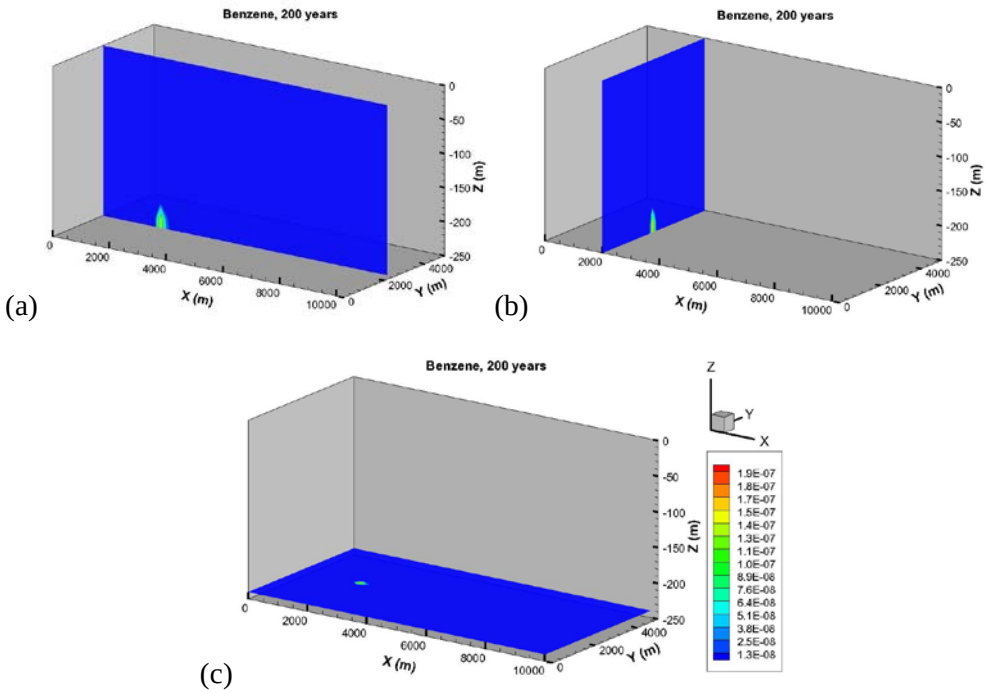

Figure 21: Cross section views of the spatial distribution of total aqueous benzene concentration at 200 years: (a) at y=2,600 m, (b) at x = 2,000 m, and (c) at z = -202.5 m

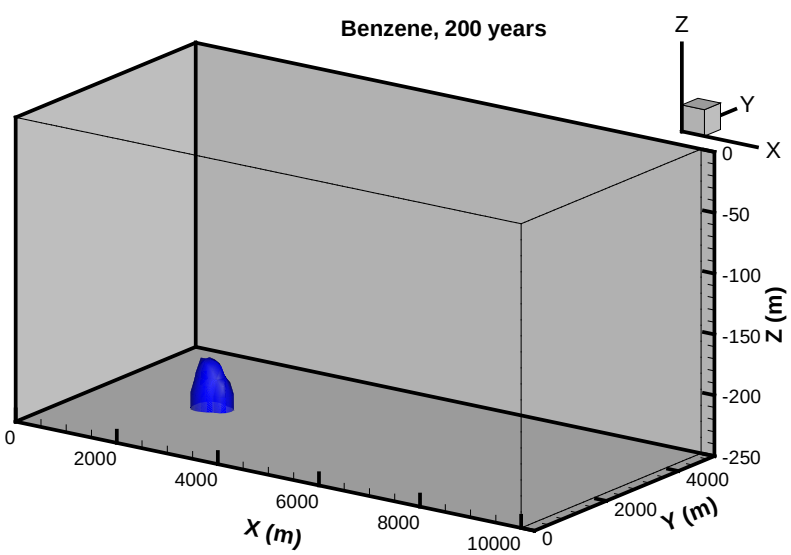

Figure 22: An iso-surface at benzene concentration of 3.84e-10 mol/L (0.03 µg/L, threshold value).

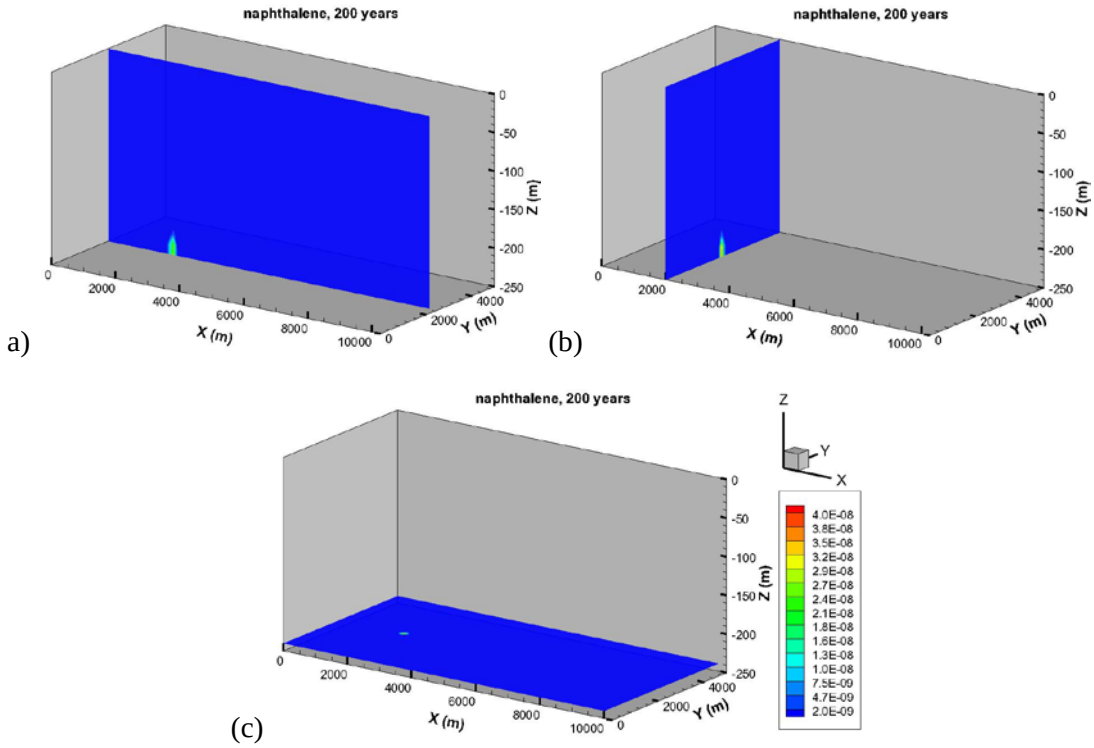

Figure 23: Cross section views of the spatial distribution of total aqueous naphthalene concentration at 200 years: (a) at y=2,600 m, (b) at x = 2,000 m, and (c) at z = -202.5 m.

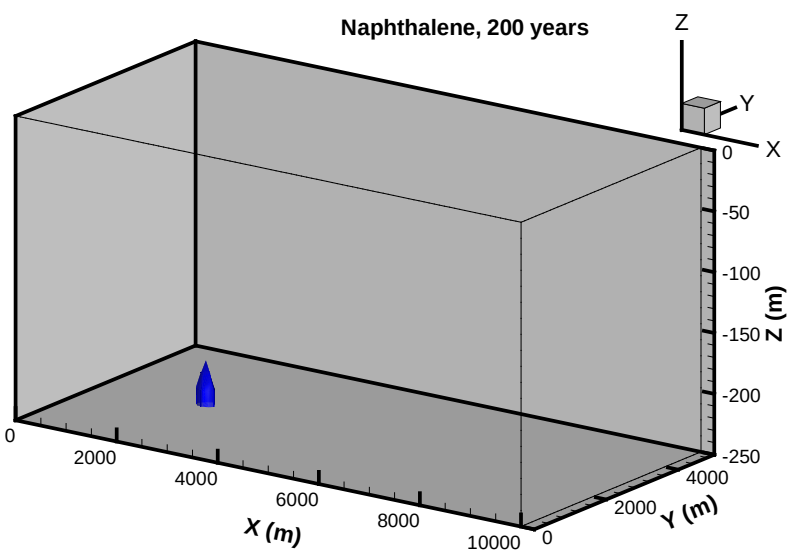

Figure 24: An iso-surface at naphthalene concentration of 1.53e-9 mol/L (0.2 µg/L, threshold value).

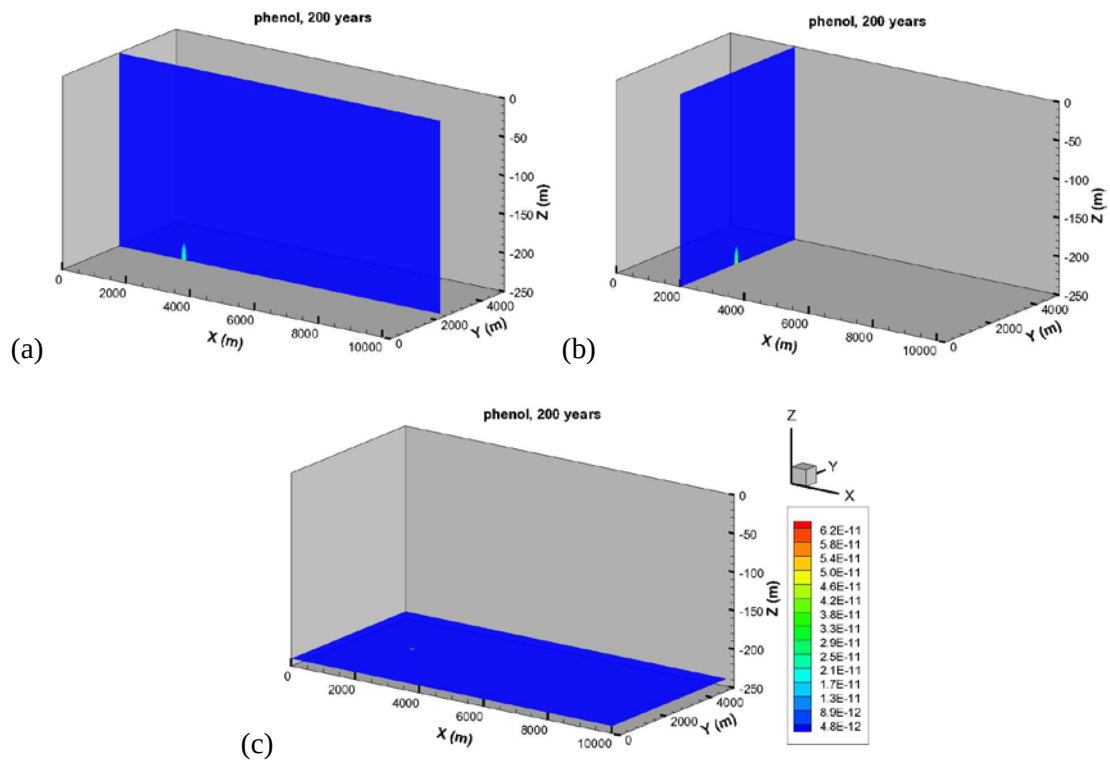

Figure 25: Cross section views of the spatial distribution of total aqueous phenol concentration at 200 years: (a) at y=2,600 m, (b) at x = 2,000 m, and (c) at z = -202.5 m

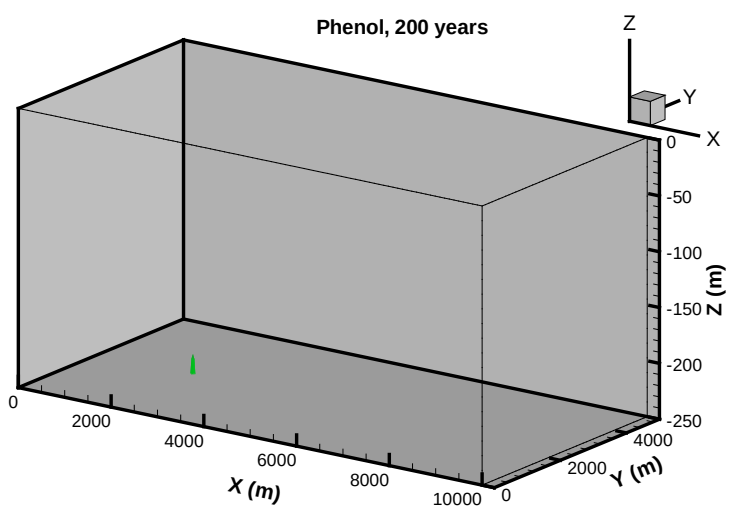

Figure 26: An iso-surface at naphthalene concentration of 3.19e-11 mol/L (0.003 µg/L, threshold value).

4.3.2 Edwards Aquifer

4.3.2.1 Modeling

The impact of organic compounds leaking into the Edwards Aquifer has been developed by Bacon et al. (2014). Three organic compounds (benzene, naphthalene, and phenol) are included in the model. As with the modeling of organic compounds in the High Plains Aquifer, benzene was included as a representative of BTEX; naphthalene as a representative of PAHs; and phenol as a representative of phenols. BTEX, phenols, and PAHs have been identified as the organic compounds that are most likely to be leached out along with CO_2 as well as pose threats on the quality of shallow groundwater (Zheng et al., 2013). The adsorption of the organic compounds was assumed to be controlled by a linear adsorption isotherm, proportional to the organic carbon content of the aquifer material. The organic carbon content of the limestone aquifer was assumed to range between 0.1 and 1% by volume. Input parameters for organic adsorption and biodegradation, along with the source of the inputs, are listed in Table 28.

Table 28: Input Parameters for Organic Adsorption and Biodegradation

Description	Minimum	Maximum	Units	Reference
Organic carbon volume fraction	1.00E-03	1.00E-02	—	Estimated
Benzene organic carbon partition coefficient	3.09E+01	5.37E+01	L/kg	(Lawrence, 2006)
Naphthalene organic carbon partition coefficient	9.93E+00	9.55E+02	L/kg	(Lawrence, 2006)
Phenol organic carbon partition coefficient	1.61E+01	3.02E+01	L/kg	(Boyd et al., 1983; Briggs, 1981)
Benzene aerobic biodegradation rate	1.00E-03	4.95E-01	day^{-1}	(Aronson et al., 1999)
Naphthalene aerobic biodegradation rate	6.40E-03	5.00E+00	day^{-1}	(Aronson et al., 1999)
Phenol aerobic biodegradation rate	6.00E-03	1.00E+01	day^{-1}	(Aronson et al., 1999)

The concentrations of organics in the leaking brine were assumed to be uncertain variables, with ranges shown in Table 29.

Table 29: Organic Concentration Ranges in Brine

Species in Brine	Minimum	Maximum	Units
Benzene	1.00E-10	6.31E-04	mol/L
Naphthalene	1.00E-10	7.94E-05	mol/L
Phenol	1.00E-10	2.00E-04	Mol/L

Initial concentrations of the organics in the aquifer were assumed to be zero, based on average aqueous concentrations for the 90 groundwater samples from the shallow, urban, unconfined portion of the Edwards Aquifer (Musgrove et al., 2010). This set of water samples was used to examine methodologies for establishing baseline datasets and statistical protocols for determining statistically significant changes between background concentrations and predicted concentrations that would be used to represent a contamination plume in the modeling presented in this report (Last et al., 2013). No-impact threshold values were determined that could be used to identify potential areas of contamination predicted by numerical models of carbon sequestration storage reservoirs (Table 30). Initial values of these concentrations were also determined using selected statistical methods; for comparison, the EPA MCL is also shown.

Table 30: Initial Values, Tolerance Limits, and Regulatory Standards for Each Variable

Analyte	Initial Value	"No-Impact" Threshold	Maximum Contaminant Level	Units
Benzene	0.000	0.016	5	µg/L
Naphthalene	0.000	0.400	0.2	µg/L
Phenol	0.000	0.005	10000	µg/L

The volume of groundwater exceeding the threshold values for organic compounds is influenced significantly by biodegradation. Volumes of groundwater with concentrations greater than the benzene, naphthalene and phenol no-impact threshold values are relatively small (Figure 27). By comparison, for the same set of simulations, the median pH-impacted aquifer volumes ranged from $1e^5$ m^3 at 10 years to $1e^7$ m^3 at 200 years.

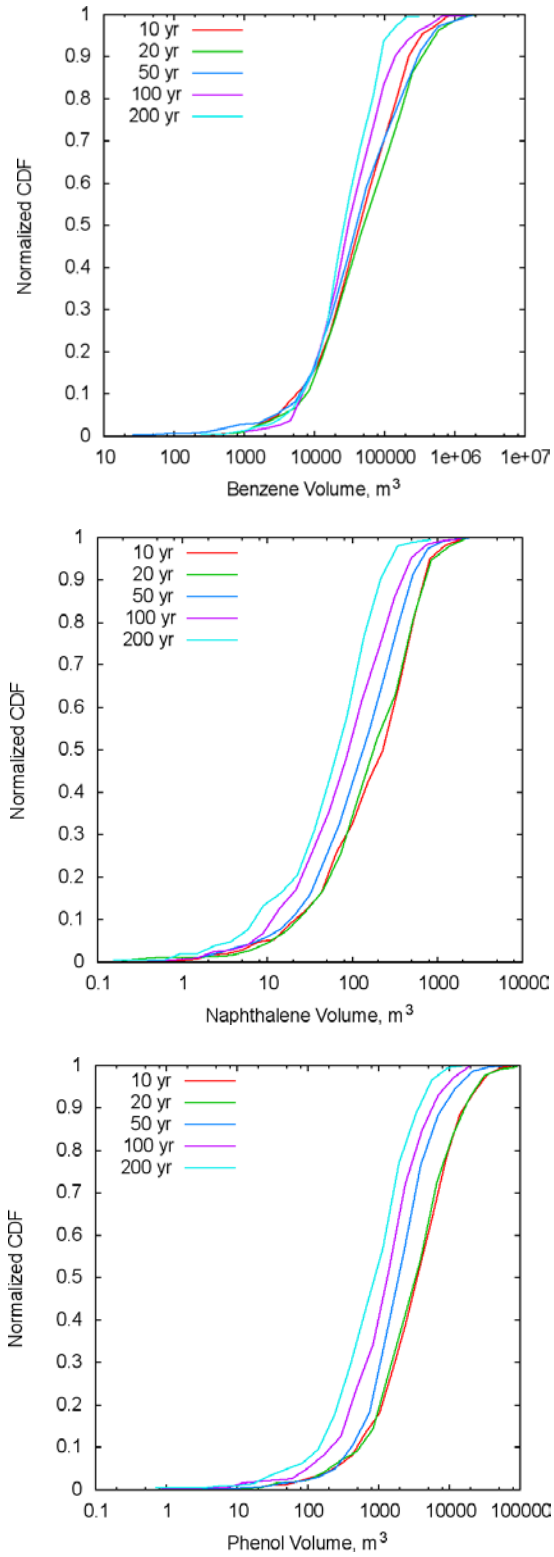

Figure 27: Cumulative density function of aquifer volume exceeding organic no-impact thresholds during 200 years of well leakage.

4.3.3 Reservoirs as a Source Term for Organic Compounds

Mobilization of toxic organic compounds, including BTEX, and PAHs by $scCO_2$, has been reported in laboratory experiments for rock samples from depleted oil reservoirs, coal deposits (Zhong et al., 2014), and sandstones (Scherf et al., 2011). Groundwater monitoring results from GCS demonstration sites have shown increased concentrations of BTEX, PAHs, phenols, and other toxic compounds in groundwater after CO_2 injection (Kharaka et al., 2009; Kharaka et al. 2010a; Kharaka et al. 2010b; Scherf et al., 2011). Zhong et al. (2014) focused on the transport and fate of toxic organic compounds mobilized by supercritical CO_2 from organic rich storage reservoirs such as unmineable coal seams and depleted oil reservoirs. Column experiments were conducted using a water wetted sandstone core installed in a tri-axial core holder to study the potential for toxic organic compounds mobilized from coal by supercritical CO_2 under simulated geologic carbon storage conditions to impact groundwater. The concentrations of the organic compounds in the column effluent and their distribution within the sandstone core were monitored. Results indicated that the mobility though the core sample was much higher for BTEX compounds than for naphthalene. Retention of organic compounds from the vapor phase to the core appeared to be primarily controlled by partitioning from the vapor phase to the aqueous phase according to Henry's Law. Accordingly, reduced temperature and elevated pressure resulted in greater partitioning of the mobilized organic contaminants into pore water. Adsorption to the surfaces of the wetted sandstone was also significant for naphthalene.

Cantrell and Brown (2014) conducted a modeling study and found that when CO_2 is introduced into a reservoir with 90 wt.% CO_2 and 10 wt.% oil, a significant fraction of the oil dissolves into the vapor phase. As the vapor phase moves up through the stratigraphic column, pressures and temperatures decrease, resulting in significant condensation of oil components. The heaviest organic components condense early in this process (at higher pressures and temperatures), while the lighter components tend to remain in the vapor phase until much lower pressures and temperatures are reached. The final concentrations to reach an aquifer at 1,520 kPa and 25°C were quite significant for benzene and toluene, indicating that these compounds could adversely impact groundwater quality (benzene in particular) in the event of a leak of CO_2 stored in a depleted oil reservoir. Conversely, it was determined that CO_2 was unlikely to transport significant concentrations of PAHs to near surface depths, limiting their potential impact to groundwater. This is particularly true for the most carcinogenic of the PAH compounds, which are relatively heavy, making them prone to condensation from the vapor phase at much higher pressures and temperatures.

5. CONCLUSIVE REMARKS

GCS is a global carbon emission reduction strategy involving the capture of CO_2 emitted from fossil fuel burning power plants, as well as the subsequent injection of the captured CO_2 gas into deep subsurface reservoirs, such as saline aquifers or depleted oil and gas reservoirs. A critical question that arises from the proposed GCS is the potential impacts of CO_2 injection on the quality of drinking-water systems overlying CO_2 sequestration storage sites.

Although storage reservoirs are evaluated and selected based on their ability to safely and securely store emplaced fluids, leakage of CO_2 from storage reservoirs is a primary risk factor and a potential barrier to the widespread acceptance of geologic CO_2 sequestration. Therefore, a systematic understanding of how CO_2 leakage would affect the geochemistry of potable aquifers, and subsequently control or affect contaminant release via dissolution, desorption, and/or redox reactions, is vital.

This report was written with the overall objective to identify the set of geochemical data and reactions and the hydrological processes required to assess and predict aquifer responses to CO_2 and brine leakage, to gather important site-specific data required to evaluate impacts, and to present and discuss potential risks for groundwater pollution due to CO_2 gas and brine exposure.

5.1 CRUCIAL SITE-SPECIFIC DATA

Establishing the mean and variance of background groundwater concentrations is necessary to determining whether there will be an impact due to leaking CO_2 and brine in groundwater aquifers. The resulting no-impact threshold values can be used to inform a “no change” scenario with respect to groundwater impacts. In some cases, the calculated no-impact threshold values may exceed regulatory standards. For instance, in the High Plains Aquifer, the no-impact threshold of 1,300 mg/L is significantly higher than the regulatory standard of 500 mg/L for TDS. Also, if there is little variability in background values there will be a higher likelihood that the threshold values will be exceeded. For instance, in the Edwards Aquifer, the mean value of pH (6.9) is only a few tenths of a pH point above the “no-impact” threshold of pH 6.6.

Determining the salinity, trace metal, and organic content of reservoir fluids is necessary to make accurate predictions of the impact to groundwater due to leaking brine. The contaminants of concern will depend on the characteristics of the reservoir brine, and whether there are significant differences between the reservoir pore water composition and the drinking water aquifer.

In order to make accurate predictions of the impact of leaking CO_2 on aquifer materials, calcite content in the sediment and/or aquifer rocks should be determined. There is a significant difference in the impact to pH on the High Plains Aquifer samples with and without calcite present. The Edwards Aquifer limestone, which consists mainly of calcite, shows a strong capacity to buffer pH changes due to interaction with CO_2.

It should also be determined whether there are other minerals in the aquifer that could dissolve under low pH conditions and contribute to increased TDS or trace metal concentrations. For instance, the dissolution of calcite can cause significant increases in dissolved calcium, raising TDS above background levels. Similarly, the dissolution of galena could cause increases in lead concentrations above background levels.

Measuring the amount and type of clays and the amount of calcite is important for estimating adsorption capacity and coefficients for trace metals. In the Edwards Aquifer, adsorption on calcite controls the release of trace metals after exposure to a lowered pH due to CO_2 exposure. In a sand and gravel aquifer like the High Plains, Fe oxides and hydroxides (such as, goethite and HFO), and clay minerals (such as illite, kaolinite, and montmorillonite) are important adsorbents.

If organic contaminants are mobilized from the injection reservoir and transported by the leaking CO_2 or brine, then determining the amount of organic matter and biodegradation potential in the aquifer is necessary in order to predict the persistence of organic contaminants in the aquifer. Establishing the redox potential of the aquifer is important, because measured biodegradation rates tend to be higher in oxidizing environments.

5.2 POTENTIAL RISK TO GROUNDWATER

Over the last decade, a number of studies have been undertaken to assess the impacts of potential CO_2 leakage from deep storage reservoirs on the quality of overlying freshwater aquifers. These studies include natural analogs, field-scale in-situ CO_2 injection, and laboratory-scale column and batch studies. However, the results of the studies are contradictory, as some indicate CO_2 leaks pose a serious risk and some indicate low levels of risk, while others have found possible benefits related to CO_2 leakage into groundwater. In an effort to reconcile these differing conclusions and to generate additional sets of data on this subject, experimental and modeling studies were conducted as part of the NRAP to define conditions under which impacts to groundwater may be significant.

Data presented in the literature and data collected from laboratory-scale experimental and modeling work conducted at PNNL and LBNL and supported by NRAP show that the aquifer responses are site-specific. Results from laboratory experimental work show that data generated from batch experiments often over predict total changes in the aquifer systems. This is due to the importance of leakage and flow rates, and because the reactions that control aqueous trace metal concentrations are time dependent (these concentrations were significantly lower during the flow portions of the column experiments but increased during stop-flows, indicating dependency on the fluid residence time and/or pH; pH also increased during the stop-flows). Additionally, both batch and columns experiments tend to be performed with size-segregated material that is more reactive due to its higher surface area to volume ratio; therefore, both types of experiments tend to provide more conservative estimates of aquifer impacts.

This report also shows that the development of site-specific conceptual and ROMs to describe and predict aquifer responses is possible. These models can then be used to estimate the degree of impact in terms of changes in the pH, major, minor, and trace element releases based on aquifer properties (e.g., initial aqueous concentration, mineralogy, etc.), changes in solid phase chemistry and mineralogy, changes in the extent and rate of reactions and processes and the establishment of a new network of reactions and processes affecting or controlling the overall response, leaking plume characteristics (gas composition, such as pure CO_2 and/or CO_2-CH_4 - H_2S mixtures), and brine concentration and composition.

These models are also able to predict the degree of impact, whether the changes in aquifer are significant or insignificant, the fate of the elements released from sediments or transported with brine, and the extent and rate of reactions such as precipitation/incorporation into minerals

(calcite and other minerals), adsorption, electron transfer reactions, and the role of natural attenuation.

Some modeling application of these models (Carroll et al., 2014) and various field studies (Table 4) indicate that results presented in this report and data from the literature estimate that there are cases where there may be measurable, long-term impacts to groundwater due to CO_2 or brine leaks.

Field-scale models of CO_2 and brine leakage, driven by models of CO_2 injection into a reservoir and leakage via abandoned wellbores of varying permeability, for the High Plains Aquifer and shallow, urban unconfined portion of the Edwards Aquifer, were used to calculate the volume of the aquifer above background thresholds due to CO_2 leaks of different rates. The volume of the impacted aquifer is very sensitive to the threshold values assumed; in most cases the regulatory threshold (EPA MCL) is significantly less limiting than the threshold value indicated by the background variability in aquifer concentrations, and so groundwater impacts are more pronounced when utilizing these no-impact thresholds.

When comparing the volumes of each of the two aquifers impacted by elevated trace metal concentrations, this study found that although initial adsorbed trace metal concentrations are lower in the Edwards sediments than the High Plains sediments, the background variability of the shallow, urban unconfined portion of the Edwards Aquifer is low compared to the High Plains Aquifer, leaving it more vulnerable to changes in groundwater quality due to CO_2 or brine leakage. A parameter sensitivity analysis shows that groundwater impacts are more sensitive to the leak rates of CO_2 and brine and hydraulic aquifer characteristics, such as permeability and groundwater flow rate, than to geochemical parameters, such as mineral dissolution rate, with the exception of the presence of calcite in the aquifer sediments.

A remaining question is whether trace metal releases due to leaking CO_2 are harmful. It could be argued that a small increase in lead concentrations above the “no-impact” threshold values in an aquifer will not have a measureable health impact. However, EPA MCL thresholds have been established to protect human health. Long-term increases above the MCL thresholds could therefore have the potential for negative impacts on human health.

Clearly, the scientific community has not yet reached an agreement on the important issue of deciding whether the impacts are negative, insignificant, or positive. One reason could be that the degree of perturbation and response to induced changes is site-specific and a function of inherent aquifer properties as well as the characteristics of the leaking plume (i.e., gas composition and brine concentration) at the specific site.

This study considered the risk to groundwater due to changes in pH, TDS, trace metals, and organics. The risk to groundwater is directly proportional to the mass of CO_2 or brine leaked. In many simulations considered in the NRAP risk analyses, the leaked mass is relatively small and plumes are not likely to be detected by the pumping of existing groundwater wells (Keating et al., 2014). However, zones of lowered pH and elevated TDS and trace metals may persist for decades. Based on biodegradation rates and sorption coefficients from the literature, organic plumes are not expected to persist in groundwater; further experimental research is needed to confirm this under site-specific conditions.

5.3 FUTURE EFFORTS

Over the last two decades, a number of laboratory and field experiments as well as modeling work have been conducted to study the impact of CO_2 and brine leakage on groundwater quality; this greatly enhances understanding on the magnitude of such impact and the controlling processes. However, questions remain and further investigations are required.

One of the remaining questions to be addressed as investigations move to the post-injection site care period is whether trace metals released during the leakage phase will recover to the background level of the aquifer and at what times scales this would happen when compared with the recovery of pH and dissolved CO_2 if the leakage were to be detected and stopped. Once the leakage stops, the plume of high CO_2 (dissolved or gaseous) and low pH will be diluted due to mixing with groundwater. As a result, the gaseous CO_2 will dissolve, and eventually, dissolved CO_2 will have a very low concentration. While it may not reach pre-leakage conditions, concentrations may become low enough to make aqueous pH return to values close to neutral (or, at least, higher than the EPA MCL of 6.5). Nevertheless, modeling studies (Zheng et al., 2015) and laboratory experiments (Fox et al., 2014) show that trace metals have fairly complex behavior in terms of recovery. Further studies are certainly warranted. Numerical models supported with laboratory experiments should be conducted to address this issue.

Organic contaminants mobilized from the injection reservoir were considered in development of the groundwater impact models for the High Plains and Edwards Aquifers. However, it is not known how these contaminants may partition between the CO_2 saturated aqueous and air phases as they travel up a borehole or other leakage path. Experiments are needed to determine how changes in pressure and temperature along the leakage path will affect phase partitioning of these contaminants. This will impact their long-term persistence once they arrive in the aquifer. Studies are also needed to determine the extent and rate of major and minor element release in the leakage pathway (i.e., from deep reservoirs to aquifers) under conditions of decreasing temperature and pressure.

While ROMs have been demonstrated as an effective tool to evaluate the risk associated with groundwater, the development of such models is challenging mainly because of the highly non-linear response of the impacted volume to the change of chemical parameters. For example, if the aquifer sediments are low in calcite content and calcite is removed due to dissolution, the volume of pH greater than the threshold changes sharply; this process is difficult to be emulated by ROMs. One potential solution is to further categorize aquifer conditions and develop ROMs for each condition. Currently, NRAP has two groundwater ROMs that are based on the Edward and High Plains Aquifers; both are designed for aquifers with appreciable pH buffering capacity. In the future, a ROM should be developed for aquifers with limited pH buffering capacity.

6. REFERENCES

Altevogt, A. S.; Jaffe, P.R. Modeling the Effects of Gas Phase CO_2 Intrusion on the Biogeochemistry of Variably Saturated Soils. *Water Resources Research* **2005,** *41*.

Annunziatellis, A.; Beaubien, S. E.; Bigi, S.; Ciotoli, G.; Coltella, M.; Lombardi, S. Gas Migration Along Fault Systems and through the Vadose Zone in the Latera Caldera (Central Italy): Implications for CO_2 Geological Storage. *Int. J. Greenhouse Gas Control* **2008,** *2*, 353–72.

Appelo, C. J. A.; Postma, D. Geochemistry, Groundwater and Pollution. A.A.Balkema: Rotterdam, Netherlands, 1994.

Apps, J. A.; Zheng, L. G.; Spycher, N.; Birkholzer, J. T.; Kharaka, Y.; Thordsen, J.; Kakouros, E.; Trautz, R. Transient Changes in Shallow Groundwater Chemistry During the MSU ZERT CO_2 Injection Experiment. *10th International Conference on Greenhouse Gas Control Technologies* **2011,** *4*, 3231–38.

Apps, J. A.; Zheng, L.; Zhang, Y.; Xu, T.; Birkholzer, J. T. Evaluation of Potential Changes in Groundwater Quality in Response to CO_2 Leakage from Deep Geologic Storage. *Transport Porous Med.* **2010,** *82*, 215–46.

Aronson, D.; Citra, M.; Shuler, K.; Printup, H.; Howard, P. H. Aerobic Biodegradation of Organic Chemicals in Environmental Media: A Summary of Field and Laboratory Studies; Technical; U.S. EPA: North Syracuse, NY, 1999.

Arthur, J.; Dabous, A.; Cowart, J. Mobilization of Arsenic and Other Trace Elements During Aquifer Storage and Recovery, Southwest Florida. In U.S. Geological Survey Artificial Recharge Workshop; Aiken, G. R., Kuniansky, E. L., Eds. USGS: Sacramento, CA, 2002.

Bachu, S. CO_2 Storage in Geological Media: Role, Means, Status, and Barriers to Deployment. *Progress in Energy and Combustion Science* **2008,** *34*, 254–73.

Bacon, D. H.; Dai, Z.; Zheng, L. Geochemical Impacts of Carbon Dioxide, Brine, Trace Metal and Organic Leakage into an Unconfined, Oxidizing Limestone Aquifer. *Energy Procedia* **2014,** *63*, 4684–707.

Bacon, D. *Reduced Order Model for the Geochemical Impacts of Carbon Dioxide, Brine, and Trace Metal Leakage into an Unconfined, Oxidizing Carbonate Aquifer, Version 2.1*; PNNL-22285; Pacific Northwest National Laboratory, 2013.

Bacon, D.; Qafoku, N.; Dai, Z.; Keating, E.; Brown, C. Modeling the Impact of Carbon Dioxide Leakage into an Unconfined, Oxidizing Carbonate Aquifer. *International Journal of Greenhouse Gas Control* **2016,** *44*, 290–99.

Birkholzer, J. T.; Apps, J.; Zheng, L.; Zhang, Y.; Xu, T.; Tsang, C.-F. *Research Project on CO_2 Geological Storage and Groundwater Resources, Quality Effects Caused by CO_2 Intrusion into Shallow Groundwater*; Technical Report; Technical, Earth Sciences Division, Lawrence Berkeley National Laboratory: Berkeley, CA, 2008.

Blanco, S. T.; Rivas, C.; Fernandez, J.; Artal, M.; Velasco, I. Influence of Methane in CO_2 Transport and Storage for CCS Technology. *Environmental Science & Technology* **2012,** *46*, 13016–23.

Boyd, S. A.; Shelton, D. R.; Berry, D.; Tiedje, J. M. Anaerobic Biodegradation of Phenolic-Compounds in Digested-Sludge. *Appl Environ Microb* **1983,** *46*, 50–54.

Briggs, G. C. Theoretical and Experimental Relationships between Soil Adsorption, Octanol-Water Partition- Coefficients, Water Solubilities, Bioconcentration Factors, and the Parachor. *J. Agric. Food Chem.* **1981,** *29*,1050–59.

Cahill, A. G.; Jakobsen, R. Hydro-Geochemical Impact of CO_2 Leakage from Geological Storage on Shallow Potable Aquifers: A Field Scale Pilot Experiment. *Int. J. Greenhouse Gas Control* **2013a,** *19*, 678–88.

Cahill, A.G.; Jakobsen, R.; Mathiesen, T. B.; Jensen, C. K. Risks Attributable to Water Quality Changes in Shallow Potable Aquifers from Geological Carbon Sequestration Leakage into Sediments of Variable Carbonate Content. *Int. J. Greenhouse Gas Control* **2013b,** *19*, 117–25.

Cantrell, K. J.; Brown, C. F. Source Term Modeling for Evaluating the Potential Impacts to Groundwater of Fluids Escaping from a Depleted Oil Reservoir Used for Carbon Sequestration. *Int. J. Greenhouse Gas Control* **2014,** *27*, 139–45.

Caritat, P. D.; Hortle, A.; Raistrick, M.; Stalvies, C.; Jenkins, C. Monitoring Groundwater Flow and Chemical and Isotopic Composition at a Demonstration Site for Carbon Dioxide Storage in a Depleted Natural Gas Reservoir. *Applied Geochemistry* **2013,** *30*, 16–32.

Carroll, S. A.; Bianchi, M.; Mansoor, K.; Zheng, L.; Sun, Y.; Spycher, N.; Birkholtzer, J. *Reduced-Order Model for Estimating Impacts from CO_2 Storage Leakage to Alluvium Aquifers: Third-Generation Combines Physical and Chemical Processes*; NRAP Technical Report Series; U.S. Department of Energy, National Energy Technology Laboratory: Morgantown, WV, 2016.

Carroll, S. A.; Keating, E.; Mansoor, K.; Dai, Z.; Sun, Y.; Trainor-Guitton, W.; Brown, C.; Bacon, D. Key Factors for Determining Groundwater Impacts Due to Leakage from Geologic Carbon Sequestration Reservoirs. *Int. J. Greenhouse Gas Control* **2014,** *29*, 153–68.

Carroll, S.; Hao, Y.; Aines, R. Geochemical Detection of Carbon Dioxide in Dilute Aquifers. *Geochem. Trans.* **2009,** 10. http://www.geochemicaltransactions.com/content/10/1/4

Celia, M. A.; Nordbotten, J. M. Practical Modeling Approaches for Geological Storage of Carbon Dioxide. *Ground Water* **2009,** *47*, 627–38.

Costagliola, P.; Bardelli, F.; Benvenuti, M.; Di Benedetto, F.; Lattanzi, P.; Romanelli, M.; Paolieri, M.; Rimondi, V.; Vaggelli, G. Arsenic-Bearing Calcite in Natural Travertines: Evidence from Sequential Extraction, Mu Xas, and Mu Xrf. *Environ. Sci. Technol.* **2013,** *47*, 6231–38.

Dafflon, B.; Wu, Y. X.; Hubbard, S. S.; Birkholzer, J. T.; Daley, T. M.; Pugh, J. D.; Peterson, J. E.; Trautz, R. C. Monitoring CO_2 Intrusion and Associated Geochemical Transformations in a Shallow Groundwater System Using Complex Electrical Methods. *Environ. Sci. Technol.* **2013,** *47*, 314–21.

Damen, K.; Faaij, A.; van Bergen, F.; Gale, J.; Lysen, E. Identification of Early Opportunities for CO_2 Sequestration-Worldwide Screening for CO_2-EOR and CO_2-ECBM Projects. *Energy* **2005,** *30*, 1931–52.

DeSimone, L. A. Quality of Water from Domestic Wells in Principal Aquifers of the United States, 1991–2004; Scientific Investigations Report 2008–5227; U.S. Geological Survey: Reston, VA, 2009.

Di Benedetto, F.; Costagliola, P.; Benvenuti, M.; Lattanzi, P.; Romanelli, M.; Tanelli, G. Arsenic Incorporation in Natural Calcite Lattice: Evidence from Electron Spin Echo Spectroscopy. *Earth and Planetary Science Letters* **2006,** *246*, 458–65.

Dixit, S.; Hering, J. G. Comparison of Arsenic(V) and Arsenic(III) Sorption onto Iron Oxide Minerals: Implications for Arsenic Mobility. *Environ. Sci. Technol.* **2003,** *37*, 4182–89.

DOE. Carbon Sequestration Technology Roadmap and Program Plan; U.S. Department of Energy (DOE), National Energy Technology Laboratory (NETL): Washington DC, 2007.

Donahue, R. B.; Barhour, S. L.; Headley, J. V. Diffusion and Adsorption of Benzene in Regina Clay. *Can. Geotech. J.* **1999,** *36*, 430–42.

Dzombak, D. A.; Morel, F. M. M. *Surface Complexation Modeling-Hydrous Ferric Oxide*; John Wiley & Sons: New York, 1990.

EPA. *Statistical Analysis of Groundwater Monitoring Data at RCRA Facilities, Unified Guidance*; Technical Rpt. EPA 530/R-09-007; U.S. Environmental Protection Agency. Washington, DC, 2009.

Fox, P. M.; Nico, P. S.; Davis, J. A.; Spycher, N. Impact of Elevated CO_2 on Release of Trace Elements from Aquifer Sediments of the San Joaquin Valley, Ca. Presented at the AGU Fall Meeting, 2014.

Frye, E.; Bao, C.; Li, L.; Blumsack, S. Environmental Controls of Cadmium Desorption During CO2 Leakage. *Environ. Sci. Technol* **2012,** *46*, 4388–95.

Goldberg, S. Competitive Adsorption of Arsenate and Arsenite on Oxides and Clay Minerals. *Soil Sci. Soc. Am. J.* **2002,** *66*, 413–21.

Gu, X.; Evans, L. J. Modelling the Adsorption of Cd(II), Cu(II), Ni(II), Pb(II), and Zn(II) onto Fithian Illite. *Journal of Colloid and Interface Science* **2007,** *307*, 317–25.

Gu, X.; Evans, L. J. Surface Complexation Modelling of Cd(II), Cu(II), Ni(II), Pb(II) and Zn(II) Adsorption onto Kaolinite. *Geochimica et Cosmochimica Acta* **2008,** *72*, 267–76.

Gu, X.; Evans, L. J.; Barabash, S. J. Modeling the Adsorption of Cd (II), Cu (II), Ni (II), Pb (II) and Zn (II) onto Montmorillonite. *Geochimica et Cosmochimica Acta* **2010,** *74*, 5718–28.

Harvey, O. R.; Qafoku, N. P.; Cantrell, K. J.; Lee, G.; Amonette, G. E.; Brown, C. F. Geochemical Implications of Gas Leakage Associated with Geologic CO_2 Storage-a Qualitative Review. *Environ. Sci. Technol.* **2013,** *47*, 23–26.

Hawthorne, S. B.; Miller, D. J. Evidence for Very Tight Squestration of Btex Compounds in Manufactured Gas Plant Soils Based on Selective Spercritical Fluid Extraction and Soil/Water Partitioning. *Environ. Sci. Technol.* **2003,** *37*, 3578–94.

Holloway, S.; Pearce, J. M.; Hards, V. L.; Ohsumi, T.; Gale, J. Natural Emissions of CO_2 from the Geosphere and Their Bearing on the Geological Storage of Carbon Dioxide. Energy **2007,** *32*, 1194–201.

Hosseini, S. A.; Mathias, S. A.; Javadpour, F. Analytical Model for CO_2 Injection into Brine Aquifers-Containing Residual CH_4. *Transport in Porous Media* **2012,** *94*, 795–815.

Hovorka, S. D.; Meckel, T. A.; Trevino, R. H.; Lu, J.; Nicot, J.-P.; Choi, J.-W.; Freeman, D.; Cook, P.; Daley, T. M.; Ajo-Franklin, J. B.; Freifeild, B. M.; Doughty, C.; Carrigan, C. R.; La Brecque, D.; Kharaka, Y. K.; Thordsen, J. J.; Phelps, T. J.; Yang, C.; Romanak, K. D.; Zhang, T.; Holt, R. M.; Lindler, J. S.; Butsch, R. J. Monitoring a Large Volume CO_2 Injection: Year Two Results from SECARB Project at Denbury's Cranfield, Mississippi, USA. *10th International Conference on Greenhouse Gas Control Technologies* **2011,** *4*, 3478–85.

Humez, P.; Lagneau, V.; Lions, J.; Negrel, P. Assessing the Potential Consequences of CO_2 Leakage to Freshwater Resources: A Batch-Reaction Experiment Towards an Isotopic Tracing Tool. *Applied Geochemistry* **2013,** *30*,178–90.

Jacquemet, N.; Picot-Colbeaux, G.; Vong, C. Q.; Lions, J.; Bouc, O.; Jeremy, R. Intrusion of CO_2 and Impurities in a Freshwater Aquifer-Impact Evaluation by Reactive Transport Modelling. *10th International Conference on Greenhouse Gas Control Technologies* **2011,** *4*, 3202–09.

Jean, J.-S.; Tsai, C.-L.; Ju, S.-H.; Tsao, C.-W.; Wang, S.-M. Biodegradation and Transport of Benzene, Toluene, and Xylenes in a Simulated Aquifer: Comparison of Modelled and Experimental Results. *Hydrological Processes* **2002,** *16*, 3151–68.

Jordan, P.; Benson, S. Well Blowout Rates and Consequences in California Oil and Gas District 4 from 1991 to 2005: Implications for Geological Storage of Carbon Dioxide. *Environ. Geol.* **2009,** *57*, 1103–23.

Jun, Y.-S.; Giammar, D. E.; Werth, C. J. Impacts of Geochemical Reactions on Geologic Carbon Sequestration. *Environ. Sci. Technol.* **2013,** *47*, 3–8.

Karamalidis, A. K.; Torres, S. G.; Hakala, J. A.; Shao, H.; Cantrell, K. J.; Carroll, S. Trace Metal Source Terms in Carbon Sequestration Environments. *Environ. Sci. Technol.* **2013,** *47*, 322–29.

Karickhoff, S. W.; Brown, D. S.; Scott, T. A. Sorption of Hydrophobic Pollutants on Natural Sediments. *Water Research* **1979,** *13*, 241–48.

Keating, E. H.; Fessenden, J.; Kanjorski, N.; Koning, D. J.; Pawar, R. The Impact of CO_2 on Shallow Groundwater Chemistry: Observations at a Natural Analog Site and Implications for Carbon Sequestration. *Environmental Earth Sciences* **2010,** *60*, 521–36.

Keating, E. H.; Hakala, J. A.; Viswanathan, H.; Carey, J. W.; Pawar, R.; Guthrie, G. D.; Fessenden-Rahn, J. CO_2 Leakage Impacts on Shallow Groundwater: Field-Scale Reactive-Transport Simulations Informed by Observations at a Natural Analog Site. *Applied Geochemistry* **2013a,** *30*,136–47.

Keating, E. H.; Newell, D. L.; Viswanathan, H.; Carey, J. W.; Zyvoloski, G.; Pawar, R. CO_2/Brine Transport into Shallow Aquifers Along Fault Zones. *Environmental Science & Technology* **2013b,** *47*, 290–97.

Keating, E.; Dai, Z.; Dempsey, D.; Pawar, R. Effective Detection of CO_2 Leakage: A Comparison of Groundwater Sampling and Pressure Monitoring. *Energy Procedia* **2014a,** *63*, 4163–71.

Keating, E.; Newell, D.; Dempsey, D.; Pawar, R. Insights into Interconnections between the Shallow and Deep Systems from a Natural CO_2 Reservoir near Springerville, Arizona. *International Journal of Greenhouse Gas Control* **2014b,** *25*, 162–72.

Kharaka, Y. K.; Campbell, P.; Thorden, J. J.; Thomas, P. B.; Cole, D. R.; Hovorka, S. D. Geologic Storage of Carbon Dioxide: Potential Environmental Impacts of CO_2-Organic Interactions. *Geochimica et Cosmochimica Acta* **2010a,** *74*, A511–A11.

Kharaka, Y. K.; Cole, D. R.; Hovorka, S. D.; Gunter, W. D.; Knauss, K. G.; Freifeld, B. M. Gas-Water-Rock Interactions in Frio Formation Following CO_2 Injection: Implications for the Storage of Greenhouse Gases in Sedimentary Basins. *Geology* **2006a,** *34*, 577–80.

Kharaka, Y. K.; Cole, D. R.; Thordsen, J. J.; Kakouros, E.; Nance, H. S. Gas-Water-Rock Interactions in Sedimentary Basins: CO_2 Sequestration in the Frio Formation, Texas, USA. *Journal of Geochemical Exploration* **2006b,** *89*, 183–86.

Kharaka, Y. K.; Hanor, J. S. Deep Fluids in the Continents: I. Sedimentary Basins. In *Surface and Ground Water, Weathering and Soil;* Drever, J. I., Ed.; Elsevier, Treatise on Geochemistry, 2007; pp 1–48.

Kharaka, Y. K.; Thordsen, J. J.; Hovorka, S. D.; Nance, H. S.; Cole, D. R.; Phelps, T. J.; Knauss, K. G. Potential Environmental Issues of CO_2 Storage in Deep Saline Aquifers: Geochemical Results from the Frio-I Brine Pilot Test, Texas, USA. *Applied Geochemistry* **2009,** *24*, 1106–12.

Kharaka, Y. K.; Thordsen, J. J.; Kakouros, E.; Ambats, G.; Herkelrath, W. N.; Beers, S. R.; Birkholzer, J. T.; Apps, J. A.; Spycher, N. F.; Zheng, L. E.; Trautz, R. C.; Rauch, H. W.; Gullickson, K. S. Changes in the Chemistry of Shallow Groundwater Related to the 2008 Injection of CO_2 at the ZERT Field Site, Bozeman, Montana. *Environmental Earth Sciences* **2010b,** *60*, 273–84.

Kirsch, K.; Navarre-Sitchler, A. K.; Wunsch, A.; McCray, J. E. Metal Release from Sandstones under Experimentally and Numerically Simulated CO_2 Leakage Conditions. *Environmental Science & Technology* **2014,** *48*, 1436–42.

Larsen, T.; Qeldsen, P. I.; Christensen, T. H. Correlation of Benzene, 1,1,1-Trichloroethane, and Naphthalene Distribution Coefficients to the Characteristics of Aquifer Materials with Low Organic Carbon Content. *Chemosphere* **1992,** *24*, 979–91.

Last, G. V.; Brown, C. F.; Murray, C. J.; Bacon, D. H.; Qafoku, N. P.; Sharma, M.; Jordan, P. D. *Determining Threshold Values for Identification of Contamination Predicted by Reduced Order Models*; Pacific Northwest National Laboratory: Richland, WA, 2013.

Lawrence, S. J. *Description, Properties, and Degradation of Selected Volatile Organic Compounds Detected in Ground Water — A Review of Selected Literature*; U.S. Geological Survey, Reston, VA, 2006.

Lawter, A.; Qafoku, N. P.; Wang, G.; Shao, H.; Brown, C. F. Evaluating Impacts of CO_2 Intrusion into an Unconsolidated Aquifer: I. Experimental Data. *International Journal of Greenhouse Gas Control* **2016,** *44*, 323–33.

Lawter, A.; Qafoku, N.; Shao, H.; Bacon, D.; Brown, C. Evaluating Impacts of CO_2 and CH_4 Gas Intrusion into an Unconsolidated Aquifer: Fate of As and Cd. *Frontiers in Environmental Science* **2015,** *3*, 49.

Lazareva, O.; Druschel, G.; Pichler, T. Understanding Arsenic Behavior in Carbonate Aquifers: Implications for Aquifer Storage Adn Recovery (ASR). *Applied Geochemistry* **2014**.

Leu, J. Y.; Lin, Y. H.; Chang, F. L. Conversion of CO_2 into CH_4 by Methane-Producing Bacterium FJ10 under a Pressurized Condition. *Chemical Engineering Research & Design* **2011,** *89*, 1879–90.

Lewicki, J. L.; Birkholzer, J.; Tsang, C.-F. Natural and Industrial Analogues for Leakage of CO_2 from Storage Reservoirs: Identification of Features, Events, and Processes and Lessons Learned. *Environ. Geol.* **2007,** *52*, 457–67.

Little, M. G.; Jackson, R. B. Potential Impacts of Leakage from Deep CO_2 Geosequestration on Overlying Freshwater Aquifers. *Environ. Sci. Technol.* **2010,** *44*, 9225–32.

Lu, J.; Partin, J. W.; Hovorka, S. D.; Wong, C. Potential Risks to Freshwater Resources as a Result of Leakage from CO_2 Geological Storage: A Batch-Reaction Experiment. *Environ. Earth Sci.* **2010,** *60*, 335–48.

Mackay, D.; Wan, Y. S.; Kuo, C. M. Lustrated Handbook of Physical-Chemical Properties and Environmental Fate for Orgwric Chemicals, Vol 1; *Monoaromatic Hydrocarbons, Chlorobenzenes, and Pcbs*; Lewis: Boca Raton, 1992.

Maclay, R. W.; Small, T. A. *Carbonate Geology and Hydrology of the Edwards Aquifer in the San Antonio Area, Texas*; OFR 83-537; U.S. Geological Survey, 1994.

McGrath, A. E.; Upson, G. L.; Caldwell, M. D. Evaluation and Mitigation of Landfill Gas Impacts on Cadmium Leaching from Native Soils. *Ground Water Monitoring and Remediation* **2007,** *27*, 99–109.

Mickler, P. J.; Yang, C. B.; Scanlon, B. R.; Reedy, R.; Lu, J. M. Potential Impacts of CO_2 Leakage on Groundwater Chemistry from Laboratory Batch Experiments and Field Push-Pull Tests. *Environmental Science & Technology* **2013,** *47*, 10694–702.

Mohd Amin, S.; Weiss, D. J.; Blunt, M. J. "Reactive Transport Modelling of Geologic CO_2 Sequestration in Saline Aquifers: The Influence of Pure CO_2 and of Mixtures of CO_2 with CH_4 on the Sealing Capacity of Cap Rock at 37°C and 100 Bar. *Chemical Geology* **2014,** *367*, 39–50.

Montes-Hernandez, G.; Renard, F.; Lafay, R. Experimental Assessment of CO_2-Mineral-Toxic Ion Interactions in a Simplified Freshwater Aquifer: Implications for CO_2 Leakage from Deep Geological Storage. *Environmental Science & Technology* **2013,** *47*, 6247–53.

Musgrove, M.; Fahlquist, L.; Houston, N. A.; Lindgren, R. J.; Ging, P. B. *Geochemical Evolution Processes and Water-Quality Observations Based on Results of the National Water-Quality Assessment Program in the San Antonio Segment of the Edwards Aquifer, 1996-2006*; Scientific Investigations Report 2010-5129; U.S. Geological Survey, Reston, VA, 2010.

Newmark, R. L.; Friedmann, S. J.; Carroll, S. A. Water Challenges for Geologic Carbon Capture and Sequestration. *Environmental Management* **2010,** *45*, 651–61.

Nicot, J.-P.; Oldenburg, C. M.; Houseworth, J. E.; Choi, J.-W. Analysis of Potential Leakage Pathways at the Cranfield, MS, USA, CO_2 Sequestration Site. *International Journal of Greenhouse Gas Control* **2013,** *18*, 388–400.

Nisi, B.; Vaselli, O.; Tassi, F.; de Elio, J.; Huertas, A. D.; Mazadiego, L. F.; Ortega, M. F. Hydrogeochemistry of Surface and Spring Waters in the Surroundings of the CO_2 Injection Site at Hontomin-Huermeces (Burgos, Spain). *International Journal of Greenhouse Gas Control* **2013,** *14*, 151–68.

Nordbotten, J. M.; Celia, M. A.; Bachu, S.; Dahle, H. K. Semianalytical Solution for CO_2 Leakage through an Abandoned Well. *Environ. Sci. Technol.* **2005,** *39*, 602–11.

Oldenburg, C. M.; Doughty, C. Injection, Flow, and Mixing of CO_2 in Porous Media with Residual Gas. *Transport in Porous Media* **2011a,** *90*, 201–18.

Oldenburg, C. M.; Rinaldi, A. P. Buoyancy Effects on Upward Brine Displacement Caused by CO_2 Injection. *Transport in Porous Media* **2011b,** *87*, 525–40.

Palandri, J.; Kharaka, Y. K. *A Compilation of Rate Parameters of Water-Mineral Interaction Kinetics for Application to Geochemical Modeling*; Open File report 2004-1068; U.S. Geological Survey, 2004.

Parkhurst, D. L.; Appelo, C. A. J. *User's Guide to Phreeqc (Version 2) : A Computer Program for Speciation, Batch-Reaction, One-Dimensional Transport, and Inverse Geochemical Calculations*; Water Resources Investigations Report 99-4259; U.S. Geological Survey, Washington, DC, 1999.

Peter, A.; Lamert, H.; Beyer, M.; Hornbruch, G.; Heinrich, B.; Schulz, A.; Geistlinger, H.; Schreiber, B.; Dietrich, P.; Werban, U.; Vogt, C.; Richnow, H. H.; Grossmann, J.; Dahmke, A. Investigation of the Geochemical Impact of CO_2 on Shallow Groundwater: Design and Implementation of a CO_2 Injection Test in Northeast Germany. *Environmental Earth Sciences* **2012,** *67*, 335–49.

Qafoku, N.; Bown, C.; Wang, G.; Sullivan, E.; Lawter, A.; Harvey, O.; Bowden, M. *Geochemical Impacts of Leaking Co2 from Subsurface Storage Reservoirs to Unconfined and Confined Aquifers*; PNNL-22420; Pacific Northwest National Laboratory: Richland, WA, 2013.

RøeUtvik, T. I. Chemical Characterisation of Produced Water from Four Offshore Oil Production Platforms in the North Sea. *Chemosphere* **1999,** *39*, 2593–606.

Romanak, K. D.; Smyth, R. C.; Yang, C.; Hovorka, S. D.; Rearick, M.; Lu, J. Sensitivity of Groundwater Systems to CO_2: Application of a Site-Specific Analysis of Carbonate Monitoring Parameters at the SACROC CO_2-Enhanced Oil Field. *International Journal of Greenhouse Gas Control* **2012,** *6*, 142–52.

Saleem, Z. A. *Anaerobic Biodegradation Rates of Organic Chemicals in Groundwater: A Summary of Field and Laboratory Studies*; U.S. Environmental Protection Agency, Office of Solid Waste: Washington, DC, 1999.

Scherer, G. W.; Kutchko, B.; Thaulow, N.; Duguid, A.; Mook, B. Characterization of Cement from a Well at Teapot Dome Oil Field: Implications for Geological Sequestration. *Int. J. Greenhouse Gas Control* **2011,** *5*, 115–24.

Scherf, A. K.; Zetzl, C.; Smirnova, I.; Zettlitzer, M.; Vieth-Hillebrand, A.; CO2SINK Grp. Mobilisation of Organic Compounds from Reservoir Rocks through the Injection of CO_2 - Comparison of Baseline Characterization and Laboratory Experiments. *Energy Procedia* **2011,** *4*, 4524–31.

Shao, H.; Qafoku, N.; Lawter, A.; Bowden, M.; Brown, C. Coupled Geochemical Impacts of Leaking CO_2 and Contaminants from Subsurface Storage Reservoirs on Groundwater Quality. *Environmental Science & Technology* **2015,** *49*, 8202–09.

Skinner L. *CO_2 Blowouts: An Emerging Problem: Well Control and Intervention*. ETATS-UNIS: Gulf, Houston, TX, 2003.

Smyth, R. C.; Hovorka, S. D.; Lu, J.; Romanak, K. D.; Partin, J. W.; Wong, C.; Yang, C. Assessing Risk to Fresh Water Resources from Long Term CO2 Injection-Laboratory and Field Studies. *Energy Procedia* **2009,** *1*, 1957–64.

Sø, H. U.; Postma, D.; Jakobsen, R.; Larsen, F. Sorption and Desorption of Arsenate and Arsenite on Calcite. *Geochimica et Cosmochimica Acta* **2008,** *72*, 5871–84.

Sonnenthal, E.; Ito, A.; Spycher, N.; Yui, M.; Apps, J.; Sugita, Y.; Conrad, M.; Kawakami, S. Approaches to Modeling Coupled Thermal, Hydrological, and Chemical Processes in the Drift Scale Heater Test at Yucca Mountain. *Int. J. Rock Mech. Min. Sci.* **2005,** *42*, 6987–719.

Spangler, L. H.; Dobeck, L. M.; Repasky, K. S.; Nehrir, A. R.; Humphries, S. D.; Barr, J. L.; Keith, C. J.; Shaw, J. A.; Rouse, J. H.; Cunningham, A. B.; Benson, S. M.; Oldenburg, C. M.; Lewicki, J. L.; Wells, A. W.; Diehl, J. R.; Strazisar, B. R.; Fessenden, J. E.; Rahn, T. A.; Amonette, J. E.; Barr, J. L.; Pickles, W. L.; Jacobson, J. D.; Silver, E. A.; Male, E. J.; Rauch, H. W.; Gullickson, K. S.; Trautz, R.; Kharaka, Y.; Birkholzer, J.; Wielopolski, L. A Shallow Subsurface Controlled Release Facility in Bozeman, Montana, USA, for Testing near Surface CO_2 Detection Techniques and Transport Models. *Environmental Earth Sciences* **2010,** *60*, 227–39.

Swedlund, P. J.; Webster, J. G.; Miskelly, G. M. Goethite Adsorption of Cu(II), Pb(II), Cd(II), and Zn(II) in the Presence of Sulfate: Properties of the Ternary Complex. *Geochimica et Cosmochimica* Acta **2009,** *73*, 1548–62.

Taggart, I. Extraction of Dissolved Methane in Brines by CO_2 Injection: Implication for CO_2 Sequestration. *Spe Reservoir Evaluation & Engineering* **2010,** *13*, 791–804.

Tesoriero, A. J.; Pankow, J. F. Solid Solution Partitioning of Sr2+, Ba2+, and Cd2+ to Calcite. *Geochimica Et Cosmochimica Acta* **1996,** *60*, 1053–63.

Trautz, R. C.; Pugh, J. D.; Varadharajan, C.; Zheng, L. G.; Bianchi, M.; Nico, P. S.; Spycher, N. F.; Newell, D. L.; Esposito, R. A.; Wu, Y. X.; Dafflon, B.; Hubbard, S. S.; Birkholzer, J. T. Effect of Dissolved CO_2 on a Shallow Groundwater System: A Controlled Release Field Experiment. *Environmental Science & Technology* **2013,** *47*, 298–305.

Underschultz, J.; Boreham, C.; Dance, T.; Stalker, L.; Freifeld, B.; Kirste, D.; Ennis-King, J. CO_2 Storage in a Depleted Gas Field: An Overview of the CO2CRC Otway Project and Initial Results. *International Journal of Greenhouse Gas Control* **2011,** *5*, 922–32.

Varadharajan, C.; Tinnacher, R. M.; Pugh, J. D.; Trautz, R. C.; Zheng, L. G.; Spycher, N. F.; Birkholzer, J. T.; Castillo-Michel, H.; Esposito, R. A.; Nico, P. S. A Laboratory Study of the Initial Effects of Dissolved Carbon Dioxide (CO_2) on Metal Release from Shallow Sediments. *International Journal of Greenhouse Gas Control* **2013,** *19*, 183–211.

Viswanathan, H.; Dai, Z. X.; Lopano, C.; Keating, E.; Hakala, J. A.; Scheckel, K. G.; Zheng, L. G.; Guthrie, G. D.; Pawar, R. Developing a Robust Geochemical and Reactive Transport

Model to Evaluate Possible Sources of Arsenic at the CO_2 Sequestration Natural Analog Site in Chimayo, New Mexico. *International Journal of Greenhouse Gas Control* **2012,** *10*, 199–214.

Vong, C. Q.; Jacquemet, N.; Picot-Colbeaux, G.; Lions, J.; Rohmer, J.; Bouc, O. Reactive Transport Modeling for Impact Assessment of a CO_2 Intrusion on Trace Elements Mobility within Fresh Groundwater and Its Natural Attenuation for Potential Remediation. 10th International Conference on Greenhouse Gas Control Technologies **2011,** *4*, 3171–78.

Wang, G.; Qafoku, N.; Lawter, A.; Bowden, M.; Harvey, O.; Sullivan, C.; Brown, C. Geochemical Impacts of Leaking CO_2 from Subsurface Storage Reservoirs to an Unconfined Oxidizing Carbonate Aquifer. *International Journal of Greenhouse Gas Control* **2016,** *44*, 310–22.

Wang, S.; Jaffe, P. R. Dissolution of a Mineral Phase in Potable Aquifers Due to CO2 Releases from Deep Formations; Effect of Dissolution Kinetics. *Energy Convers. Manage.* **2004,** *45*, 2833–48.

Wei, Y.; Maroto-Valer, M.; Steven, M. D. Environmental Consequences of Potential Leaks of CO_2 in Soil. *Energy Procedia* **2011,** *4*, 3224−30.

White, M. D.; Bacon, D. H.; McGrail, B. P.; Watson, D. J.; White, S. K.; Zhang, Z. F. STOMP Subsurface Transport over Multiple Phases: STOMP-CO2 and STOMP-CO2e Guide: Version 1.0; PNNL-21268; Pacific Northwest National Laboratory: Richland, WA, 2012.

White, M. D.; McGrail, B. P. *Stomp, Subsurface Transport over Multiple Phases, Version 1.0, Addendum: Eckechem, Equilibrium-Conservation-Kinetic Equation Chemistry and Reactive Transport*; PNN-15482; Pacific Northwest National Laboratory: Richland, WA, 2005.

Wilkin, R. T.; Digiulio, D. C. Geochemical Impacts to Groundwater from Geologic Carbon Sequestration: Controls on pH and Inorganic Carbon Concentrations from Reaction Path and Kinetic Modeling. *Environ. Sci. Technol.* **2010,** *44*, 4821–27.

Witter, A. E.; Jones, A. D. Chemical Characterization of Organic Constituents from Sulfide-Rich Produced Water Using Gas Chromatography/Mass Spectrometry. *Environ. Toxicol. Chem.* **1999,** *18*, 1920–26.

Wolery, T. W.; Jarek, R. L. *Software User's Manual, Eq3/6, Version 8.0*; Sandia National Laboratories: Albuquerque, NM, 2003.

Wunsch, A.; Navarre-Sitchler, A. K.; Moore, J.; McCray, J. E. Metal Release from Limestones at High Partial-Pressures of CO_2. *Chemical Geology* **2014,** *363*, 40–55.

Wunsch, A.; Navarre-Sitchler, A. K.; Moore, J.; Ricko, A.; McCray, J. E. Metal Release from Dolomites at High Partial-Pressures of CO_2. *Applied Geochemistry* **2013,** *38*, 33–47.

Xu, T.; Sonnenthal, E.; Spycher, N.; Pruess, K. Toughreact: A Simulation Program for Non-Isothermal Multiphase Reactive Geochemical Transport in Variably Saturated Geologic Media. *Computers and Geosciences* **2006,** *32*, 145–65.

Yang, C. B.; Mickler, P. J.; Reedy, R.; Scanlon, B. R.; Romanak, K. D.; Nicot, J. P.; Hovorka, S. D.; Trevino, R. H.; Larson, T. Single-Well Push-Pull Test for Assessing Potential Impacts of CO2 Leakage on Groundwater Quality in a Shallow Gulf Coast Aquifer in

Cranfield, Mississippi. *International Journal of Greenhouse Gas Control* **2013,** *18*, 375–87.

Yang, C.; Dai, Z.; Romanak, K. D.; Hovorka, S. D.; Trevino, R. H. Inverse Modeling of Water-Rock-CO2 Batch Experiments: Potential Impacts on Groundwater Resources at Carbon Sequestration Sites. *Environ Sci Technol* **2014,** *48*, 2798–806.

Yokoyama, Y.; Tanaka, K.; Takahashi, Y. Differences in the Immobilization of Arsenite and Arsenate by Calcite. *Geochimica Et Cosmochimica Acta* **2012,** *91*, 202–19.

Zheng, L.; Apps, J. A.; Spycher, N.; Birkholzer, J. T.; Kharaka, Y. K.; Thordsen, J.; Beers, S. R.; Herkelrath, W. N.; Kakouros, E.; Trautz, R. C. Geochemical Modeling of Changes in Shallow Groundwater Chemistry Observed During the MSU-ZERT CO_2 Injection Experiment. *International Journal of Greenhouse Gas Control* **2012,** *7*, 202–17.

Zheng, L.; Apps, J. A.; Zhang, Y.; Xu, T.; Birkholzer, J. T. On Mobilization of Lead and Arsenic in Groundwater in Response to CO_2 Leakage from Deep Geological Storage. *Chemical Geology* **2009,** *268*, 281–97.

Zheng, L.; Qafoku, N. P.; Lawter, A.; Wang, G.; Shao, H.; Brown, C. F. Evaluating Impacts of CO2 Intrusion into an Unconsolidated Aquifer: II. Modeling Results. *International Journal of Greenhouse Gas Control* **2016,** *44*, 300–09.

Zheng, L.; Spycher, N.; Birkholtzer, J.; Xu, T.; Apps, J.; Kharaka, Y. On Modeling the Potential Impacts of CO_2 Sequestration on Shallow Groundwater: Transport of Organics and Co-Injected H_2S by Supercritical CO_2 to Shallow Aquifers. *International Journal of Greenhouse Gas Control* **2013,** *14*, 113–27.

Zheng, L.; Spycher, N.; Birkholzer, J.; Xu, T.; Apps, J. *Modeling Studies on the Transport of Benzene and H_2S in CO_2-Water Systems*; Lawrence Berkeley National Laboratory: Berkeley, CA, 2010.

Zheng, L.; Spycher, N.; Varadharajan, C.; Tinnachera, R. M.; Pugh, J. D.; Bianchi, M.; Birkholzer, J.; Nico, P. S.; Trautz, R. C. On the Mobilization of Metals by CO_2 Leakage into Shallow Aquifers: Exploring Release Mechanisms by Modeling Field and Laboratory Experiments. *Greenhouse Gases: Science and Technology* **2015,** *5*, 403–18.

Zhong, L. R.; Cantrell, K.; Mitroshkov, A.; Shewell, J. Mobilization and Transport of Organic Compounds from Reservoir Rock and Caprock in Geological Carbon Sequestration Sites. *Environmental Earth Sciences* **2014a,** *71*, 4261–72.

Zhong, L.; Cantrell, K. J.; Bacon, D. H.; Shewell, J. Transport of Organic Contaminants Mobilized from Coal through Sandstone Overlying a Geological Carbon Sequestration Reservoir. *International Journal of Greenhouse Gas Control* **2014b,** *21*, 158–64.

NRAP is an initiative within DOE's Office of Fossil Energy and is led by the National Energy Technology Laboratory (NETL). It is a multi-national-lab effort that leverages broad technical capabilities across the DOE complex to develop an integrated science base that can be applied to risk assessment for long-term storage of carbon dioxide (CO_2). NRAP involves five DOE national laboratories: NETL, Lawrence Berkeley National Laboratory (LBNL), Lawrence Livermore National Laboratory (LLNL), Los Alamos National Laboratory (LANL), and Pacific Northwest National Laboratory (PNNL).

Technical Leadership Team

Diana Bacon
Lead, Groundwater Protection Working Group
Pacific Northwest National Laboratory
Richmond, WA

Jens Birkholzer
LBNL Lab Lead
Lawrence Berkeley National Laboratory
Berkeley, CA

Grant Bromhal
Technical Director, NRAP
Research and Innovation Center
National Energy Technology Laboratory
Morgantown, WV

Chris Brown
PNNL Lab Lead
Pacific Northwest National Laboratory
Richmond, WA

Susan Carroll
LLNL Lab Lead
Lawrence Livermore National Laboratory
Livermore, CA

Abdullah Cihan
Lead, Reservoir Performance Working Group
Lawrence Berkeley National Laboratory
Berkeley, CA

Tom Daley
Lead, Strategic Monitoring Working Group
Lawrence Berkeley National Laboratory
Berkeley, CA

Robert Dilmore
NETL Lab Lead
Research and Innovation Center
National Energy Technology Laboratory
Pittsburgh, PA

Nik Huerta
Lead, Migration Pathways Working Group
Research and Innovation Center
National Energy Technology Laboratory
Albany, OR

Rajesh Pawar
LANL Lab Lead
Lead, Systems/Risk Modeling Working Group
Los Alamos National Laboratory
Los Alamos, NM

Tom Richard
Deputy Technical Director, NRAP
The Pennsylvania State University
State College, PA

Josh White
Lead, Induced Seismicity Working Group
Lawrence Livermore National Laboratory
Livermore, CA

Sean Plasynski
Executive Director
Technology Development and Integration Center
National Energy Technology Laboratory
U.S. Department of Energy

Heather Quedenfeld
Associate Director
Coal Development and Integration
National Energy Technology Laboratory
U.S. Department of Energy

Traci Rodosta
Technology Manager
Strategic Planning
Science and Technology Strategic Plans and Programs
National Energy Technology Laboratory
U.S. Department of Energy

Mark Ackiewicz
Director
Division of Carbon Capture and Storage
Office of Fossil Energy
U.S. Department of Energy

NRAP Executive Committee

Cynthia Powell
Executive Director
Research and Innovation Center
National Energy Technology Laboratory

Donald DePaolo
Associate Laboratory Director
Energy and Environmental Sciences
Lawrence Berkeley National Laboratory

Roger Aines
Chief Energy Technologist
Lawrence Livermore National Laboratory

Melissa Fox
Program Manager
Applied Energy Programs
Los Alamos National Laboratory

George Guthrie
Chair, NRAP Executive Committee
Earth and Environmental Sciences
Los Alamos National Laboratory

Alain Bonneville
Laboratory Fellow
Pacific Northwest National Laboratory

Grant Bromhal
Technical Director, NRAP
Senior Research Fellow
Research and Innovation Center
National Energy Technology Laboratory

NRAP Technical Report Series